(2)

Mechanisms of Microwave Induced Damage In Biologic Materials

Annual Report

January 1990

By

T.A. Litovitz, R. Meister, R.K. Mohr., C.J. Montrose, J.M. Mullins, R.M. Nardone, and M. Penafiel

Contract DAMD17-86-C-6260

The Catholic University of America
Washington, D.C. 20064

SECURITY CLASSIFICATION OF THIS PAGE

REPORT DOCUMENTATION PAGE

Form Approved OMB No. 0704-0188

1a. REPORT SECURITY CLASSIFICATION Unclassified	1b. RESTRICTIVE MARKINGS
2a. SECURITY CLASSIFICATION AUTHORITY	3. DISTRIBUTION/AVAILABILITY OF REPORT Approved for public release; distribution unlimited
2b. DECLASSIFICATION/DOWNGRADING SCHEDULE	
4. PERFORMING ORGANIZATION REPORT NUMBER(S)	5. MONITORING ORGANIZATION REPORT NUMBER(S)
6a. NAME OF PERFORMING ORGANIZATION The Catholic University of America 6b. OFFICE SYMBOL (If applicable)	7a. NAME OF MONITORING ORGANIZATION
6c. ADDRESS (City, State, and ZIP Code) Washington, DC 20064	7b. ADDRESS (City, State, and ZIP Code)
8a. NAME OF FUNDING/SPONSORING ORGANIZATION U.S. Army Medical Research & Development Command 8b. OFFICE SYMBOL (If applicable)	9. PROCUREMENT INSTRUMENT IDENTIFICATION NUMBER DAMD17-86-C-6260
8c. ADDRESS (City, State, and ZIP Code) Fort Detrick Frederick, MD 21701-5012	10. SOURCE OF FUNDING NUMBERS

PROGRAM ELEMENT NO.	PROJECT NO.	TASK NO.	WORK UNIT ACCESSION NO.
62787A	3E1-62787A878	BB	021

11. TITLE (Include Security Classification)

(U) Mechanisms of Microwave Induced Damage in Biologic Materials

12. PERSONAL AUTHOR(S) T.A. Litovitz, R. Meister, R.K. Mohr, C.J. Montrose, J.M. Mullins, R.M. Nardone, and M. Penafiel

13a. TYPE OF REPORT	13b. TIME COVERED	14. DATE OF REPORT (Year, Month, Day)	15. PAGE COUNT
Annual	FROM 9/22/88 TO 9/21/89	1990 January	

16. SUPPLEMENTARY NOTATION

17. COSATI CODES			18. SUBJECT TERMS (Continue on reverse if necessary and identify by block number)
FIELD	GROUP	SUB-GROUP	RA 3; Microwave; Irradiation; Cell Cultures; Deoxyribonucleic acid
06	03		
06	01		

19. ABSTRACT (Continue on reverse if necessary and identify by block number)

This report is divided into four chapters which correspond to the four main lines of research being carried out under the contract. In brief, these are (1) mathematical modeling studies, (2) experimental spectroscopic studies, (3) engineering design research, and (4) experimental biological studies.

The research program is structured to attempt to discover the biological effects at the cell and molecular level that result from exposure to electromagnetic radiation. The main thrust is on the athermal effects of exposure to microwaves. Because recent work has suggested that significant cellular effects occur only when the microwaves are amplitude modulated, either with extremely low frequency (ELF) sinusoids or with pulses, we have hypothesized that the interaction of the microwave fields with cells must involve a demodulation or detection step. As a result, research designed to develop an understanding of the effects of direct ELF exposure becomes not only relevant, but vital.

20. DISTRIBUTION/AVAILABILITY OF ABSTRACT	21. ABSTRACT SECURITY CLASSIFICATION
☐ UNCLASSIFIED/UNLIMITED ☒ SAME AS RPT. ☐ DTIC USERS	Unclassified

22a. NAME OF RESPONSIBLE INDIVIDUAL	22b TELEPHONE (Include Area Code)	22c. OFFICE SYMBOL
Mary Frances Bostian	301-663-7325	SGRD-RMI-S

DD Form 1473, JUN 86 *Previous editions are obsolete.* SECURITY CLASSIFICATION OF THIS PAGE

19. The first chapter of the work develops some of the theoretical ideas that connect the augmentation of transcription with the exposure of cells to electromagnetic fields. Among the major ideas that are explored are transient response mechanisms and so-called "power windows." The implications of the theory as regards the outcomes of a number of experimental configurations and protocols are discussed.

In the second chapter we report on a fundamental study involving the frequency dependence of the dielectric response of DNA solutions of variable salt content. Using the data it has been possible for the first time to sort out the roles of the various constituents of the ionic atmosphere (condensed counter-ions, diffuse ions and bulk ions) in determining the relaxation of the conductivity and thus the nature of the coupling of DNA molecules to electric fields.

Chapter three discusses the experimental configurations that have been used in exposing cells to both microwave and ELF electromagnetic fields. Measurements of the field distributions within the sample chambers are reported for a variety of orientations within the exposure reion. The effect of the settling of cells in their suspension medium is explored. Dielectric response and electrical conductivity studies in aqueous solutions of polyelectrolytes of varying ionic strength are also reported.

The last chapter summarizes the activity of the biology group. Included in this work is a study using 2-D gel electrophoresis of EM field induced changes in the synthesis of certain proteins and an examination of possible ELF enhancement of mRNA synthesis. In addition very promising results are reported in experiments examining the enhancement of total RNA production following short-term ELF exposure and in the increased activity of the enzyme ornithine decarboxylase to ELF and microwave irradiation.

Foreward

Citations of commercial organizations and trade names in this report do not constitute an official Department of the Army endorsement or approval of the products or services of these organizations.

Table of Contents

CHAPTER I

MATHEMATICAL MODELLING STUDIES

Power windows and transiently augmented transcription from exposure to electromagnetic radiation

The exposure of cells to relatively low intensity pulsed and low frequency electromagnetic fields results in a transient augmentation of transcriptional activity. Under certain irradiation conditions, the increases exhibit maxima when regarded as a function of the strength of the electromagnetic fields. A linear multi-step chemical reaction model that accounts for many of the principal features that are observed both in the time and power variation of the transcriptional effects is described. The crucial hypothesis of the model is the supposition that the direct effect of cell exposure to electromagnetic fields is an increase in the rate constant characterizing one of the intermediate sequential reactions in the mRNA synthesis. The implications of the model for a variety of experimental circumstances are explored.

INTRODUCTION

Under certain exposure conditions the effect of extremely low frequency (ELF) exogenously applied electromagnetic fields on certain measured properties of a biological system is a transient one.[1,2,3,4] The system's response, determined by some well-defined endpoint, first rises following the switching on of the irradiating field, reaches some maximum value, and then decays, ultimately approaching some steady-state value (which may be the original equilibrium or basal value). It has also been reported that the magnitude of a system's response both to ELF and to ELF-modulated RF fields depends sensitively on the field strength, exhibiting maxima, or so-called power-windows[1-4,5] when regarded as a function of the exogenous field strength. This paper suggests an intimate connection between these two observations, in particular, that the latter may arise simply from observing the former at a fixed exposure time following the switching-on of the exogenous field.

As an example, suppose that we are monitoring the concentration of some particular messenger RNA species as a function of time following the switching on of the field at t=0. We suppose that, as a function of time, the mRNA concentration initially rises to some maximum value and then decays back to a steady-state level (the exogenous field remaining on). Let us further suppose that the system's response depends upon the strength of the irradiating field (or power density) such that increasing the strength of the field

(1) increases the maximum value of the system's response (the peak is higher); and

(2) accelerates the system's response (the peak occurs sooner after switching on the field).

Under such conditions the results for three different field strengths will look something like those shown in Figure 1.

Next consider that rather than being monitored as a function of time, the mRNA composition (or any other suitable endpoint) is measured only for some fixed exposure time T following the initial switching on of the field. Such an experiment might be designed to probe, for instance, the response of the system to the time = T exposure as a function of the field strength (irradiating power density). For the curves shown in Figure 1, the time = T exposure data would be represented by the bar graph in Figure 2. There is apparently a power region of maximum sensitivity--a power window--even though our assumptions above would seem to legislate explicitly against such behavior. The conclusion to be drawn is clear:

> Observations of power windows must be viewed cautiously, especially if they involve measurements made not as a function of exposure time, but rather for a single

exposure duration.

Observe that this conclusion rests on three perhaps-not-too-unreasonable assumptions--(1) transient response to an impressed field; (2) a maximum response that increases with increasing irradiating power; and (3) a peak location that shifts to earlier time as the power is increased. Is there some simple physical model that suggests this kind of behavior? In the next section, we suggest that there is, and that this simple model--which is surely much too crude to portray accurately a process as complex as, for instance, RNA or protein synthesis--can nevertheless prove useful as a guide for designing and a vehicle for interpreting electromagnetic field in vitro exposure experiments.

1. DESCRIPTION OF THE MODEL

For the sake of definiteness we shall present the model as one intended to describe field-enhanced transcription, although it can profitably be used in conceptualizing a variety of field-altered processes. We envision a series of events, modeled by a set of sequential first-order chemical reactions:

$$\left[\begin{array}{c}\textit{Nucleotide}\\ \textit{reservoir}\end{array}\right] \longrightarrow \left[\begin{array}{c}\textit{Positioned}\\ \textit{G, C, A, U}\end{array}\right] \longrightarrow [\,\textit{mRNA}\,] \longrightarrow \cdots$$

Diffusion : Polymerization Degradation

$$[A] \xrightarrow[k_1]{} [X] \xrightarrow[k_2]{} [Y] \xrightarrow[k_3]{} \cdots$$

The first step (rate constant = k_1) represents the diffusion-controlled migration to, and the "positioning" and orienting of the various nucleotides from the cellular pool (we designate the nucleotide reservoir concentration by A) in their "correct" sites in the neighborhood of the DNA molecule. The second reaction step (rate constant = k_2) is the polymerization of the positioned and oriented G, C, A and U nucleotides (the concentration of which we designate by x) to form messenger RNA (concentration denoted by y). The final step (rate constant = k_3) is the degradation of messenger RNA by cytoplasmic nucleases. We assume that the reactions are strongly biased in the forward direction, and that only these rate constants need be considered.

Of course, we recognize that what we have described as a single reaction step in actuality consists of a number of complex

individual processes. Our assumption is that among these processes there is one that is "rate-determining" so that the simplification shown above is meaningful. No qualitative changes in the model's predictions would result if additional steps were added to the sequence, although the equations would become more complicated and the exact shapes of the response curves would be altered.

Mathematical Formulation

We assume that the nucleotide reservoir is rapidly replenished (that is, that it is not depleted) and, as noted above, that any back-reactions can be neglected. We then describe these reactions by a set of linear first order differential equations

$$dx/dt = + k_1 A - k_2 x; \tag{1a}$$

$$dy/dt = + k_2 x - k_3 y. \tag{1b}$$

The equilibrium values (in the absence of any external electromagnetic fields) are easy to determine from dx/dt = dy/dt = 0:

$$x_{eq} = x_0 = k_1 A/k_2; \tag{2a}$$

$$y_{eq} = y_0 = k_2 x_0/k_2 = k_1 A/k_3. \tag{2b}$$

We now make our hypothesis regarding the effect of the exogenous electromagnetic field:

> Switching on the electromagnetic field at t = 0 produces a "sudden" increase in k_2, that is
>
> $$k_2 \longrightarrow k_2^*$$
>
> with this change occurring on a time scale that is short compared with the inverse reaction rates.

With this hypothesis, it is now a straightforward matter to solve the differential equations to determine the concentrations as functions of time:

$$x(t) = \frac{k_1 A}{k_2^*} \left[1 + \frac{\Delta k}{k_2} e^{-k_2^* t} \right]; \tag{3}$$

and

$$y(t) = \frac{k_1 A}{k_3} + \frac{k_1 A}{k_3 - k_2^*} \frac{\Delta k}{k_2} \left[e^{-k_2^* t} - e^{k_3 t} \right], \qquad (4)$$

where

$$\Delta k = k_2^* - k_2. \qquad (5)$$

The quantities x(t) and y(t) (the mRNA concentration) are plotted in Figs. 3 and 4 for three values of the altered rate constant k_2^*.

The parameters for the plots are given in a set of reduced units. From the differential equations (1), it is clear that the rate constants (the k_j) have units of $(\text{time})^{-1}$. It is therefore sensible to choose one of them as defining the basic time unit: we do this by setting $k_1 \equiv 1$. In a similar fashion, we take A as the basic concentration unit, i.e., $A \equiv 1$. Equivalently we may regard all rate constants and concentrations as being given by ratios with k_1 and A respectively:

$$k_j \longrightarrow k_j/k_1, \quad x \longrightarrow x/A \text{ and } y \longrightarrow y/A.$$

Similarly times an be regarded as products with k_1:

$$t \longrightarrow k_1 t$$

For the plots in Figures 3 and 4 we have taken $k_2 = 1$, $k_3 = 10$, and $k_2^* = 3$, 10 and 30.

Observe from Figure 4 that, independent of the value of k_2^*, the long-time steady-state field-on concentration is the same as the zero-field concentration--the basal level, i.e., $y(\infty) = y(0)$. The transient character of the response in this model is relatively easy to understand. The initial rise in y(t) arises from the enhanced rate k_2^* (the polymerization rate); the drop off at long times (back to the equilibrium value) comes from the depletion of the precursors x (the "positioned and oriented" nucleotides). Note in particular that

(1) the maximum of y(t), marked by "|" on the plots, moves toward t = 0 with increasing k_2^*, and

(2) the peak height increases with increasing k_2^*.

Apparent Power Windows

If we were now to assume that Δk increases with irradiating field strength (or power density) that is, the change in the rate

constant governing the x → y reaction (the production of mRNA) increases with the electromagnetic intensity, then all of the features of transient responses would be qualitatively reproduced by this simple model.

Note in particular that for the parameters chosen for this sample calculation, an exposure time of 0.25 (marked on Figure 4 by a vertical line) leads to the appearance of a maximum in the response considered as a function of k_2^*, field strength or power density, i.e., a so-called power window. This is illustrated on the bar graph in Figure 5. Note that for shorter exposure times (illustrated in Figure 5 is the case of an exposure time of 0.12) the maximum shifts to higher power densities. The point is that, within the context of the linear reaction model, fixed observation times will always lead to the appearance of a maximum in the response regarded as a function of the field strength, with the location of the maximum being a function of the exposure time.

The Peak in the Transient Response

The location in time of the peak that is observed in the response of the system can be determined by differentiating Equation (4). The result is

$$t_{max} = \frac{1}{k_3 - k_2^*} \ln(k_3/k_2^*), \qquad (6)$$

and the magnitude of the maximum response is given by substituting this back in Equation (4). Defining $y_{max} \equiv y(t_{max})$ leads to

$$y_{max} = \frac{k_1 A}{k_3} + \frac{k_1 A}{k_3 - k_2^*} \frac{\Delta k}{k_2^*} \left[(k_2^*/k_3)^{k_2^*/(k_3 - k_2^*)} - (k_2^*/k_3)^{k_3/(k_3 - k_2^*)} \right]. \qquad (7)$$

Both t_{max} and y_{max} are plotted as functions of the changed rate constant k_2^* in Figure 6. Observe that y_{max} saturates as k_2^* is increased so that the peak height cannot be used as a measure of the change in k_2. That is, for large values of k_2^* the peak height does not change although the location of the peak does shift to shorter times. This saturation occurs when k_2^* has become so large that it no longer limits the polymerization rate; the production of mRNA is controlled exclusively by the availability of the positioned nucleotide precursors.

Short-time and Long-time Behavior

The change in k_2 produced by switching on the field can be found from the initial rate of change of the response. Expanding Equation (4) about t = 0 shows that y increases linearly for short times:
From this it follows that the initial slope of the response is

$$y(t) - y_0 = \delta y(t) - \frac{k_3}{k_2}\,\Delta k\, t \qquad (t \ll t_{max}). \tag{8}$$

directly proportional to the magnitude of the change in k_2, that is to Δk.

Note also the behavior of the response at long times. With the field remaining on, the system marker (mRNA) returns to its equilibrium value at a rate determined by the <u>smaller</u> of the reaction rates k_2^* and k_3. Specifically, if one of the rates is much larger than the other, we have

$$\left[\frac{d}{dt}\ln \delta y\right]_{t\to\infty} \approx -k_<, \qquad (k_< \ll k_>) \tag{9}$$

where $k_<$ ($k_>$) is the smaller (larger) of k_2^* and k_3.

The Effect of mRNA Stabilization

In the reaction model just described, the transient increase and subsequent fall of the measured marker (mRNA) was produced by supposing that the effect of the impressed field is to <u>increase the polymerization rate (the rate of mRNA production)</u>. It is reasonable to inquire if a similar result can be derived if we assume that the effect of the field is to stabilize the mRNA, that is, to decrease its rate of degradation. The answer is that within the context of this elementary linear picture, it is not. If we had assumed, for example, that switching on the field at t = 0 causes k_3 to be suddenly changed to some new value k_3^* ($< k_3$), then we would obtain for the response

$$x = \frac{k_1 A}{k_2} = \textit{a constant, i.e., no change,}$$

and

$$y = \frac{k_1 A}{k_3}\left[1 - \frac{k_3 - k_3^*}{k_3}\, e^{-k_3^* t}\right].$$

The mRNA concentration simply rises monotonically from its initial level k_1A/k_3 to an increased level k_1A/k_3^*; there is no later return to the pre-exposure level.

The Rebound Effect

We close this section by noting the effect of switching off

the impressed field. Assuming that the effect of the electromagnetic field on the rate constant is reversible (which seems reasonable since we are considering relatively weak fields), then the task is to re-solve the differential equations for $t \geq t_0$ (the time at which the field is switched off) using k_2 rather than k_2^*. For simplicity we consider first the effect of turning off the field after the mRNA concentration has returned to its pre-irradiation equilibrium value. This is shown for $k_2^* = 30$ in Figure 7. Note the drop below the steady-state value immediately following the cessation of the irradiation; the concentration reaches a minimum, and then slowly return to its equilibrium value. The "rebound" is easily understood as resulting from the suddenly decreased rate of mRNA production ($k_2 < k_2^*$) coupled with the depleted population appropriately positioned nucleotides.

If the exogenous field is switched off at a time prior to the system's response returning to its pre-exposure level, then the effect is a sudden decrease in the system's response (the mRNA concentration) leading to an overshoot of the basal value, and finally a slow return to this equilibrium value. This is illustrated for two different "switch-off" times in Figure 8.

2. IMPLICATIONS OF THE MODEL FOR EXPERIMENTS

For a variety of reasons experiments are seldom carried out as a function of exposure duration. Even in those instances where time-dependent responses are measured, the data are usually confined to measurements made at rather widely separated times, and perhaps at only a few field strengths so that the actual character of the variation may not be apparent. In the paragraphs below, we consider a few examples of the difficulties that may be encountered.

A. Experimental Difficulties: Detecting Transient Responses

Generally experimental data on, for example, mRNA production are monitored neither continuously as a function of time after switching on the external field, nor are the measurements routinely carried on for very long times, it is quite possible that for the specific set of experimental parameters chosen for a given investigation that the "true" nature of the system's behavior might be missed. This is illustrated by considering the "data" shown in Figure 9. These data were created by using the same parameters as those that generated Figures 3 and 4, taking as the defining time unit $k_1 = 0.3\ hr^{-1}$ ($= 0.005\ min^{-1}$), and then assuming that measurements of mRNA concentration were made after exposure intervals of 10, 20 and 40 minutes. These "data" are plotted in Figure 9(a) for three external field strengths $E_0 = E_1$, E_2, and E_3 ($E_1 < E_2 < E_3$) corresponding to the three values of k_2^* used to generate Figure 4. No unifying theme is obvious in these plots: for the highest field, the data decrease monotonically; for the lowest field they

increase; and for the intermediate field strength they exhibit a maximum at t = 20 minutes. When the time = 0 point ($\delta y(0) = 0$) is added, and the set of curves computed from the model are superimposed, as in Figure 9(b), a coherent picture is seen to emerge. Of course, when the data are "real" laboratory measurements, there are no predetermined curves to superimpose on the results, and consequently the interpretation of the measurements is not nearly so straightforward. The point is that it is difficult (at best) to infer the correct nature of a transient biological response from a small set of isolated points measured over a limited time range.

B. Experimental Difficulties: Non-zero Quenching Times

Another factor complicating the measurements especially at the higher field strengths (larger k_2^* values) is the rapid fall in the system's response that occurs immediately after the sample is removed from the electromagnetic field (see Figure 8). To clarify the nature of this problem we consider a specific example.

Consider the "data" shown in Figure 9. If these had been real data, they would have been obtained by exposing a suitably prepared cell sample to the desired electromagnetic field (produced perhaps by a solenoid or a Helmholtz coil arrangement) with adequate provision being made to maintain the experimental system at the desired temperature, usually 37°. After exposure for the desired time, the sample is removed from the exposure chamber and is quenched--its temperature is quickly reduced to the neighborhood of 0°C--so that biological processes are thermally arrested. Suitable assays are then carried out to obtain the desired concentration values (or quantities that are proportional to them).

Suppose that samples are removed for assay after 5, 10, 20 and 40 minutes of electromagnetic field exposure. Further suppose that three minutes are required for quenching the samples; that is, for three minutes following their removal from the field, the mRNA levels decrease in the manner shown in Figure 8 because of the reduction in the polymerization rate from k_2^* to the original rate k_2. As a result of this the measured mRNA concentrations will differ from the "correct" values; this is shown in Table 1. The differences are in a range from about 10 to 15%, but the qualitative behavior of the data are unchanged. Also shown is a similar comparison obtained by assuming that one minute is required for quenching the samples. Here the differences are significantly less (only 3 to 5%) as would be expected.

If the first point (the five-minute point) is used to determine the initial slope of the response-versus-time curve, and then this is combined with Equation (8) to obtain Δk, one must be concerned both with the errors that are introduced due to non-zero quenching times and with the fact that the curves may not be linear at times as long as 5 minutes. For the examples discussed in this section with $k_2^* = 0.05$ and 0.15 min^{-1} ($k_1 = k_2 = 0.005$ min^{-1}

and $k_2 = 0.05\ min^{-1}$) the errors in Δk that would result from assuming linearity out to 5 minutes are of the order of 30 to 40%. As a specific case examine the data set corresponding to $k_2^* = 0.05\ min^{-1}$ ($\Delta k = 0.045\ min^{-1}$). The peak in the response-versus-time curve occurs at about t = 20 minutes. Assuming a linear increase and using Equation (8) one would calculate an increased mRNA concentration at 5 minutes of

$$y(t) = 0.100 + (0.045\ min^{-1})(5\ min) = 0.325$$

(all concentrations in reduced units, i.e. relative to $A \equiv 1$); the correct value is y(t) = 0.275. Using this would lead to a value of the slope, and thus of Δk, some 22% too low even with instantaneous quenching. For the finite (1- and 3-minute) quenching times illustrated in Table 2, the y(t) values of 0.266 and 0.248 increase these errors to 26% and 34%, respectively. Even for measurements made 2 minutes after switching on the field the errors would still be 10%, 16% and 28% for zero-, one- and three-minute quenching times respectively.

At lower field strengths, the situation is somewhat better. For $k_2^* = 0.015\ min^{-1}$ ($\Delta k = 0.010\ min^{-1}$, peak at about 35 minutes), the errors resulting from a five-minute measurement are 15%, 19%, and 28% for zero-, one-, and three-minute quenching times. For a two minute measurement the comparable errors are 6%, 13% and 26%. The message is simply that while (we feel) the multistep reaction model is a useful for the conceptualization and understanding of the responses to exogenous fields, as well as for guiding and designing experiments, experimental determinations of the model parameters are subject to quite large errors (as high as 30 to 40%) even without accounting for uncertainties in the data. These latter uncertainties may also lead to errors or this same order of magnitude.

C. The Relationship between k_2^* and the External Field Strength

In the sections above the appearance of a so-called power window was shown to follow from some elementary considerations regarding transient phenomena. These were embodied in the multistep reaction model discussed in the immediately preceding section providing that we assume a monotonically increasing relationship between the change in k_2 (or k_2^*) and the impressed field strength E_0. Examples of possible functional dependencies of Δk on E_0 that one might think about include

$$\Delta k \propto E_0, \qquad \Delta k \propto E_0^2, \qquad \textit{and} \qquad \Delta k \propto \exp(\mu E_0 / k_B T) - 1,$$

among others (in the last of these μ is a constant parameter, k_B is Boltzmann's constant, and T is the temperature). To determine the relationship between Δk and E_0 it is probably simplest to make use of Equation (8), which connects the initial slope of the response versus time curve to the change in k_2. We have already noted that neither y_{max} or t_{max} are simply related to k_2^*. Observe from Figure 4 that for large changes in k_2, i.e., large field strengths, these might well be very difficult measurements, in that data at rather short times would be required. For instance if the units of time axis in Figure 4 were assumed to be hours (the rate constants would then be measured in hours^{-1}), then, for the larger values of k_2^* or field strength, measurements would have to be made on time scales on the order of a few minutes. This is a very challenging experimental task, and it suggests that the dependence of Δk on E_0 can most effectively be determined by measurements made with relatively weak impressed fields. Of course the fields must be large enough that the system response (the increase in mRNA levels over the unexposed controls) can be accurately determined.

3. SOME SPECULATIVE IDEAS

A. Protein Synthesis

We can think about the effect of all this on the production of protein in the cytoplasm by recognizing that the rate of synthesis of a protein is proportional to the amount of its corresponding mRNA that is present. The increased amount of mRNA resulting from the EM field ($k_2^* > k_2$) means an enhanced rate of protein production. Designating the excess protein concentration by z, we can then write the governing differential equation as

$$dz/dt = K\delta y - \alpha z \qquad (10)$$

where K is the rate constant describing the protein production and α is the reciprocal lifetime describing the rate at which it is degraded. The solution to Equation (10) is straightforward:

$$z = K \frac{k_1 A}{k_3 - k_2^*} \frac{\Delta k}{k_2} \left[\frac{(e^{-k_2^* t} - e^{-\alpha t})}{\alpha - k_2^*} - \frac{(e^{-k_3 t} - e^{-\alpha t})}{\alpha - k_3} \right]. \qquad (11)$$

This is plotted--along with x(t) and y(t) from Equations (3) and (4)--in Figure 10 for the intermediate field value (i.e., $k_2^* = 10$) considered in Figures 3 - 5. Observe that the peak in excess protein concentration is delayed relative to the mRNA peak. This is significant in terms of the field's effect on the organism, as it is certainly the altered protein production that would be the controlling factor in this. Note also that the peak in the protein response is generally broader than that for mRNA.

B. Regulatory Feedback Effects

A central feature in the mathematical model presented in this paper as well as in the discussion is that of linearity. Once the rate constant k_2 is altered by the field, the subsequent behavior is prescriptively and predictively determined by a set of rate equations in which the governing rate parameters (k_1, k_2, k_3, K, α) are independent of the local concentrations (x, y, z) of the various species. This is, of course, not the situation at long times. Cells do indeed regulate the production of proteins by a rather complex set of biochemical "sense-and-feedback" mechanisms. Depending upon what precisely is sensed, the regulatory processes will operate in different ways to restore the basal levels.

Consider the situation reached depicted in Figure 10 at time = 0.8. At this point the mRNA concentration has returned to its basal level. However the nucleotide concentration, x, is not at its pre-exposure equilibrium level, being reduced by the ratio k_2^*/k_2. Suppose that the cell senses this low value and attempts to correct the deficiency by, for example, increasing the rate k_1 at which nucleotides are brought to the immediate vicinity of DNA. The effect would be to cause a second rise in the production of mRNA and also of its corresponding protein. This second rise might also trigger additional regulatory responses.

Alternatively suppose that it is the presence of excess protein that is sensed by the cell. Possible responses designed to eliminate the excess could include destabilizing the protein (increasing α) to hasten the degradation of the excess, or decreasing the protein production rate K. Alternatively, it is perhaps not inconceivable that the cellular response would be to effect an increase in k_3, the rate of mRNA degradation. This would have the desired effect of reducing the excess protein, but would also cause the mRNA to drop below its basal level to which it has returned by $t \approx 0.6$.

In the preceding few paragraphs, we have anticipated the likelihood that the simple linear model presented in this paper is incomplete. We would like to emphasize that a valuable feature of such a linear model is that it can provide a "baseline" against which to compare the results of experiments. From these paragraphs we see that by probing the directions and magnitude of the deviations from the linear model predictions one can hope to acquire insight into the cell's regulatory responses. For instance, we have suggested that one possibility is the cell's sensing a low value of x and reacting by increasing k_1 leading to a rise in mRNA levels. Comparing this with the possibility of the second rise in mRNA discussed in the preceding paragraph (in which an excess of protein causes an increase in k_3 and subsequently a fall in the mRNA level) suggests a class of experiments that might prove useful in probing the nature of cellular regulatory mechanisms.

Additional information might be available in this regard by exploiting the "rebound effect" that results when the field is switched off to examine the response to sub-equilibrium values of mRNA. Indeed one might find that, although the field has been switched off (at say time ≈ 0.6 in Figure 10), the delayed cellular regulatory processes might lead to "unexpected" time dependencies in the mRNA or protein concentrations that act to enhance or to offset the predicted variations.

4. MEASUREMENTS USING A RADIOACTIVE PRECURSORS

If a small amount of radioactive precursor, such as ^{3}H-uridine, is included in the nucleotide pool, then time dependent measurements of the nuclear activity of the RNA will yield a measure of RNA synthesis. In this section we examine a simple theoretical calculation that illuminates the specific character of that "measure of RNA synthesis" under a variety of conditions.

The specific time variation of the activity that is observed will, of course, depend on the time instant t_0 at which the radioactive precursor presented to the cells in relation to the instant (in this paper taken to be time = 0) at which the exogenous field is switched on. We consider the following situations:

(1) the ^{3}H-uridine is presented at times prior to t = 0 (including the remote past, i.e., $t_0 = -\infty$);

(2) the ^{3}H-uridine is presented simultaneously with the switching on of the field, at $t_0 = 0$; and

(3) the ^{3}H-uridine is presented at specific instants t_i (i = 1, 2, 3...) following the switching on of the field, and its incorporation is measured as a function of the time difference $\tau_i = t - t_i$.

As the model system on which to examine these cases we consider the linear multi-step chemical reaction model presented above. Here we shall assume that the simple three-step process is adequate for characterizing transcription, at least to the extent that it can serve as a useful "zeroeth-order" approximation in terms of which we can understand the usefulness of various measurement approaches. Initially we adopt the point of view that we are given a well-defined model system, and it is incumbent upon the experimenter employing various radiographic techniques to explain how these techniques produce data from which one could infer the characteristics of the system. This can also demonstrate why a given set of procedures is more or less effective in revealing the behavior. Secondarily, we shall comment on how one might interpret departures from the results that are predicted.

Suppose that at some instant t_0 the nucleotide pool is

"loaded" with a small concentration of radioactive precursor, i.e., ^{3}H-uridine. The concentration of the pool associated with the radioactive species is designated by A and those for the resulting radioactive products X and Y are denoted by x and y, respectively (definitions of the important symbols have been collected in Table 2). Since x can be produced only when A > 0, and y only when x > 0, it follows that for $t \leq t_0$, $x = y = 0$. For $t \geq t_0$, one has the governing differential equations:

$$d\tilde{x}/dt = + k_1\tilde{A} - k_2\tilde{x}; \qquad (12a)$$
$$dy/dt = + k_2x - k_3y \qquad (12b)$$

for $t \leq 0$. For $t \geq 0$, i.e., after the external field has been switched on, the rate constant k_2 must be replaced by k_2^*.

Note that the development in time of the concentrations of the labeled species x and y proceed independently of the variation in x and y. This is a consequence of the initial hypothesis that the dynamics are governed by a sequence of <u>linear</u> chemical reactions. That is, the reaction rate constants k_1, k_2, k_2^*, and k_3 are not functions of the concentrations x and y (or $\tilde{x}$ and $\tilde{y}$).

CASE I: $t_0 < 0$.

We examine the situation where the loading is done prior to the irradiation. We assume that the fraction of labeled precursor is so small, that the unlabeled precursor concentration A is unaffected. Then

$$x(t<0) = x_0 \quad \text{and} \quad y(t<0) = y_0.$$

The concentrations $\tilde{x}$ and $\tilde{y}$ will develop in time as governed by Eqs. (12). The solutions to these are

$$\tilde{x}(t) = \frac{k_1}{k_2}\tilde{A}\,[1 - e^{-k_2(t - t_0)}] \qquad (13)$$

and

$$\tilde{y}(t) = k_1\tilde{A}\,\{\frac{1}{k_3}[1 - e^{-k_3(t-t_0)}] - \frac{1}{k_3 - k_2}[e^{-k_2(t-t_0)} - e^{-k_3(t-t_0)}]\} \qquad (14)$$

for $t_0 \leq t \leq 0$. Observe that while both t_0 and t are negative the time factor $(t - t_0)$ appearing in the exponentials is positive. For times after the field has been switched on $(t \geq 0)$, the differential equations to be solved are the same as those in Eq. (6) with k_2^* replacing k_2. The initial conditions to be imposed are obtained by putting $t = 0$ in Eqs. (13) and (14):

$$\tilde{x}(0) = \tilde{x}_0 - \frac{k_1}{k_2}\tilde{A}\,[1 - e^{-k_2|t_0|}] \tag{15a}$$

and

$$\tilde{y}(0) = \tilde{y}_0 - k_1\tilde{A}\,\{\frac{1}{k_3}[1 - e^{-k_3|t_0|}] - \frac{1}{k_3 - k_2}[e^{-k_2|t_0|} - e^{-k_3|t_0|}]\}. \tag{15b}$$

The time evolution of the labeled species for $t \geq 0$ is then given by

$$\tilde{x}(t) = \tilde{x}_0\, e^{-k_2^* t} + \frac{k_1}{k_2^*}\,\tilde{A}\,(1 - e^{-k_2^* t}) \tag{16}$$

and

$$\tilde{y}(t) = \tilde{y}_0\, e^{-k_3 t} + k_1\tilde{A}\,[\frac{1}{k_3}(1 - e^{-k_3 t}) - \frac{k_1\tilde{A} - k_2^*\tilde{x}_0}{k_3 - k_2^*}(e^{-k_2^* t} - e^{-k_3 t})]. \tag{17}$$

The time dependence described by Eqs. (13)-(17) is plotted in Figure 11 for three values of the "presentation time" t_0. In fact what is plotted is the difference between the values of x and y calculated from Eqs. (13) - (17) and the "control results" which are obtained by putting $k_2^* = k_2$ in these equations. That is,

$$\Delta\tilde{y}(t) = \tilde{y}(t) - \tilde{y}_c(t),$$

where the subscript "c" denotes the control.

The effect of deceasing the interval between the presentation

of the labeled precursor and switching on the field is to reduce both the initial rate of growth and the maximum value of y while shifting the location of that maximum to longer times. That this is behavior that might be anticipated can be appreciated by noting that the growth in the labeled species [Y] following the application of the field is driven by the product $k_2^*x(0)$. When the interval $|t_0|$ is small, there has been little growth in x so that its value at $t = 0$ is small, and consequently the impetus for the growth of y is small. As $|t_0|$ is increased the value of x(0) approaches its steady-state saturation value of k_1A/k_2, and thus the bias for rapid growth of y is enhanced.

Two special cases are of interest. The first that in which the radioactive precursors are presented in the "remote past," i.e., the case for which $t_0 \rightarrow -\infty$. The second is the situation in which the radioactive precursor is presented simultaneously with the switching on of the exogenous field, i.e., $t_0 = 0$.

Labeled precursor presented in the remote past ($t_0 \rightarrow -\infty$). In this case the $t \rightarrow 0^-$ values of x and y are proportional to the equilibrium zero-field values of x and y. Moreover the values of x(t>0) and y(t>0) are proportional to--and are therefore a measure of--x(t) and y(t), respectively. The governing equations in this case for $t \geq 0$ are the same as Eqs. (3) an (4) with x, y and A replacing x, y and A, respectively. The time dependence is as presented in Fig. 1.

Labeled precursor presented at $t_0 = 0$. The governing equations are obtained by setting $t_0 = 0$ in Eqs. (13) and (14) and replacing k_2 by k_2^*. The results are

$$\tilde{x}(t) = \frac{k_1}{k_2^*}\tilde{A}\left(1 - e^{-k_2^* t}\right) \tag{18}$$

and

$$\tilde{y}(t) = k_1\tilde{A}\left[\frac{1}{k_3}\left(1 - e^{-k_3 t}\right) - \frac{1}{k_3 - k_2^*}\left(e^{-k_2^* t} - e^{-k_3 t}\right)\right]. \tag{19}$$

The time-dependent behavior is shown in Figure 12 where, as in Figure 11, the behavior of the control ($k_2^* = k_2$) has been subtracted, i.e., $\Delta y(t)$ has been plotted. Observe that the behavior simply represents a continuation of the trend that is evident in Figure 11: for $t_0 \leq 0$, reducing $|t_0|$ causes the maximum in the Δy versus t curve to be both less pronounced and shifted to later times.

CASE II: $t_0 > 0$.

In this section we examine two specific cases. In both the field is switched on at time = 0. In the first case the labeled precursor is presented at time $t_0 > 0$, and the time evolution of y is considered as a function of $\tau = t - t_0$. In the second case precursors are presented to <u>different but identically treated samples</u> at a series of time instants t_i ($i = 1, 2, 3...$) and the behavior of y is examined at a fixed interval τ_0 after this. The dependence of y on t_i is considered.

<u>**Labeled precursor presented at $t_0 > 0$.**</u> Clearly

$$\tilde{x}(t<t_0) = \tilde{y}(t<t_0) = 0.$$

The equations for $\tilde{x}$ and $\tilde{y}$ for $t \geq t_0$ are obtained by replacing k_2 by k_2^* in Equations (13) and (14). The resulting formulas are

$$\tilde{x}(t) = \frac{k_1}{k_2^*} \tilde{A} \left[1 - e^{-k_2^*(t - t_0)}\right] \tag{20}$$

and

$$\tilde{y}(t) = k_1 \tilde{A} \left\{\frac{1}{k_3}\left[1 - e^{-k_3(t-t_0)}\right] - \frac{1}{k_3 - k_2^*}\left[e^{-k_2^*(t-t_0)} - e^{-k_3(t-t_0)}\right]\right\} \tag{21}$$

These are graphed in Figure 12 for two different values of $t_0 > 0$. The results are clear. As compared with the $t_0 = 0$ behavior, the initial rise in Δy, indeed the entire curve, is simply delayed for a time interval t_0. The shape of the curve is unchanged. Phrased another way, the time variation of Δy is a function only of the <u>**difference**</u> $t - t_0$ (for $t_0 > 0$).

<u>**Labeled precursor presented at $t_i > 0$ ($i = 1, 2, 3...$).**</u>

Clearly, for any of the presentation times t_i the values of $x(t \geq t_i)$ and $y(t \geq t_i)$ are given by Eqs. (20) and (21) with t_0 replaced by t_i. If we were then to denote the intervals by

$$\tau_i \equiv t - t_i,$$

then the formulas are

$$\tilde{x}(t \geq t_i) = \frac{k_1}{k_2^*} \tilde{A} \left[1 - e^{-k_2^* \tau_i}\right] \tag{22}$$

and

$$\bar{y}(t \geq t_i) = k_1 \tilde{A} \left\{ \frac{1}{k_3} [1 - e^{-k_3 \tau_i}] - \frac{1}{k_3 - k_2^*} [e^{-k_2^* \tau_i} - e^{-k_3 \tau_i}] \right\} \quad (23)$$

From these and, as was said in the paragraph immediately following Eq. (21), $\bar{y}(t)$ and $\Delta\bar{y}(t)$ depend only on the interval τ_i following the presentation of the labeled precursor, and <u>not</u> on the actual time of presentation.

> The implication is that if measurements are made at a fixed time interval τ following presentations (on different samples) at time instants t_i ($i = 1,2,3 \ldots$), the measured response $\bar{y}(t)$ or $\Delta\bar{y}(t)$ will yield a constant <u>when considered as function of t_i</u>. The value of this constant depends only upon the length of the interval τ.

This is illustrated in Figure 13 for two different values of the labeled precursor interval τ. At least for the linear model considered here this "pulse technique" of measurement yields no information about the dynamics of RNA production during exposure to an external electromagnetic field.

If one were to observe a dependence on the instant at which the precursor was presented (for a fixed τ), then this would have to be interpreted as resulting from the type of non-linear "sense-and-feedback" effects discussed in Section III, Part B of this Chapter.

5. SUMMARY

The main results of this work include the following:

(1) the demonstration that transient response to EM fields can lead to apparent power windows;

(2) the description of a multi-step reaction model that predicts transient behavior and power windows if one assumes that

  (a) switching on the field causes a sudden increase in an intermediate reaction rate, and

  (b) the change in the reaction rate increases with the strength of the EM field;

(3) the prediction that switching off the field leads to a "rebound effect" in which the mRNA levels drop below the

basal levels;

(4) the recognition that these predictions imply that certain precautions must be taken to avoid significant errors in experimentally determining the model parameters;

(5) the suggestion that deviations from the model predictions provide a useful probe for attempting to gain insight into the nature of cellular regulatory mechanisms;

(6) the demonstration that measurements of the time dependence of RNA production using a radioactive precursor technique depend sensitively on the time interval prior to switching on the field at which the labeled precursor is presented;

(7) the demonstration that if the precursor is presented after the switching on of the field, the measured change in labeled RNA production depends only on the time interval after the labeled precursor was presented; and

(8) the demonstration that if a linear description of mRNA production is adequate, this "pulse labeling technique" of measurement yields no information about the dynamics of mRNA production during exposure to an external electromagnetic field. Alternatively, we may say that the technique, since it is completely insensitive to linear features of the response, reveals only those nonlinear aspects of the system behavior.

Table 1. The Effect of "Slow" Quenching

Exposure Time (min)	Strong Field ($k_2^* = 0.15$)*		Weak Field ($k_2^* = 0.05$)*	
	"Measured" [mRNA]	"Actual" [mRNA]	"Measured" [mRNA]	"Actual" [mRNA]
	Three Minute Quenching			
5	0.475	0.544	0.248	0.275
10	0.568	0.656	0.330	0.373
20	0.484	0.561	0.377	0.431
40	0.253	0.293	0.299	0.344
	One Minute Quenching			
5	0.520	0.544	0.266	0.275
10	0.635	0.656	0.358	0.373
20	0.534	0.561	0.412	0.431
40	0.279	0.293	0.328	0.344

* The value of k_2^* is given here in units of min^{-1}. These are related to the reduced unit values of k_2^* by taking $k_1 = 0.005\ min^{-1} = 0.3\ hr^{-1}$. Given here are results for $k_2^* = 30\ k_1$ and $k_2^* = 10\ k_1$, with $k_2 = k_1$ and $k_3 = 10\ k_1$.

Table 2. Definition of Symbols

Symbol	Definition
A	Nucleotide pool concentration (constant)
k_1	Rate constant for A → X reaction
k_2	Rate constant for X → Y reaction with no exogenous field
k_2^*	Rate constant for X → Y reaction with exogenous field switched on
k_3	Rate constant for degradation of Y
t	Time variable; at t = 0 the exogenous field is switched on
t_0	Time at which the radioactively labeled precursor is introduced into the nucleotide pool
τ	$t - t_0$, time after the introduction of the radioactive precursor
x, y	Time dependent concentrations of species X and Y
x_0, y_0	Zero-field equilibrium concentrations of X and Y
$\tilde{x}$, $\tilde{y}$, $\tilde{A}$	Time dependent concentrations of radioactively labeled species X, Y and A
Δy	Difference between y (in the presence of an exogenous field) and the control
Δk	$k_2 - k_2^*$, field-induced change in k_2

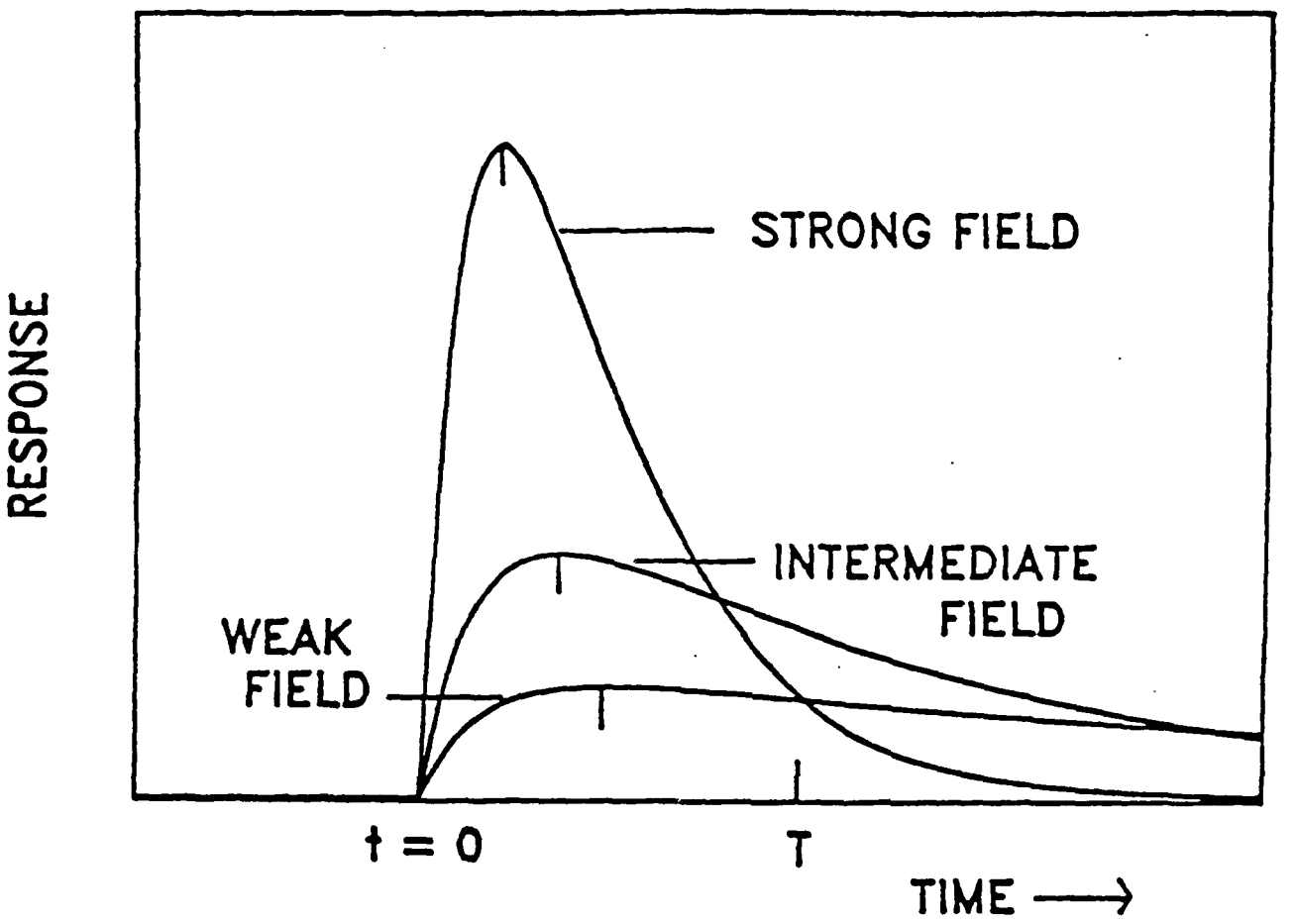

Figure 1. The schematic representation of a transient response by a system to three different electromagnetic field exposure levels switched on at time t = 0.

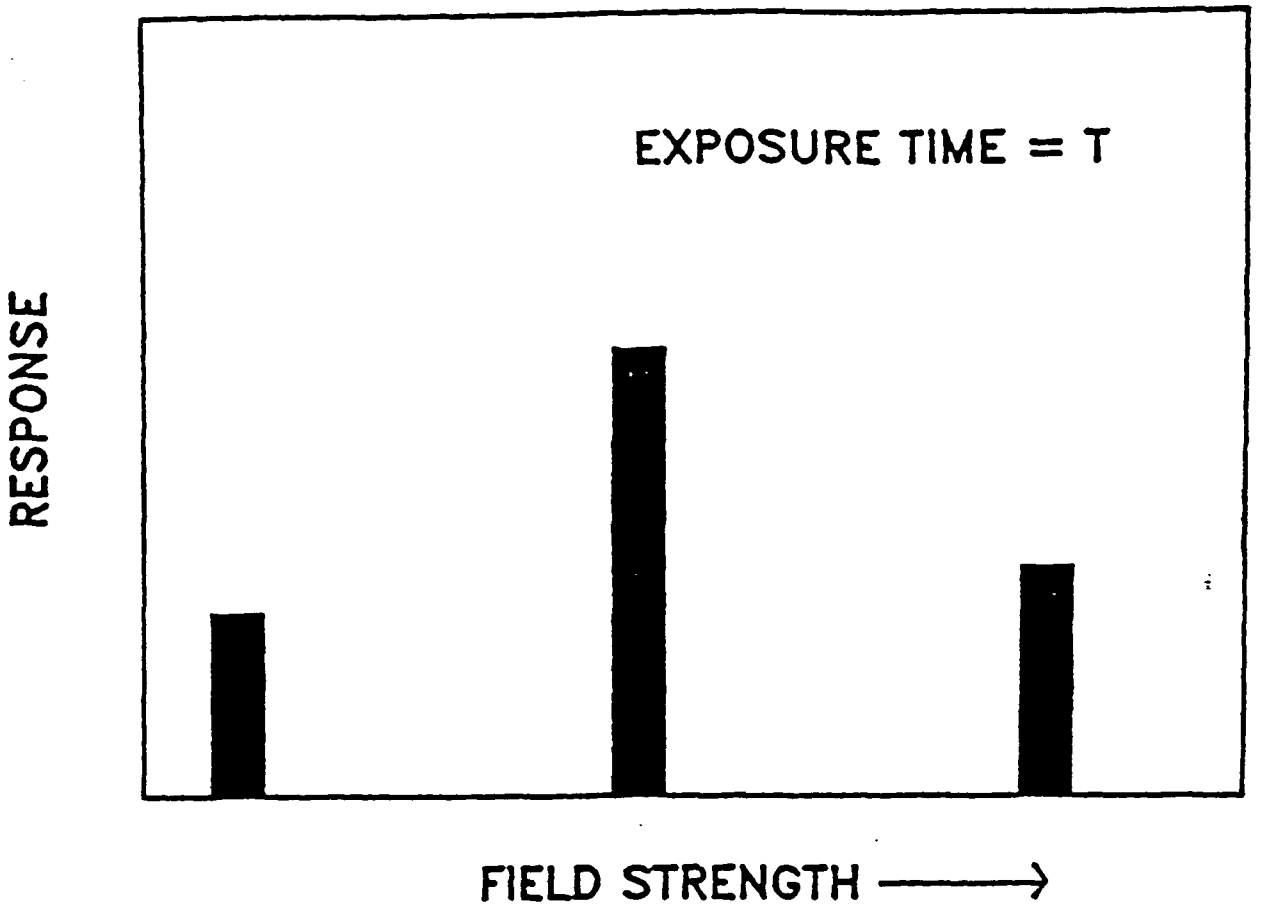

Figure 2. The schematic representation of an apparent power window resulting from observing the system's response only for a fixed exposure time T in Figure 1.

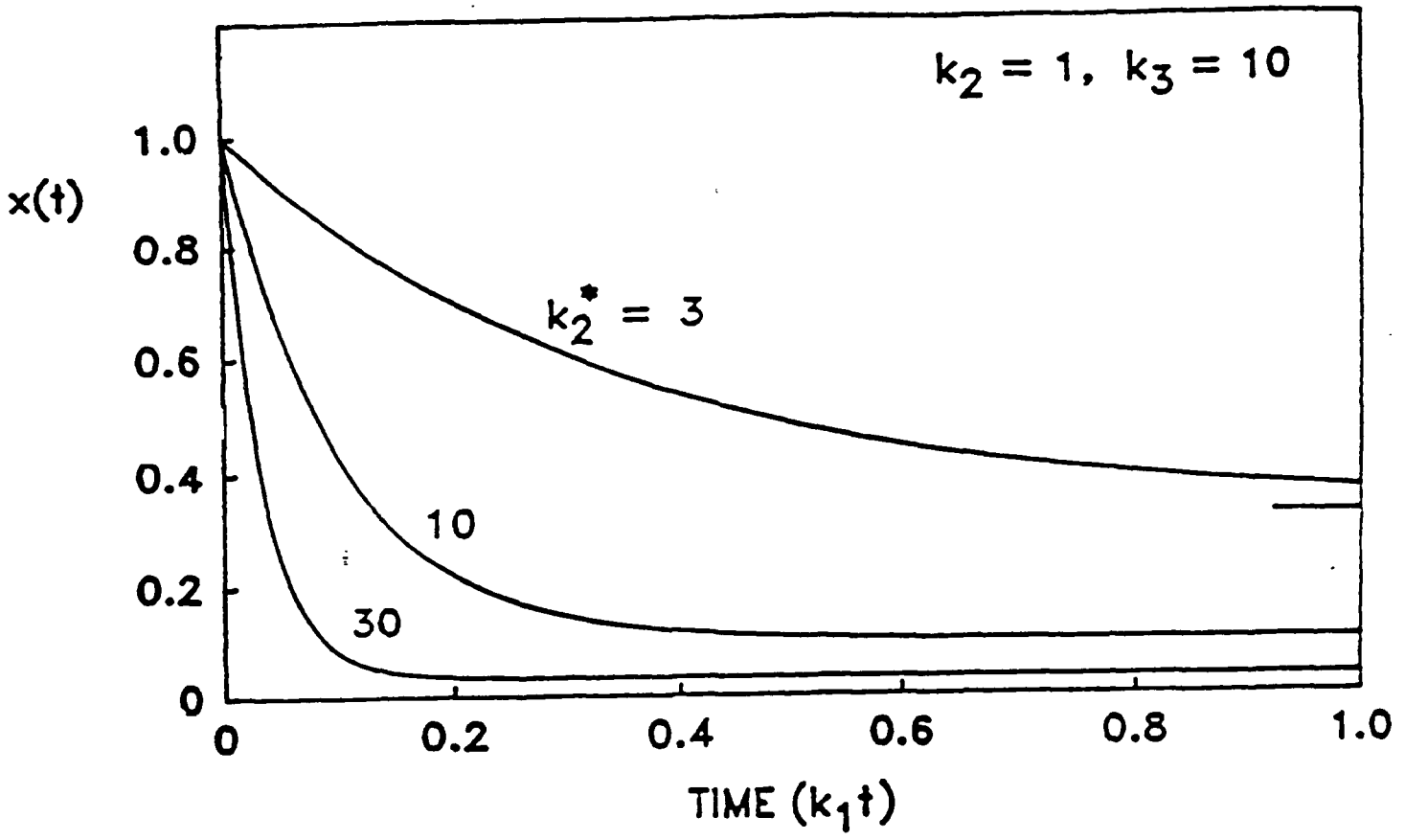

Figure 3. The prediction of the multistep model for the time evolution of the concentration x(t) following the switching on of the exogenous electromagnetic field at time = 0. The curves are calculated from Equation (3) for the three values of k_2^* shown.

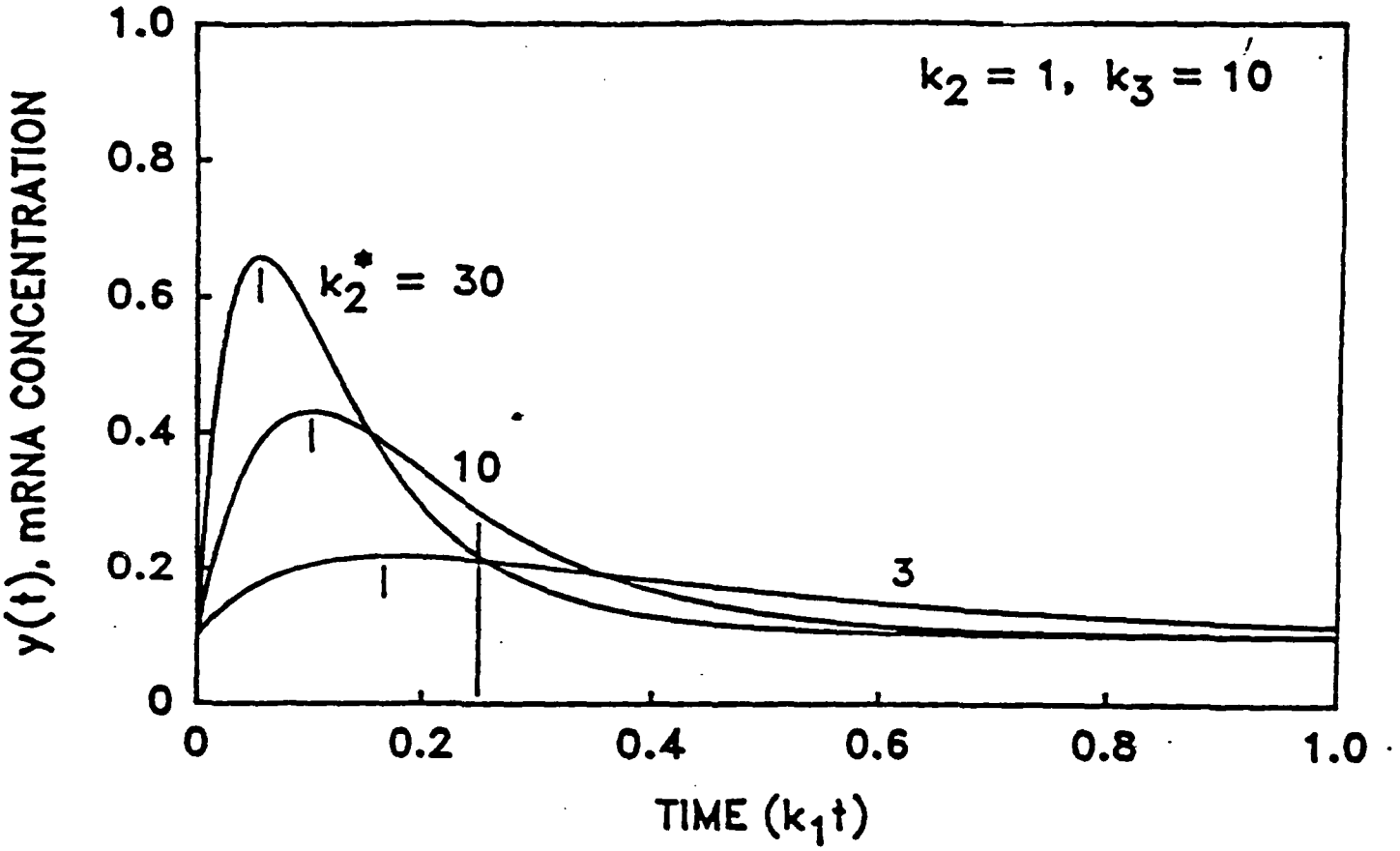

Figure 4. The prediction of the multistep model for the time evolution of the concentration y(t) following the switching on of the exogenous electromagnetic field at time = 0. The curves are calculated from Equation (3) for the three values of k_2^* shown.

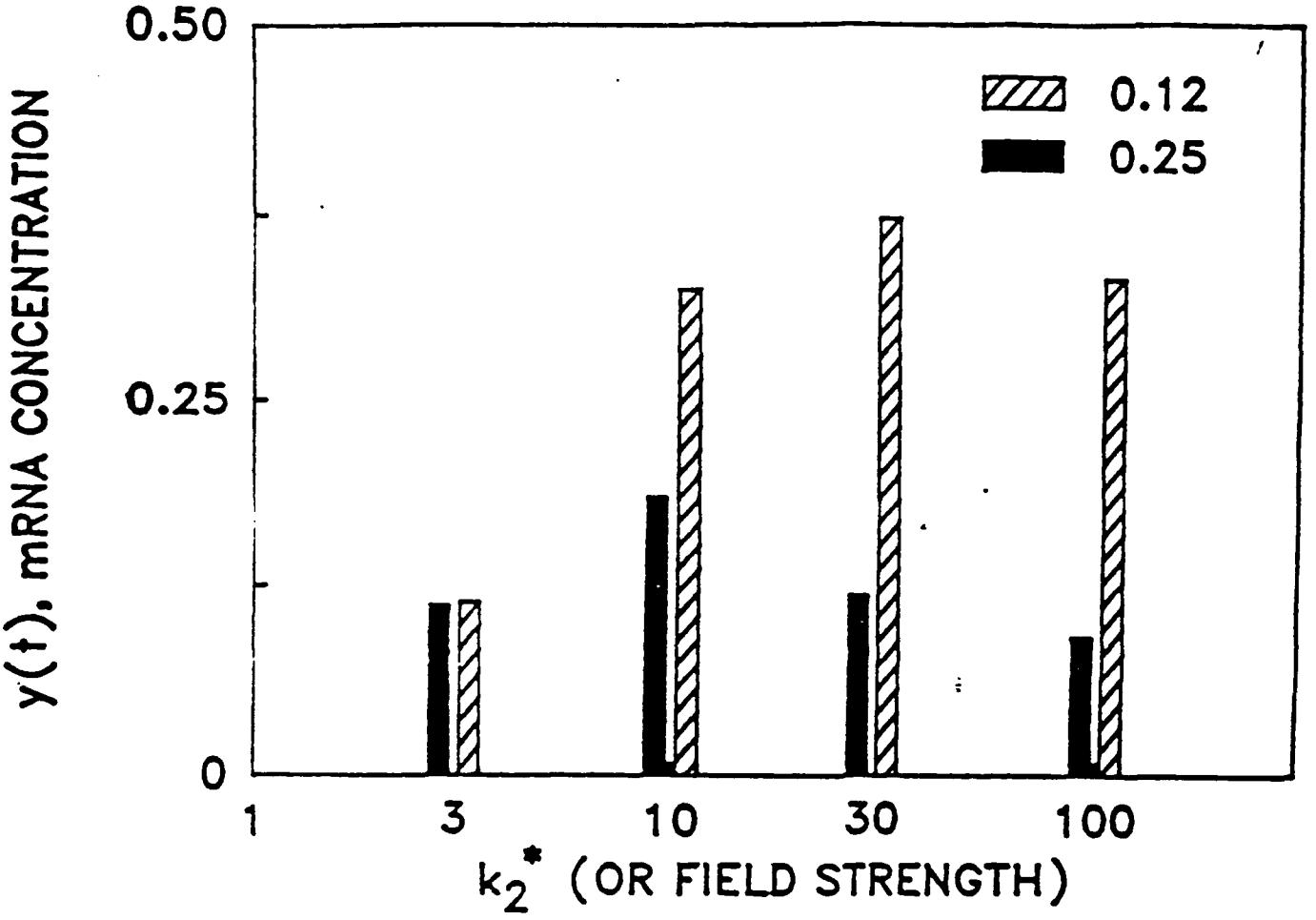

Figure 5. The resulting power windows that result from observing the response shown in Figure 4 as a function of field strength (k_2^*) for two fixed exposure times: $k_1t = 0.12$ and $k_1t = 0.25$.

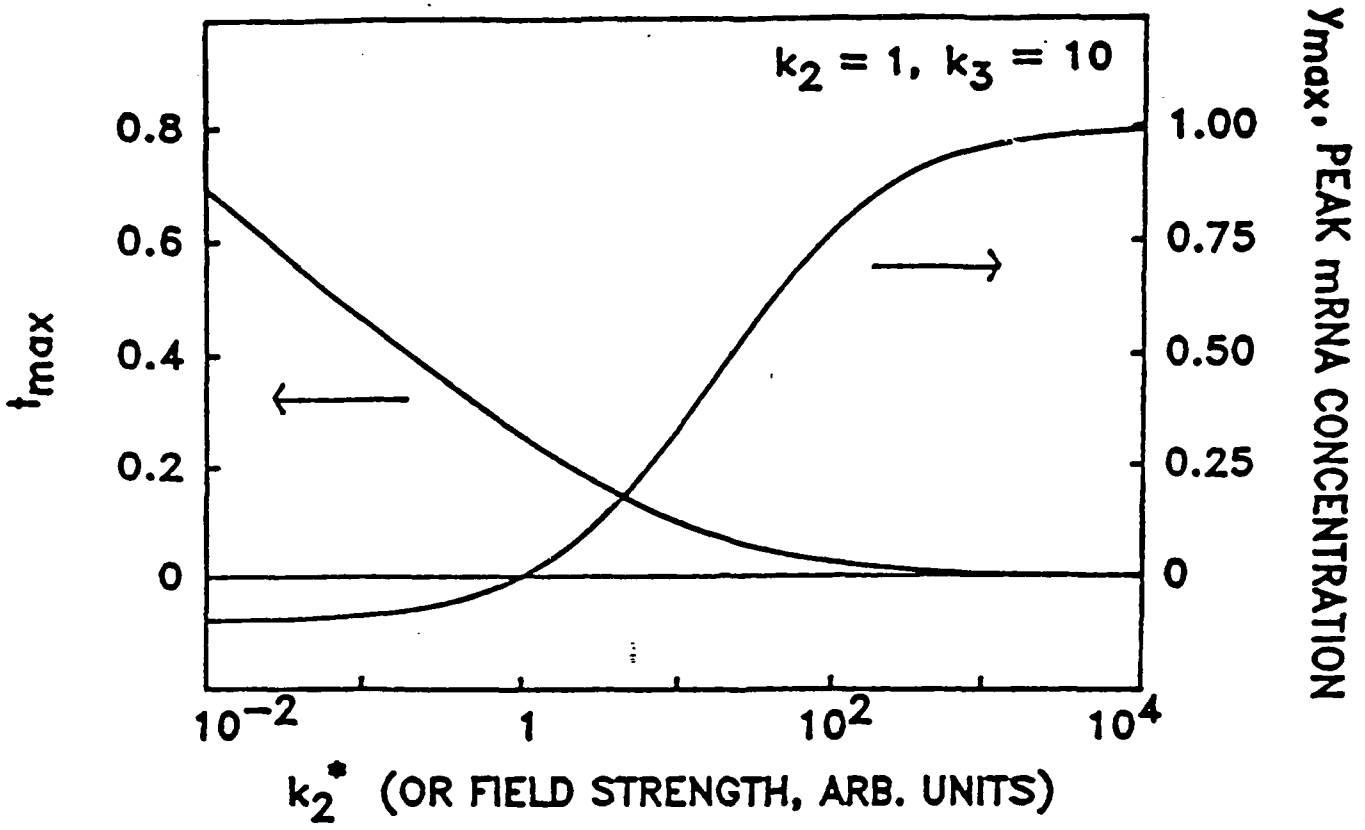

Figure 6. The dependence on field strength (or k_2^*) of the location in time (left scale) of the peak value of $y(t)$, i.e., t_{max} and the variation of the magnitude of the peak value $y_{max} = y(t_{max})$ (right scale) with field strength.

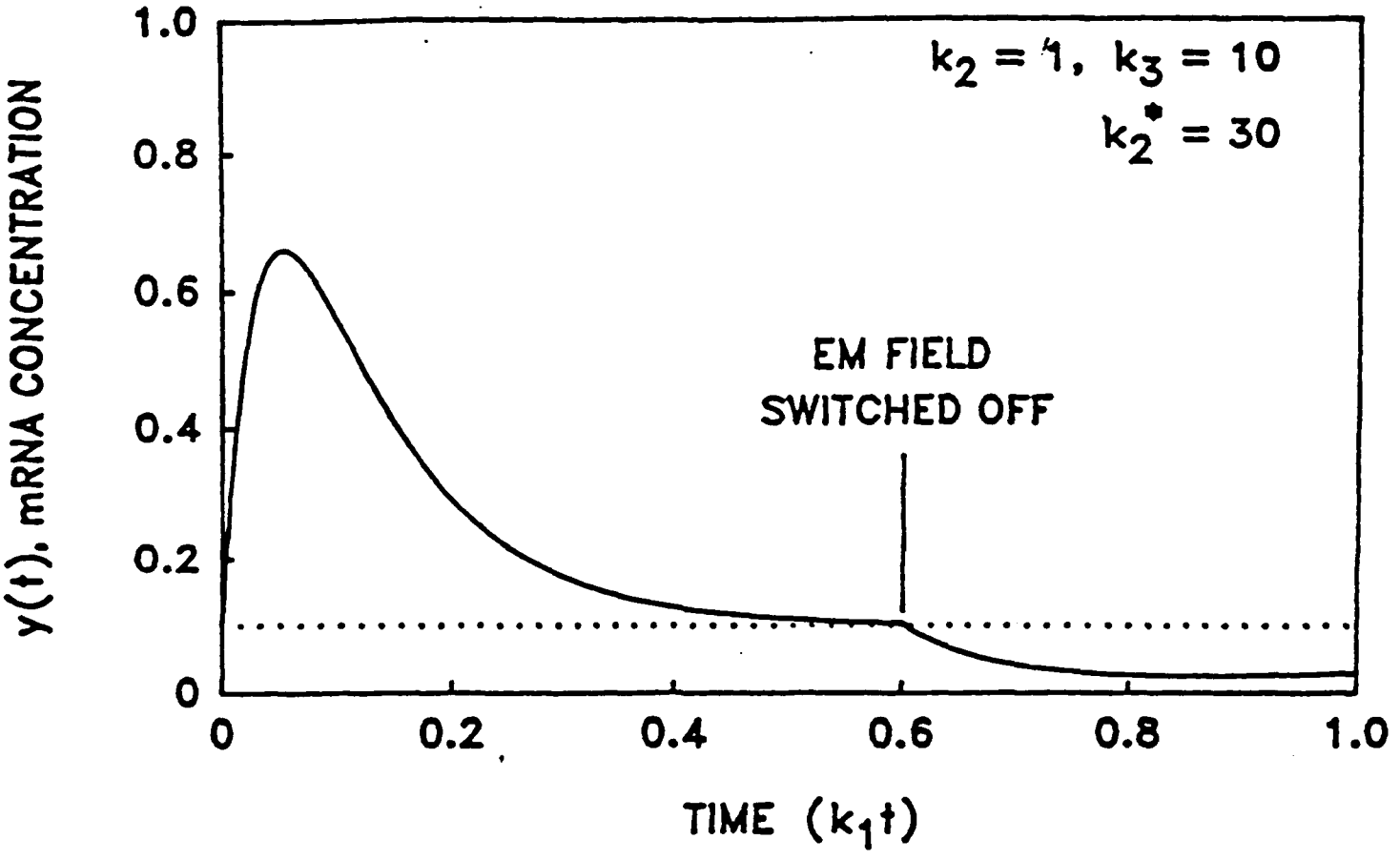

Figure 7. The time dependence of the concentration y(t) for exposure conditions in which the EM field is switched on at time = 0 and off at time = 0.6 (after y has returned to its basal level). At long times (not shown) the "rebound effect" vanishes as the concentration returns to its equilibrium pre-exposure value, here 0.1.

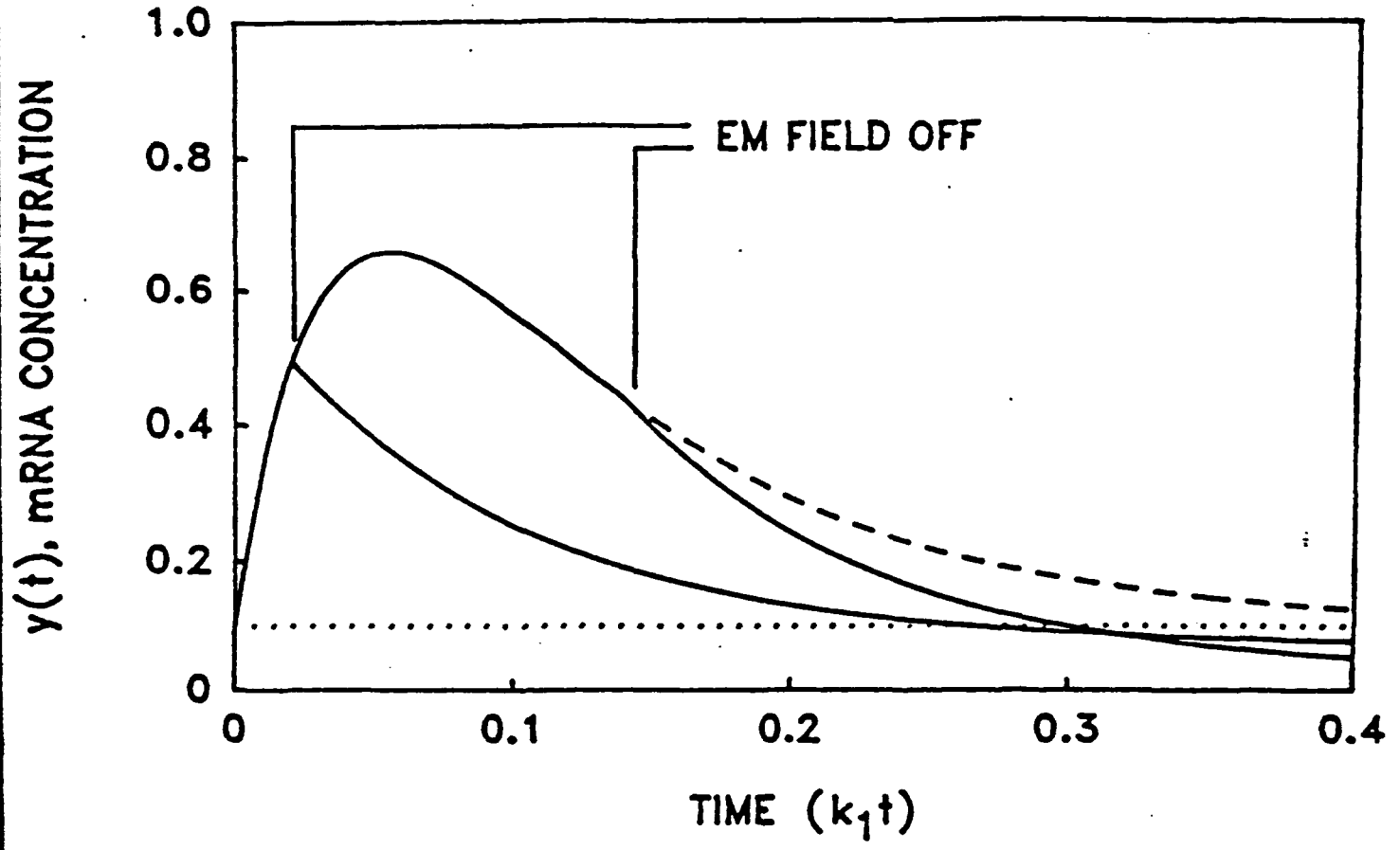

Figure 8. The time dependence of the concentration of y(t) for exposure conditions under which the EM field is switched on at time = 0 and off at two different times (0.03 and 0.14) during the transient response period. The broken curve illustrates the behavior when the field is allowed to remain on. All curves return to the equilibrium level of 0.1 at long times.

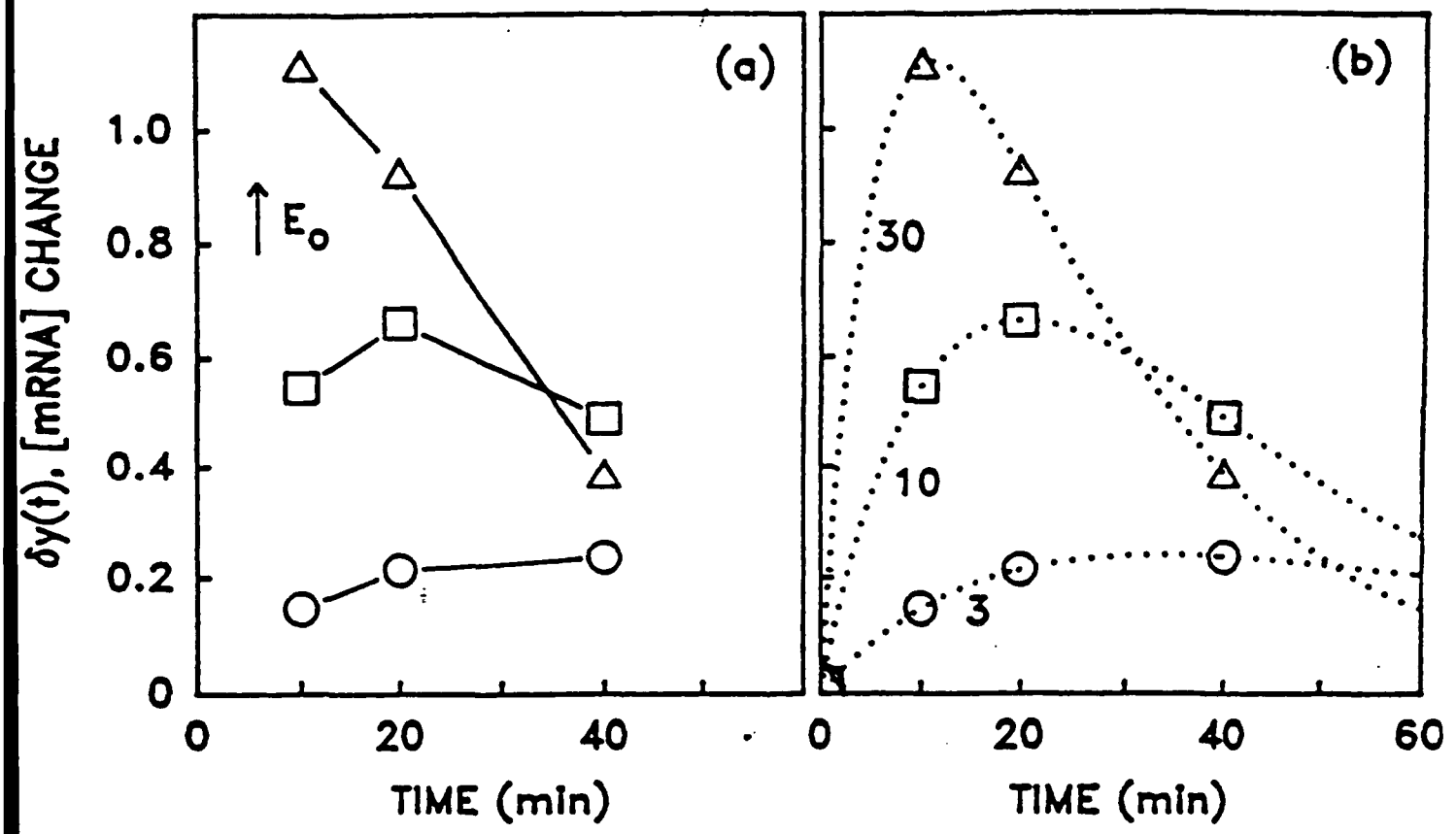

Figure 9. (a) "Data" on the deviation of y from its equilibrium value obtained from evaluating Equation (4) at times of 10, 20 and 40 minutes assuming $k_1 = 0.005\ min^{-1}$ and other parameters as shown in Figure 4. The circles, squares and triangles represent values of $k_2^*/k_1 = 3$, 10 and 30 respectively. (b) The same data with the time = 0 data points and the full curves shown in Figure 4 added.

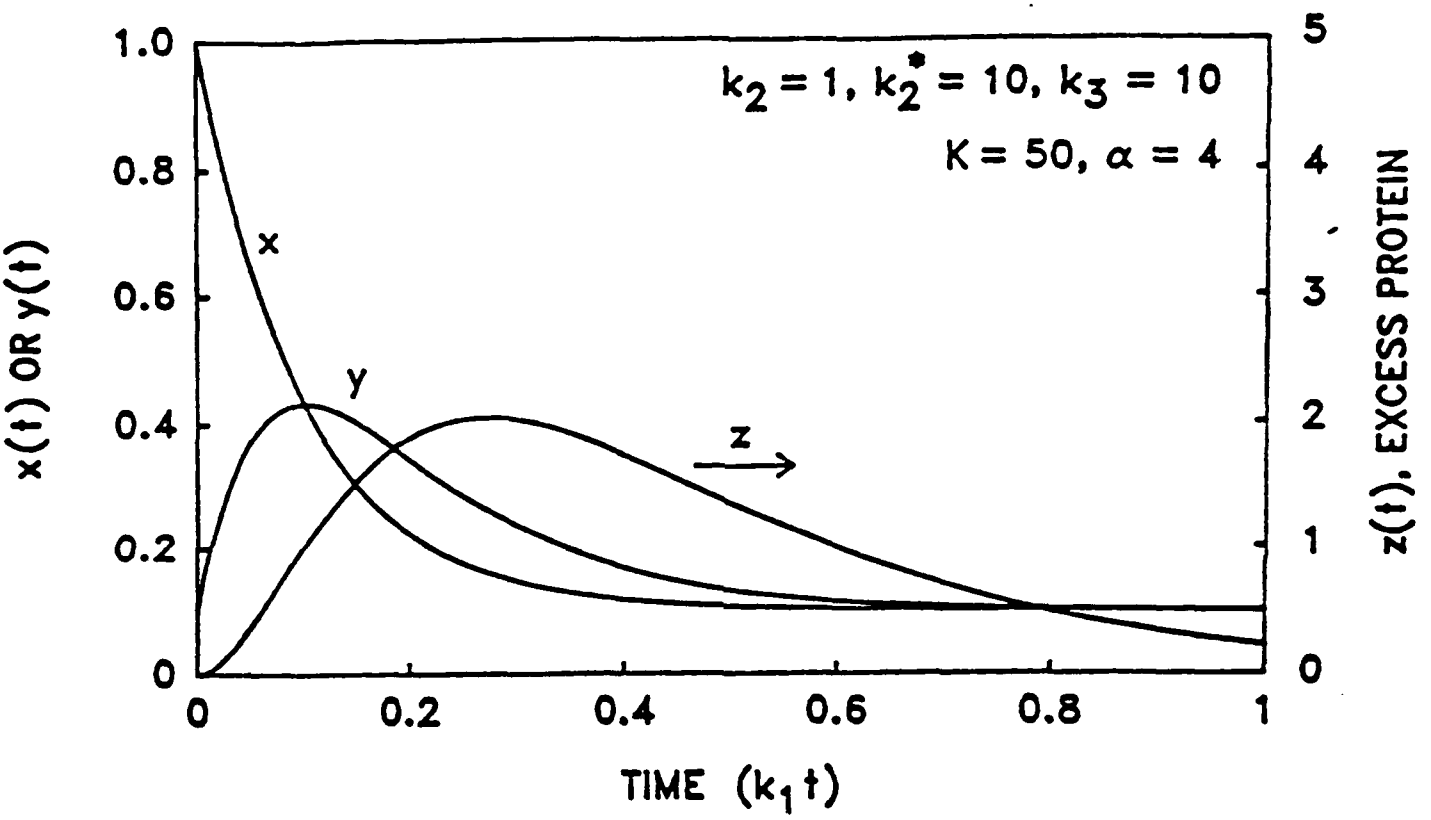

Figure 10. The time variation of the excess protein, z(t) (right side scale), calculated using Equation (11), for an EM field exposure switched on at time = 0 (note that reduced units are used). The time evolution of x(t) and y(t) (left side scale) for the same conditions are shown for comparison.

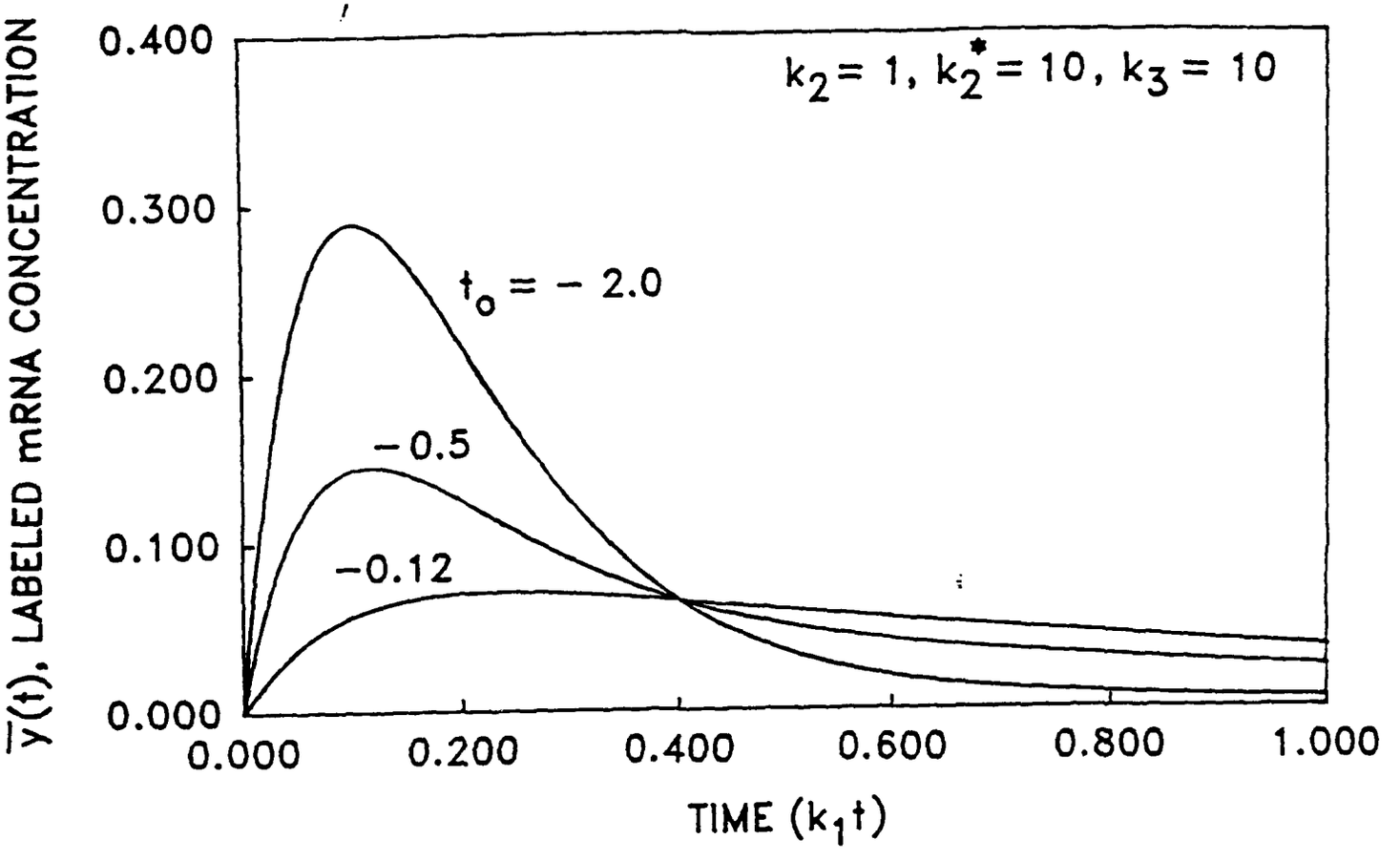

Figure 11. The time variation of the radioactively labeled mRNA following the switching on of the exogenous field at time = 0. The control (zero-field) values have been subtracted out, and the results are for three different instants ($t_0 < 0$) at which the labeled precursors are presented.

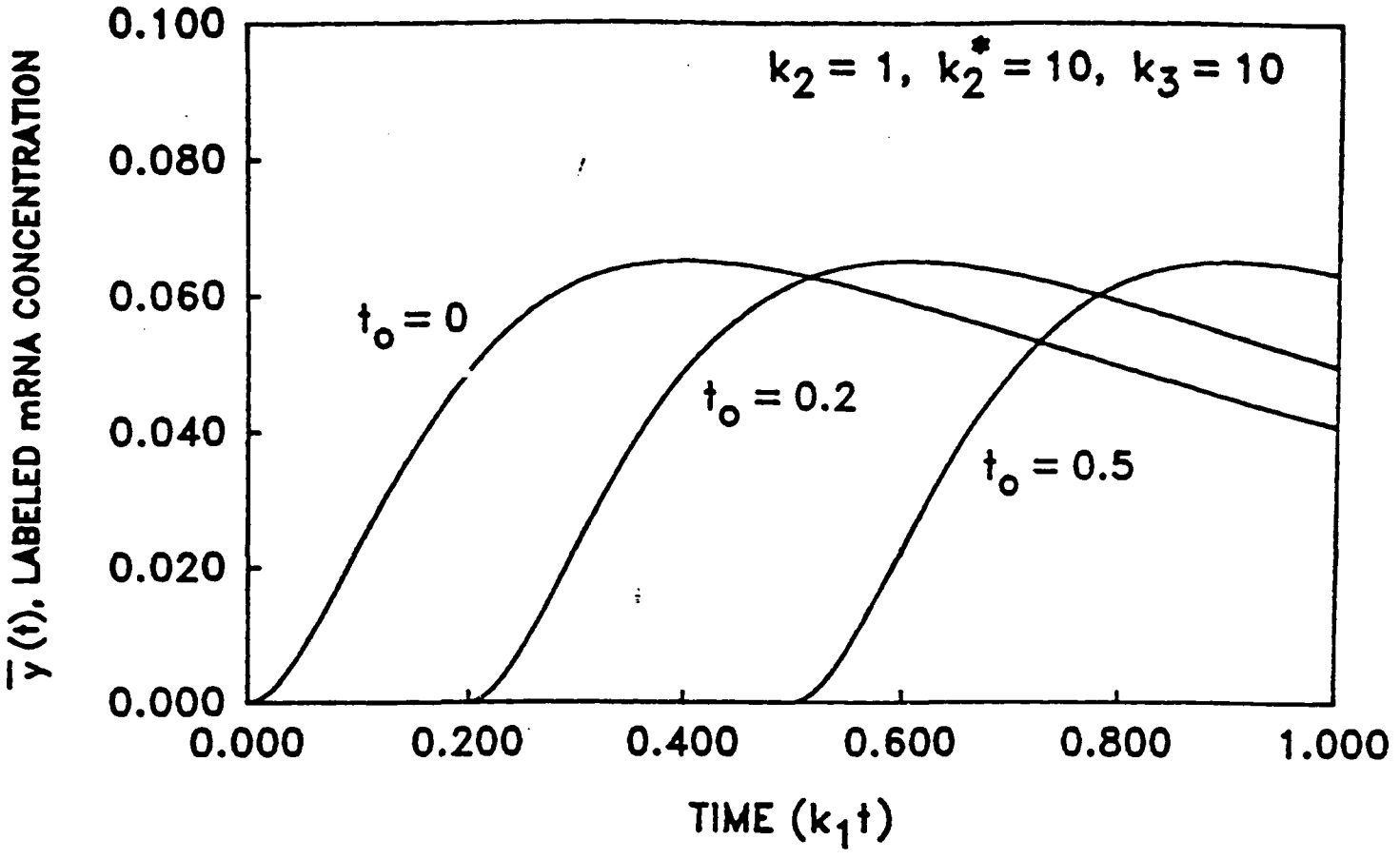

Figure 12. The time variation of the radioactively labeled mRNA following the switching on of the exogenous field at time = 0. The control (zero-field) values have been subtracted out, and the results are for three different instants ($t_0 \geq 0$) at which the labeled precursors are presented.

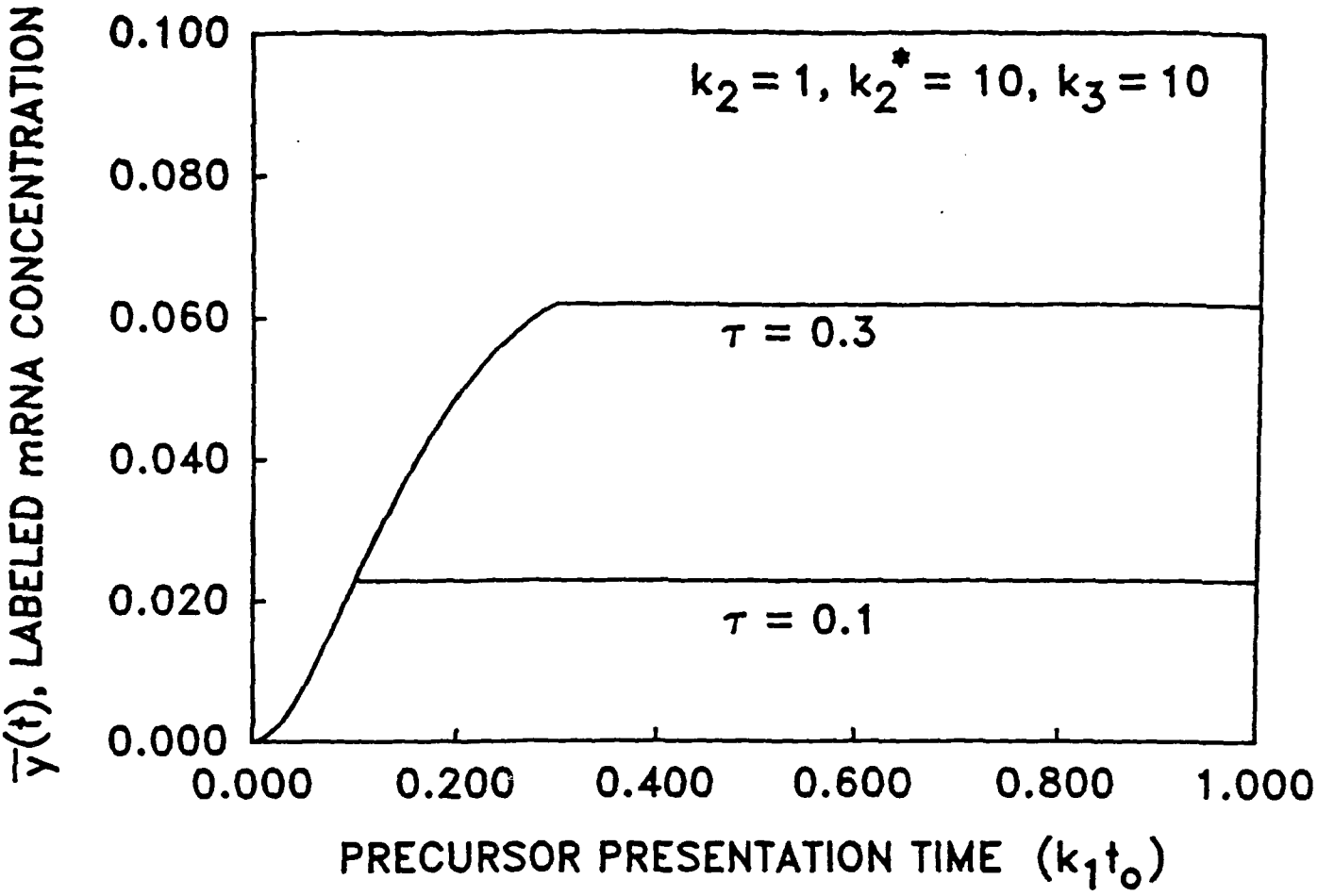

Figure 13. The variation of the radioactively labeled mRNA as a function of the time instant t_0 at which the radioactively labeled precursor is presented. The external field is switched on at time = 0. The control (zero-field) values have been subtracted out, and the results are for two different presentation intervals τ.

REFERENCES

1. R. Goodman, C. A. L. Bassett and A. S. Henderson, "Pulsing electromagnetic fields induce cellular transcription," Science 22: 128-1285 (1983).

2. R. Goodman and A. S. Henderson, "Sine waves enhance cellular transcription," Bioelectromagnetics 7: 23-29 (1986).

3. R. Goodman, L-X. Wei, J-C. Xu, and A. S. Henderson, "Relationship of transcript quantity to signal amplitudes," paper presented at the Eleventh Annual Meeting of the Bioelectromagnetics Society, Tucson, AZ, June 18-22, 1989.

4. R. Goodman, L-X. Wei, J-C. Xu, and A. S. Henderson, "Exposure of human cells to electromagnetic fields," (to be published).

5. C. F. Blackman, L. S. Kinney, D. E. House and W. T. Joines, "Multiple power-density windows and their possible origin," Biolelectromagnetics 10: 115-128 (1989). See also the references cited in this paper's "Introduction."

CHAPTER II

SPECTROSCOPIC STUDIES

The Dynamical Response of DNA Solutions: the Motion of Condensed and Diffuse Counter-ions

1. Introduction to Dielectric and Optical Measurements

This report summarizes the third year of a study of microwave interactions with DNA molecules. DNA plays a key role in determining and controlling the storage and transmission of genetic information. It also provides information for protein production and participates in many metabolic processes. For these reasons it is a likely material to suspect for involvement in any nonthermal effects of electromagnetic radiation. To understand any such effects it is essential that the nature of the interaction of this radiation with DNA be explored and understood in detail. We have been using two different experimental approaches to examine DNA at microwave and near microwave frequencies. These approaches are dielectric and optical spectroscopy both of which can yield information about the dynamics of DNA at frequencies in the microwave range.

A. Dielectric Measurements

Since the magnetic permittivity of DNA solutions is essentially a constant, the interaction with electromagnetic fields is described by the frequency dependent complex dielectric constant. The dielectric properties have been examined in numerous studies since the 1940's and several review papers exist which summarize the results for DNA specifically and more generally for DNA as one of the naturally occurring polyelectrolytes[6,7]. One of the best and perhaps the most critical of these reviews is by Mandel[8]. From his review one can conclude that much remains to be done in this field. Both theoretical and experimental difficulties are abundant. The result is that theoretical treatments exist only under simplifying assumptions which are not consistent with most of the experiments or are semiempirical in nature. On the experimental side only sketchy data is available from experiments which are often poorly described in the literature. He concludes that studies are needed which systematically vary such parameters as polyelectrolyte (DNA) concentration and molecular weight, counterion type and charge, concentration of added salts and temperature. Despite these criticisms we can still make some general remarks concerning the experimental observations that have been previously reported and the requirements they make on theoretical predictions.

The dielectric behavior is characterized by the existence of

dispersions in three frequency ranges. These dispersions are sometimes called the α, δ and τ dispersions[9]. The first two of these are generally agreed to be due to the DNA and its counterions. The last is due to the perturbation of the dielectric behavior of water caused by the presence of DNA.

For highly polymerized DNA the α dispersion occurs primarily in the region below 1 kHz but its high frequency tail can be observed above 1 MHz. It is responsible for a large (often > 1000 dielectric units) dielectric increment which depends on the size of the DNA molecule examined as well as its concentration and on the type of counterions in the solution. A major experimental difficulty in this region is due to electrode polarization which increases in severity with solution conductivity. The phenomenon increases the apparent dielectric increment and requires elaborate correction schemes and or complicated measuring cell designs to minimize its effects. Several theoretical treatments that have been applied to this dispersion although crude do predict semiquantitatively the length dependence of the magnitude of the dielectric increment and of the relaxation time. As stated above a series of carefully controlled experiments in which a variety of parameters are systematically varied is required to clarify the experimental situation and to test the applicable theories.

The τ relaxation occurs above 1 gHz and is due primarily to water which is the usual solvent for DNA solutions. The presence of DNA may cause some minor shifts in the spectrum relative to pure water due to the fraction of water molecules characterized as bound water or to minor effects on unbound water molecules. This region has been briefly studied and is thought to be reasonably well understood, at least in a qualitative way, as a perturbation of the normal water relaxation[10]. The perturbation is small however and very careful studies will be required to fully characterize it.

The δ relaxation appears as a relatively small, broad dispersion in the frequency range 1 MHz to 1 gHz. There have been several reports of its existence[5,11] but none of the measurements were sufficiently detailed to permit the assignment of a mechanism with a high degree of certainty. Polar groups, the Maxwell-Wagner effect, bound water and counterion fluctuations have been suggested as sources of the dispersion.

It is this δ dispersion region which has been the major subject of the PhD thesis research of Babak Saif, a graduate student in our laboratory. For DNA solutions of similar DNA concentration he studied the effect of varying the ionic strength of his solutions. To do this he measured the low frequency conductivity, and the dielectric and conductivity increments relative to the bulk solvent from 1 MHz to 1 gHz as a function of ionic strength. His results appear to characterize the dispersion sufficiently to allow quantitative comparisons between these results and those models sufficiently developed to allow that

comparison. The models proposed by Mandel[12] and by Manning[13] relating the dispersion to motions in the counterion layer surrounding DNA appear to explain both the real and imaginary parts of the dielectric relaxation. A complete explanation of the effective time constant for the phenomenon remains to be made, however. An important result of this analysis is that the local concentration of ions and thus the conductivity near the DNA can be relatively high compared to the bulk of the solution. This results in a disproportionately high absorption of electromagnetic energy near the DNA. This high energy absorption may in turn have some effect on the manner in which DNA functions.

B. Optical Spectroscopy Measurements

Although it is predicted that the upper limit for biologically significant modes in DNA is about 250 cm^{-1} it is only recently that the frequency range below this value has seen much attention. Urabe and coworkers[14] and Lindsay and coworkers[15] have examined both Raman and Brillouin scattering in this frequency range. They have had some success in characterizing the coupling of the DNA modes with its solvent and have observed the effects of different counterions.

The lowest Raman mode examined was near 20 cm^{-1} (60 gHz). This mode has been observed in solid DNA[10] and in highly concentrated gels[9]. The assignment of this mode is tentatively as an interhelical mode which is modified by interactions between DNA and its surrounding solution. The mode may be a shearing mode of adjacent helices[16]. Recent theoretical work suggests several other possible explanations[17]. More experimental work is required to fully determine the nature of the mode.

Our work in this area has thus far only been preparatory. We purchased a high resolution, high contrast monochromator from Sopra in France. It was received in January of 1989. This instrument should allow us to look for possible modes closer than the mode discussed above. In principle the instrument will permit us to look for modes with frequencies corresponding to the microwave region to 10 gHz and perhaps below.

2. Experimental methods - Dielectric Measurements

A. Sample Preparation

Calf Thymus DNA was purchased from Sigma Chemical Company. We

used ultrapure type D 4764 or preparations purified by standard phenol extraction methods[18] from type D 4522. Both are supplied as highly polymerized DNA. The type D 4522 DNA on which most of our experiments were made was sheared prior to purification to reduce the average molecular weight and lower the viscosity. Although a wide range of concentrations were examined in preliminary measurements the results we report here are for concentrations near 6 mg/ml. This concentration is relatively high but is necessary to obtain dielectric and conductivity increments large enough to measure with high accuracy. The NaCl concentrations of the solutions were fixed by dialysis for two to four days against known concentrations of salt. The salt concentrations were zero, 30 mM and 90 mM added salt. The added salt does not include the Na^+ counterions bound to the DNA and not removed by dialysis.

B. Dielectric Measurements

To characterize the high frequency δ relaxation for calf thymus DNA samples required that we measure their complex dielectric response over the frequency range 1 MHz to 1 gHz. In addition it was useful to determine the low frequency (100Hz) conductivity of the samples. The measurements were all made at 25°C using a circulating water bath to control the temperature of the sample and measuring cell. The 100 Hz conductivity measurements were made with a commercial conductivity probe (Beckman CEL-G50-Y184) capable of measuring less than 150 μl of sample. The measurements to 40 MHz were made with a parallel plate capacitance cell having platinum black electrodes similar in design to cells used by Foster[19]. The measurements above 45 MHz were made with open ended coaxial probes as described by Stuchly[20].

These measurements required the use of two instruments. The low frequency range from 100 Hz to 40 Mhz was covered by a Hewlett Packard 4194A impedance analyzer (an automatic impedance bridge). The high frequency range from 45 MHz to 1 gHz was covered by a Hewlett Packard 8510B network analyzer, an instrument capable of detecting and comparing the amplitudes and phases of the signal incident on and reflected from the sample. These two instruments use very different techniques to measure parameters from which the dielectric response of a material can be deduced.

The impedance analyzer as its name implies determines the impedance of a test circuit which in our case is either a conductance cell or a capacitance cell containing a DNA solution. The analyzer is capable of representing the measured complex impedance in terms of a variety of equivalent circuits. The correct equivalent circuit must be selected from knowledge concerning the actual circuit. In both of the measurement cells we have used it is most convenient to consider an equivalent circuit consisting of a parallel conductance ,G, (G = 1/resistance) and

capacitance, C, due to the solution held between a pair of conducting wires or plates. In the ideal case, a capacitance cell consists of a pair of parallel plates between which the sample is held. Ignoring stray capacitance, leakage currents and other difficulties the measured conductance and capacitance are related to the conductivity, σ, and relative permittivity, ϵ', of the sample through the simple relations:

$$G = \sigma A/D \qquad (1)$$

and

$$C = \epsilon'\epsilon_o A/D \qquad (2)$$

where A is the area of the plate, D the plate separation and ϵ_o the permittivity of free space. In practice one usually determines an effective A/D (also known as the cell constant) empirically by measuring materials of known ϵ' and σ.

The upper operating frequency of the impedance analyzer is 40 MHz. Although it is possible to build impedance bridges which operate at higher frequency it becomes more and more difficult to avoid parasitic impedances and or correct for them. The network analyzer provides another more convenient method for determining impedances above a few tens of MHz. This instrument uses the fact that signals transmitted by or reflected from a test device will be related in amplitude and phase to the incident signal. The relationship is determined, in the case of reflection, by the impedance mismatch at the input to the test device. In our case the test device consists of the sample itself which is in intimate contact with the flat end of a teflon filled coaxial waveguide. This so called open ended waveguide forms a dielectric probe.

The network analyzer determines the complex reflection coefficient, Γ, which is related to the impedance mismatch at the end of the probe by the relation:

$$\Gamma = (Z_i - Z_o)/(Z_i + Z_o) \qquad (3)$$

where Zi and Z_o are the impedance of the test sample and the characteristic impedance of the waveguide respectively. As in the case with the impedance analyzer one must choose an appropriate equivalent circuit to represent the sample. If we choose the same circuit as before (neglecting fringe capacitance and radiation conductance) we can relate the reflection coefficient to the conductance and capacitance of the probe. We must then extract the relative permittivity and conductivity of the sample as before from the conductance and capacitance. For the open ended probe (coaxial waveguide) we of course do not have the simple geometry of a parallel plate capacitor and so the equations 1 and 2 must be replaced with ones appropriate to the geometry of the probe. Although it is possible to obtain analytic expressions analogous to

equations 1 and 2 for the open ended probe they are only valid in limiting cases which do not match the experimental conditions[21]. It is more appropriate, as was the case for the impedance analyzer, to use empirical relations determined by measuring the reflection coefficients from samples of known relative permittivity and conductivity.

The above discussion is an over simplification of the actual measuring conditions for both the impedance analyzer and the network analyzer. Substantial corrections must be applied using well established techniques to correct for stray impedances. The corrections are generally determined by measuring materials for which the response is known and then calculating correction terms based on an assumed equivalent circuit for the measurements.

In the case of the impedance analyzer the machine has a resident program to make corrections for stray series and parallel impedances based on measurements of an open and short circuited cell. This standard correction procedure accounts for stray impedances in the circuit up to the measurement cell. It does not fully correct for stray capacitance or residual inductance associated with the cell. The effects of these uncorrected errors can be observed by making impedance measurements of materials with known dielectric behavior such as salt solutions and alcohol water mixtures. We determined that the errors due to residual inductance were negligible in our case. The stray capacitance however was significant and we corrected for it.

To determine the stray capacitance and cell constant for the cell we can measure a series of liquids with known ϵ'. The observed capacitance, C_T, is due to the parallel combination of the stray fringe, C_f, and cell, $\epsilon' C_o$, capacitances and is given by:

$$C_T = C_f + \epsilon' C_o \qquad (4)$$

By measuring a series of liquids with known ϵ' and plotting the capacitance versus ϵ' we can determine both the cell constant and C_f. The slope of the line is C_o. The cell constant is obtained by dividing by ϵ_o. C_f is the intercept of the curve at ϵ' equal to zero.

In the case of the network analyzer there are a number of corrections that must be made to account for error signals in the instrument itself. These corrections are determined from measurements of three conditions for which the instrument response can be accurately predicted. In our case we measure a shorted probe, an open probe in air and a liquid having the same or similar salt concentration as our sample. A series of equations are solved

based on an equivalent circuit for the analyzer. The results are correction coefficients which correct the response of the instrument up to a reference plane which in our case is the end of the probe. In addition to these corrections it is known from the theory of the open ended probe[22] that there is a fringe capacitance and a radiation conductance for the probe. These depend on frequency and on the dielectric constant of the sample. In the frequency range below 1 gHz the radiation conductance should be small and we neglect it. The fringe capacitance is assumed to be constant and is determined by measuring a series of liquids for which the complex dielectric constant is known and then solving for C_f using the equivalent circuit. Values for C_f have been reported in the literature for probes based on standard coaxial cable and are consistent with our measured values[23].

The effects of DNA on the dielectric behavior of aqueous salt solutions is relatively small in the δ relaxation frequency regime. In order to more clearly observe the effects of DNA and its associated counterions we assumed that the various contributions to ϵ' and σ were simply additive as will be explained in more detail in section ( ). We determined increments for the relative permittivity and conductivity by measuring the properties of the bulk solvent with and without DNA and finding the difference. This procedure has the advantage of making the effects of DNA visible and also partially correcting for certain calibration errors and neglected stray impedances[24]. Since the errors are nearly the same in both sample solution and solvent they are removed in the subtraction.

3. Dielectric Relaxation Data

Dielectric relaxation measurements were made on three different DNA solutions over a frequency range of 1 to 1000 MHz. These solutions contained calf thymus DNA molecules , NaCl , and water. The solutions differed in the concentrations of both the DNA and the salt. The solutions were the following : (1) a 5.7 g/l DNA solution that was dialyzed against distilled water for 4 days (yielding a zero bulk salinity); (2) a 6.1 g/l DNA solution that was dialyzed for 2 days against a 30 mN NaCl salt solution (yielding a bulk salinity of 30 mN); and (3) a 3.9 g/l DNA solution that was dialyzed 2 days against 90 mN NaCl salt solution (yielding a bulk salinity of 90 mN).

To analyze the relaxation data we proceeded as follows:

We assumed that the conductivity contribution of each entity in the solution is additive. Thus, the total conductivity of the DNA solution , σ_T , is given by:

$$\sigma_T = \sigma_D + \sigma_C + \sigma_B + \sigma_{WD} \qquad (5)$$

where σ_D , σ_C , σ_B , are the conductivity contributions of the diffuse counter ions, condensed counter ions, and bulk (i.e. added salt) ions respectively. σ_{WD} is the dipolar conductivity contribution of the water molecules.

If, as the data below show, the relaxing part of the total conductivity , $\Delta\sigma$, is related to motion of the condensed ions, (i.e. a frequency dependent condensed ion conductivity) then $\Delta\sigma = \sigma_C$. To extract $\Delta\sigma$ from the measured values of σ_T we obtained values of $\sigma_B + \sigma_D$ by assuming that at 1 MHz the contributions of σ_C and σ_{WD} are negligible thus:

$$\sigma_{1MHz} = \sigma_B + \sigma_D \qquad (6)$$

The value of σ_D should be constant over the range 1 to 1000 MHz because it is not relaxing . These ions are associated with low frequency relaxation occurring in the kHz region. Thus $\Delta\sigma(\omega)$ at all frequencies above 1 MHz was obtained by subtracting the constant conductivity , σ_{1MHz} , and the measured values of σ_{WD} (of course corrected for the excluded volume caused by the presence of the DNA) from σ_T . We used the expression:

$$\Delta\sigma(\omega) = \sigma_T - \sigma_{1MHz} - (1 - V)\,\sigma_{WD} \qquad (7)$$

to obtain the relaxing condensed ion conductivity. The quantity V is the volume fraction of the sample occupied by the DNA.

Eq. (7) assumes that the dipolar contribution of the water is not affected by the presence of the DNA molecules in solution, and that the conductivity of the DNA molecule itself is zero. Using Eq.

(7) we obtained values of $\Delta\sigma(\omega)$ for each of the three DNA solutions. We show as typical data the values obtained for the zero bulk salinity sample in Fig. 1.

Following the logic of the conductivity discussion above, one can write an expression for $\Delta\epsilon'$, the dielectric increment of our DNA solution (i.e. the relaxing component of the real part of the dielectric permittivity) as follows:

$$\Delta\epsilon' = \epsilon'_T - (1 - V)\,\epsilon'_{WD} \qquad (8)$$

ϵ'_T is the real part of the permittivity of the DNA solutions and ϵ'_{WD} is the dielectric permittivity of water in the presence of DNA and salt. Since the relaxation frequency of water in DNA solutions is still of the order of 10GHz or higher ϵ'_{WD} is constant over the range of our measurements. The assumption above that the dipolar water contribution to the conductivity is not much affected by the presence of the DNA turned out to be quite reasonable. However the data at 1 GHz clearly show that DNA lowers the ϵ' of the aqueous salt solution. The value of ϵ'_T at 1 GHz is less than that of a salt water solution of the same salinity (even after correction for excluded volume caused by the presence of the DNA). This is consistent with the notion that some of the water is bound to the DNA[5].

To obtain an estimate of the value of ϵ'_{WD} in the presence of the DNA we assumed (after analyzing the frequency dependent conductivity data) that by 1 GHz the condensed ion relaxation had effectively reached its limiting values (i.e. $\omega\tau \gg 1$)). Thus ϵ'_T at 1 GHz is given by:

$$[\,\epsilon'_T\,]_{1GHz} = (1 - V)\,\epsilon'_{WD} \qquad (9)$$

and $\Delta\epsilon' = 0$ at this frequency. The dielectric increment of the DNA solutions in the range from 1 to 1000 MHz can then be written:

$$\Delta\epsilon'(\omega) = \epsilon'_T - [\epsilon'_T]_{1GHz} \,. \qquad (10)$$

The conductivity data were fitted to commonly used functions. First an attempt to describe the data with a single Debye was tried. For a single Debye the frequency dependent permittivity, $\epsilon'(\omega)$, and conductivity, $\sigma(\omega)$ are given by the following equations:

$$\epsilon'(\omega) = \epsilon_\infty + \frac{\epsilon_s - \epsilon_\infty}{1+\omega^2\tau^2} \qquad (11)$$

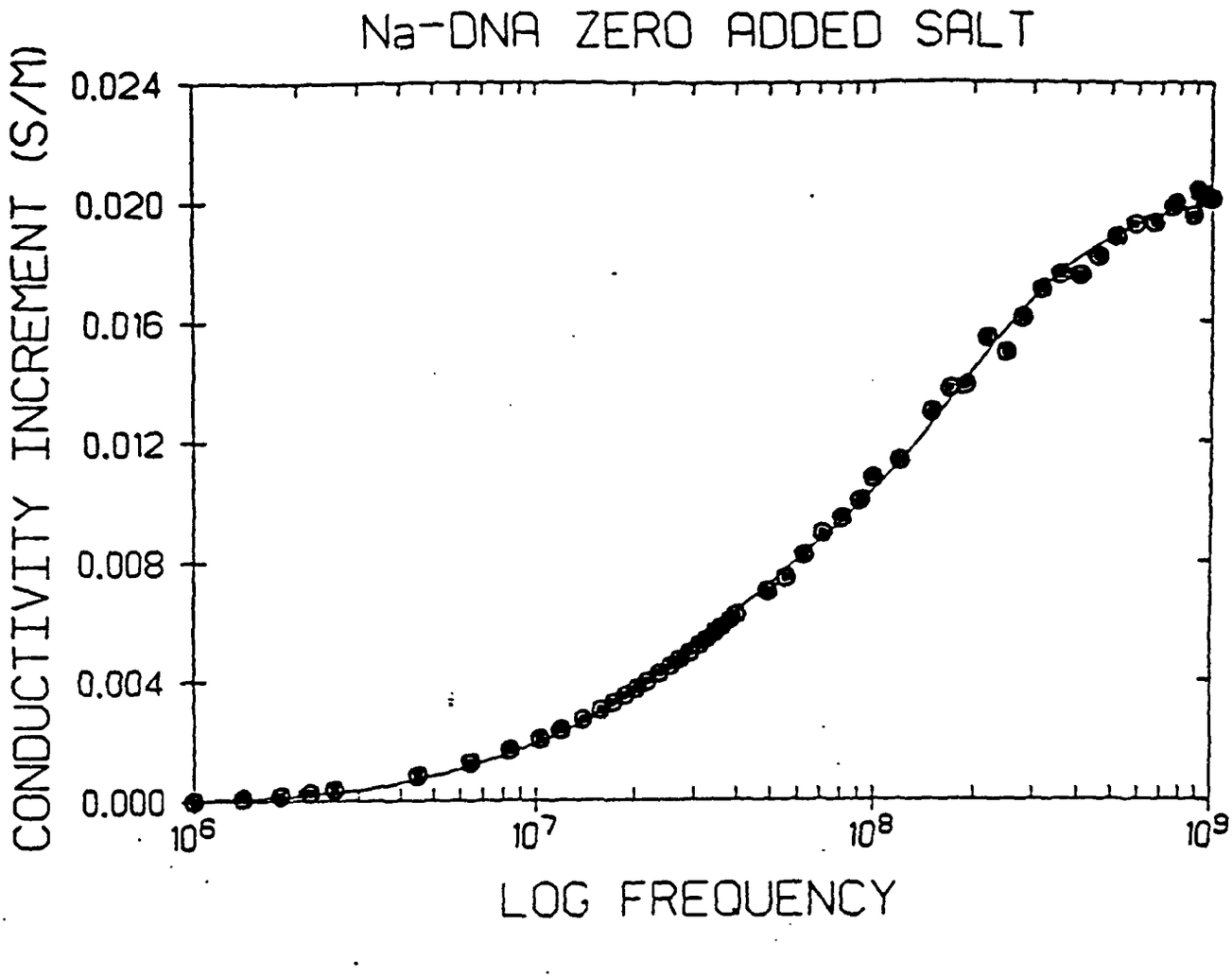

Figure 1. The conductivity increment for a zero added salt DNA solution.

and

$$\sigma(\omega) = \frac{(\epsilon_s - \epsilon_\infty)\omega^2\tau}{1+\omega^2\tau^2} \qquad (12)$$

where ϵ_s and ϵ_∞ are the low frequency and high frequency relative permittivities for the relaxation, ω is the angular velocity and τ is the relaxation time. The fit of the data to a single Debye was not good. The standard deviations of the fit parameters were bigger than the parameters themselves. Similar poor fits resulted from a superposition of two Debye processes. However a superposition of three Debye processes yielded an excellent fit. The relevant formulas are:

$$\Delta\epsilon(\omega) = \epsilon_\infty + \frac{\Delta\epsilon_1}{1+\omega^2\tau_1^2} + \frac{\Delta\epsilon_2}{1+\omega^2\tau_2^2} + \frac{\Delta\epsilon_3}{1+\omega^2\tau_3^2} \qquad (13)$$

and

$$\Delta\sigma(\omega) = \frac{\Delta\epsilon_1\omega^2\tau_1}{1+\omega^2\tau_1^2} + \frac{\Delta\epsilon_2\omega^2-\tau_2}{1+\omega^2\tau_2^2} + \frac{\Delta\epsilon_3\omega^2\tau_3}{1+\omega^2\tau_3^2} \qquad (14)$$

where the subscripts 1,2 and 3 refer to the three relaxations.

Table I

Superposition of 3 Debyes
Least squares fit parameters*

Sample	0 mM	30 mM	90 mM
$\Delta\epsilon_1$	5 ±.7	10.4 ±.8	4.7 ±.8
$\Delta\epsilon_2$	3.6 ±.7	2.7 ±.3	2.1 ±.3
$\Delta\epsilon_3$	1.1 ±.1	1.3 ±.1	.85 ±.04
f_1 (MHz)	7 ±2.4	7 ±1.1	7 ±2.1
f_2 (MHz)	33 ±4.6	54 ±7	56 ±6.7
f_3 (MHz)	200 ±9	300 ±13	400 ±12
f_{avg} (MHz)	38.5 ±4.5	38.4 ±3.1	64 ±6.6
$\Delta\epsilon_{Total}$	9.7 ±1	14.4 ±.9	7.6 ±.9
$\Delta\sigma_{Total}$ (s/m)	.021±.004	.034 ±.004	.028 ±.003

*The uncertainties represent the 90% confidence level of least squares fit parameters. f_{avg} is the average of the 3 frequencies weighted by magnitude of the $\Delta\epsilon$ associated with each.

The fit of the $\Delta\sigma$ data to Eq. 14 was excellent. This is shown

in Fig. 1. The relaxation parameters determined by the fit procedure are listed in Table I. Using these parameters the dielectric increment over the same frequency range was calculated using Eq. 13. The comparison of the calculated and experimental results are shown in Fig. 2.

Above 8 MHz the calculated curve is in good agreement with the dielectric increment data . Below 8 MHz significant departures from the predictions of Eq. 13 occur. These departures are consistent with the existence of a low frequency relaxation ($f_{rel} < 500$ Hz) reported by Mandel[3] and by Takishima[19]. This is known as the α relaxation.

The effects of a tail of the α relaxation are to be expected in both the $\Delta\sigma$ and $\Delta\epsilon$ data. However these effects are negligible in the $\Delta\sigma$ data. This is so because although the dielectric increment is quite large the corresponding conductivity increment is small, being proportional to ϵ_0/τ. This is a relatively small number for the α relaxation. Thus, to find parameters which would be insensitive to the tail of the α relaxation, we fit the $\Delta\sigma$ data first.

Because it has been proposed in the literature[7] that there are several relaxation mechanisms which one might associate with the dispersion in the 1 to 1000 MHz region we found the good fit to 3 Debyes intriguing. We made some attempts to relate the predicted relaxations with our results as we discuss below. It may also be that the large number of adjustable parameters in a fit to three Debyes is responsible for the good fit and there may be no relation to three distinct relaxation mechanisms.

IV Interpretation of Results

We examined several models which have been proposed to explain the δ relaxation. These include a modified Maxwell Wagner type model due to Grosse[20] and models due to Mandel[7] and to Manning[8] for condensed counterions. Grosse's model was modified by Babak Saif to account for the experimentally observed[21] thickness of the ion layer around DNA molecules. Based on this model, predictions for the conductivity increment were approximately correct but predictions for the permittivity increment and the relaxation times were incorrect by more than an order of magnitude. This model was rejected.

The condensed counterion model as developed by Manning[8] correctly predicts the magnitudes of both the conductivity and permittivity increments. There is some qualitative agreement between the observed relaxation times and the times predicted in Mandel's development of the model. The magnitudes of the relaxation times are not completely understood, however. Although the condensed counterion model involves approximations due to the complexity of dealing with macromolecular solutions it does appear

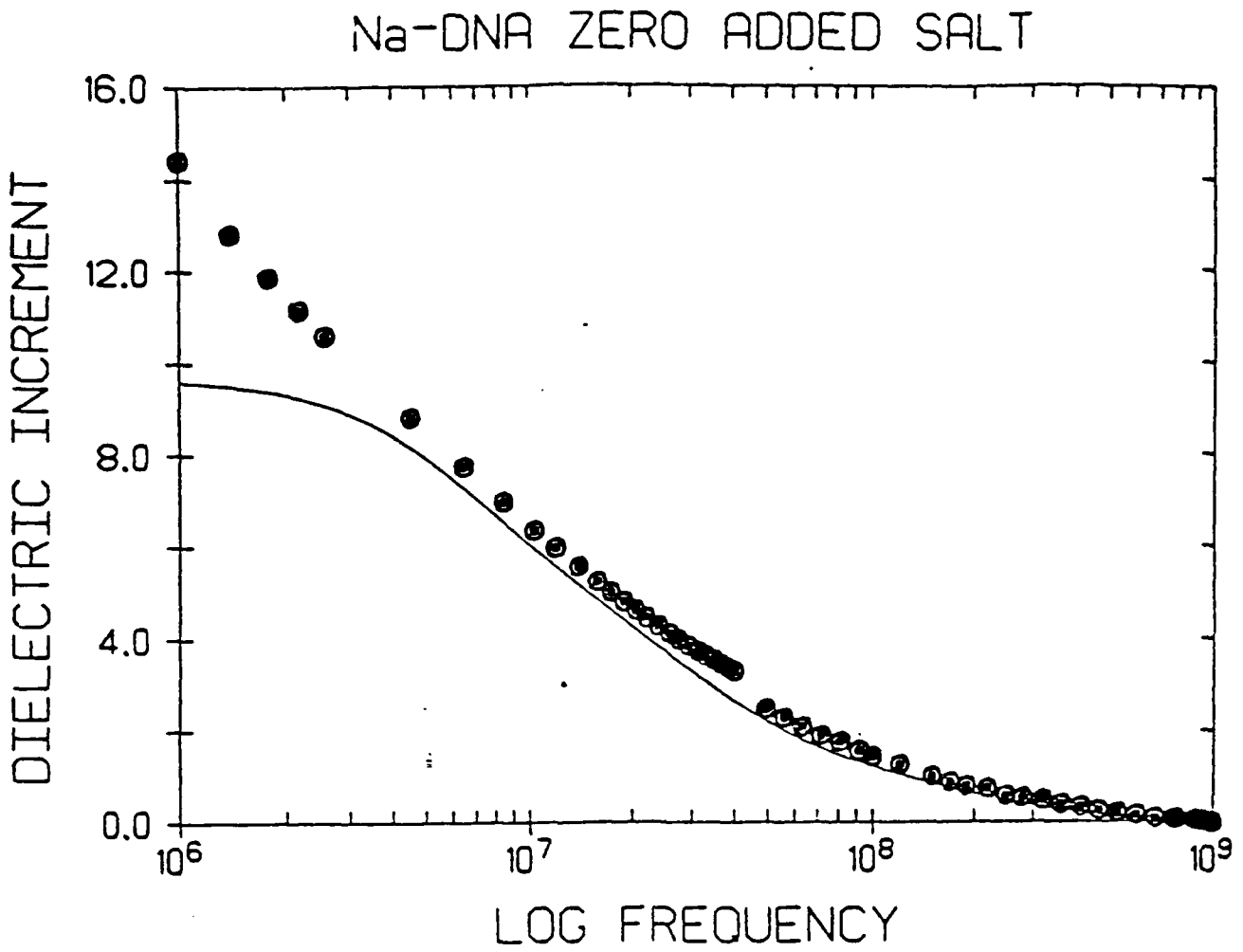

Figure 2. The dielectric increment for a zero added salt DNA solution.

to explain the general dielectric behavior of the δ relaxation well.

To simplify our discussion of the data we have normalized the results shown in Table I to a DNA concentration of 1 g/l. This normalized data is shown in Table II.

Table II
Sum of Three Debyes
Summary of normalized least squares fit parameters*

	0 mN Na-DNA (5.7 g/l)	30 mN Na-DNA (6.1 g/l)	90 mN Na-DNA (3.9 g/l)
f_1(MHz)	7 ± 2.4	7 ± 1.1	7 ± 2.1
f_2(MHz)	33 ± 4.6	54 ± 7	56 ± 6.7
f_3(MHz)	200 ± 8.9	300 ± 13.5	400 ± 12.5
$\Delta\epsilon_1$	.88 ± .12	1.70 ± .13	1.2 ± .2
$\Delta\epsilon_2$	.63 ±.12	.44 ± .05	.54 ± .08
$\Delta\epsilon_3$	.19 ± .02	.21 ± .02	.22 ± .01
$\Delta\sigma_1$ (s/m x 10^4)	3.5 ± 1.8	6.6 ±.6	5.1 ± 2.6
$\Delta\sigma_2$ (s/m x 10^4)	12.3 ± 3.5	13.1 ± 1.6	18 ± 2.6
$\Delta\sigma_3$ (s/m x 10^4)	21 ± 1.8	36 ±.3	49 ± 2.6
$\Delta\epsilon_T$	1.7 ± .2	2.4 ± .2	2 ± 2
$\Delta\sigma_T$ (s/m x 10^4)	37 ± 7	56 ± 6.6	72 ± 7.7
f_{avg} (MHz)	38.5 ± 4.5	38.4 ± 3.1	64 ± 6.6

* All values of $\Delta\epsilon$ and $\Delta\sigma$ have been normalized to 1 g/l.

In the condensed counterion model the DNA is modeled as a series of connected rigid rods or subunits of length b = 300 ± 50 Å as determined from measurements of the persistence length for DNA molecules[22]. The rods are permitted free rotation around the joint but maintain a fixed bond angle. In solution, there are enough counterions associated with the DNA to yield electrical neutrality for the DNA i.e. sufficient positive ions to balance the negatively charged phosphate groups in the DNA. The associated counterions are either condensed or diffuse. The former are found in a thin shell around the DNA and are bound to rodlike subunits by potential barriers at the ends of each subunit. The latter are loosely bound to the DNA molecule as a whole and behave similarly to ions in the bulk solvent.

In the Manning model[8] the fraction of associated ions which are condensed is determined by the parameter, ξ, the ratio of the electrostatic energy between polyion sites and condensed counterions to the thermal energy :

$$\xi = \frac{q^2}{\epsilon kTd} \tag{15}$$

where q is the protonic charge, ϵ is the permittivity of the bulk solvent, k is Boltzmann's constant, T is the absolute temperature and d is the distance between charge sites. In Manning's model the fraction of associated ions which are condensed is given by $(Z\xi)^{-1}$. Where Z is the valence of the counterion. For Na^+ ions we find that 76% of the associated ions are condensed and 24% are diffuse. These values have been confirmed by NMR measurements[21].

Manning uses the condensed ion model for DNA to derive expressions for the polarizability of the DNA in the presence of an external field[23]. The expressions are based on calculations of the free energies due to the electrostatic interaction of charge sites, g_{el}, in the presence of excess salt, the free energy of mixing for Na^+ ions, g_m, and the free energy due to the interaction of the external field with the condensed counterions, g_{ex}. From conditions which the total free energy must satisfy he obtains an expression for the charge distribution and thus the polarizability of the system.

Manning's expression for the polarizability for the condensed counterion layer parallel to the DNA axis, α_l is given by:

$$\alpha_l = \left[\frac{Z^2q^2nL^2}{12kT}\right] A(N) \tag{16}$$

where A(N) is given by:

$$A(N) = \frac{1}{1 - 2(|Z|\xi - 1)\ln(K_s d)} \qquad (17)$$

and n is the total number of condensed counterions, L is the length of the DNA parallel to the external field, K_s is proportional to the square root of the ionic strength and the other parameters are as previously defined. In our case we are interested in the polarizability of a subunit. We thus replace L by b, the length of a subunit, in Eqs. 6 and 7.

We can now calculate the dielectric and conductivity increments according to the expressions:

$$\Delta\epsilon' = \frac{N\alpha_1}{3\epsilon_o} \qquad (18)$$

and

$$\Delta\sigma = \frac{ne\mu}{3} \qquad (19)$$

where N is the total number of rod subunits, μ is the free ion mobility, e is the electronic charge and the factor of 1/3 is due to the random orientation of the rods with respect to the applied field.

In Table III we show the results of the calculations and the corresponding results from the measurements.

TABLE III

Relaxation Parameters Calculated Using Manning's Model
Comparison of Experiment and Theory

SAMPLE	0 mN Na-DNA	30 mN Na-DNA	90 mN Na-DNA
$\Delta\epsilon_{Exp}$	1.7 ±0.2	2.4 ±.2	2 ±.2
$\Delta\epsilon_{Calc}$	.84 ±0.4	1.44 ±.5	1.7 ±.6
α_{1Exp} x10^{33} (of a subunit)	4.5 ±.5	6.5 ±.5	5.4 ±.8
$\alpha_{1\,Calc}$ x10^{33} (of a subunit)	2.3 ±1.1	3.9 ±1.4	4.6 ±.5
$\Delta\sigma_{Exp}$ x10^{3} (s/m)	3.7 ±.7	5.6 ±.7	7.2 ±.8
$\Delta\sigma_{Calc}$ x10^{3} s/m)	3.8 ±??	3.9 ±?	3.8 ±??

In the Manning model only the contributions to ϵ' and σ due to the movement of the condensed counterions over a subunit are considered. The calculated values thus represent a lower bound to the expected values. Other relaxation mechanisms may be contributing to the total observed increments as we will discuss further below. In any case, the results shown in Table III indicate that the there is general agreement between the magnitudes of the measured and calculated values of both the conductivity and dielectric increments. The general features of the condensed ion model give a good picture of the behavior of the DNA solutions.

We now consider the ionic strength dependence of the relaxation parameters. Equations 6 and 7 indicated that an increase in the bulk ionic strength should cause an increase in the polarizability. The reason for this is that the higher the ionic strength, the stronger the Debye shielding. This weakens the electrostatic interactions between the fixed negative charge sites and the condensed counterions, and also between the condensed counterions themselves. Therefore at the higher ionic strengths it is easier for an external electric field to displace the Na^+ condensed counterions over a subunit. As a result the polarizability increases with increasing ionic strength.

In Table III the measured and calculated polarizabilities are listed for various ionic strengths. From the table we see that there is reasonable agreement between the calculated and measured polarizabilities. We believe this agreement to be strong evidence that the δ relaxation is due to condensed counterion motions.

It was mentioned previously that Mandel[7] suggested several mechanisms which could account for the relaxation we have observed. These mechanisms are:

1) The orientational motion of the DNA molecule,

2) The migration of the condensed ions over a subunit,

3) Fluctuations in the concentration of the condensed counterions with the bulk and diffuse ions.

The slowest of these mechanisms should be the orientational motion of the molecule. Based on orientation times of other macromolecules we would judge that this mechanism is too slow to contribute to the δ relaxation. The fastest mechanism should be the fluctuations of the concentration of condensed counterions as ions move into and out of the condensation layer. One would expect to see a faster exchange rate between the bulk, diffuse, and condensed ions as ionic strength is increased. When a condensed counterion leaves the layer, the probability of it being replaced with a diffuse or bulk ion is higher. Thus the process is faster

at higher bulk ionic strengths because more ions are available. Looking at the data in Table II the value of f_1 does increase with ionic strength and may correspond to Mandel's concentration fluctuation mechanism.

Lastly we consider the mechanism involving the diffusion of the Na^+ condensed counterions over a subunit. This is the only mechanism for which we can calculate an expected relaxation frequency, f. The calculation is based on the diffusion of an ion along a rod subunit according to the equation:

$$f = \pi\mu kT/2b2 \qquad (20)$$

where b is a subunit length, k is the Boltzmann's constant, T is the absolute temperature, and μ is the ion mobility. Assuming that the ions have the same mobility along the subunit as in the bulk we obtain an estimate for f of approximately 2 MHz. Our lowest observed relaxation frequency is 7 MHz which is at least the same magnitude as this estimate.

Without more precise predictions of the dynamics of the relaxation processes it is not possible to make more meaningful comparisons between theory and experiment. More theoretical work needs to be done to make this possible. We conclude, however, that since the measured dielectric and conductivity increments of the relaxation were accounted for by using Manning's model it remains the prime candidate for explaining the observed δ relaxation.

As a further and final test of our conclusions above, we tried to use the concept of condensed and diffuse ions to account for the "excess" dc conductivity measured in our DNA samples dialyzed against deionized water. In one of these samples containing 1 g/l DNA the dialysis was performed for 7 days. It is thought that this is sufficient time to remove nearly all of the bulk Na^+ ions. The DNA must remain electrically neutral so sufficient ions must be present to balance the charges on the phosphate groups. If these are the condensed and diffuse ions of the Manning theory we can estimate their contributions to the low frequency conductivity.

The normality of a 1 g/l DNA solution is 3 mN. From the Manning theory 24% of the charge is neutralized by diffuse ions which behave like bulk ions and can thus contribute to the low frequency (100 Hz) conductivity. Using equation 19 without the factor 1/3, since the diffuse ions are not forced to move along the DNA subunits, we find that the conductivity is 0.004 ± 0.001 s/m. This is in excellent agreement with the measured value of 0.005 ± 0.001 s/m. The condensed counterions do not contribute to the low frequency conductivity because they are bound to their subunits and are prevented from following the field by the potential barriers at the subunit ends. Thus the magnitude of the excess low frequency conductivity adds support to the concept of counterion condensation.

We would like to point out a further consequence of the condensed counterion theory. Although the condensed ions do not contribute to the low frequency conductivity they do contribute to the high frequency conductivity and energy absorption. In fact, the local conductivity and absorption may be relatively high. In a cell the bulk saline concentration is about 0.1 N corresponding to a conductivity of 1.27 S/m at 37 °C. From the conductivity contribution of the condensed counterion layer measured in our experiments and the volume fraction occupied by that layer we can estimate that the local conductivity for DNA segments aligned with an external field is about 7.5 S/m at 37 °C. Whether this enhanced conductivity will have any biological effect cannot be answered at this point.

V Conclusions

This study of the dielectric properties of DNA-saline solutions has led to several important conclusions. It confirms the existence of a small dispersion in the frequency range 1 MHz to 1 gHz. The data give strong support for the condensed ion models of Mandel and Manning. Finally, a consequence of the condensed ion model is that the local conductivity and thus the absorption of electromagnetic energy at the surface of the DNA is almost an order of magnitude higher than it is in the bulk for physiological concentrations. This may or may not have biological significance but it is encouragement for further study.

REFERENCES

6. S. Takashima and A. Minakata, Digest of Dielectric Literature 37, 602 (1975)

7. G. Schwarz, Adv. Mol. Relax. Processes 3, 281 (1972)

8. M. Mandel and T. Odijk, Ann. Rev. Phys. Chem. 35, 75 (1984)

9. K. R. Foster and H. P. Schwan, "dielectric Properties of Tissues," CRC Handbook of Biological Effects of Electromagnetic Fields,

10. S. Takashima, C. Gabriel, R. J. Sheppard, and E. H. Grant, Biophys. J. 46, 29 (1984)

11. M. Mandel, Ann. NY. Acad. Sci. 303, 74 (1977)

12. F. Van Der Touw and M. Mandel, Biophys. Chem., 2, 218 (1974)

13. G. S. Manning, J. Chem. Phys. 51, 924 (1969)

14. Y. Tominaga, M. Shida, K. Kubota, H. Urabe, Y. Nishimura, and M Tsuboi, J. Chem, Phys. 83, 5972 (1985)

15. C. Demarco, S. M. Lindsay, M. Pokorny, J. Powell, and A. Rupprecht, Biopolymers 24, 2035 (1985)
N. J. Tao, S. M. Lindsay, and A. Rupprecht, Biopolymers 26, 171 (1987)
M. B. Hakim, S. M. Lindsay, and J. Powell, Biopolymers 23, 1185 (1984)

16. T. Weidlich, "Raman Spectroscopy from the Low Frequency Vibrations of DNA in Highly Crystalline Films, Oligonucleotide Crystals and Polynucleotide Solutions," Ph.D. dissertation, Arizona State University (1989)

17. L. L. Van Zandt and V. K. Saxena, Phys Rev. A 39, 2672 (1989)

18. L. G. Davis, M. D. Dibner and J. F. Battey, "Molecular Biology," (Elsevier, New York, 1986)

19. K. Foster, University of Penn. private communication

20. T. W. Athey, M. A. Stuchly, and S. S. Stuchly, IEEE Tran, Microwave Th. and Tech. MTT-30, 82 (1982)

21. N. Marcuvitz editor, "Waveguide Handbook," (McGraw-Hill, New York, 1951)

22. M. A. Stuchly, M. M. Brady, S. S. Stuchly, and G. Gajda, IEEE Trans. Inst. and Meas. IM-31, 116 (1982)

23. M. A. Stuchly, T. W. Athey G. M. Samaras, and G. E. Taylor, IEEE Tran. Microwave Th. and Tech. MTT-30. 87, (1982)

24. D. Misra, M. Chabbra, B. R. Epstein, M Mirotznik, and K. Foster, IEEE Tran. on Microwave Th. and Tech. 38, 8 (1990)

CHAPTER III

DESIGN AND EVALUATION OF MICROWAVE IRRADIATION SYSTEMS

1. Microwave irradiation of cells in suspension

Two microwave irradiation systems were used during this reporting period, one operating at 915 MHz and the other one at 2.45 GHz. Both systems have been fully described in the previous two annual reports.

The 2.45 GHz system has a waveguide applicator within which a sample tube containing the biological cell suspension is placed. The cells are maintained in suspension with a stirring bar and magnetic stirrer. Use of this irradiation system was restricted to studies with HL-60 cells carried out to investigate possible changes in cell viability and ornithin-decarboxylase (ODC) and RNase L activities. Exposures were performed with both CW and pulsed microwaves. In the later case, the microwave signal was pulsed with a period of 10 ms and pulse duration of 100 μs. The irradiations were generally carried out at a nominal SAR of 300 W/Kg. Results of this work are being reported in another section.

The 915 MHz system uses a Crawford cell within which tissue culture flasks containing the biological cell sample are placed. Four 25 cm^2 tissue culture flasks were used for each exposure to most effectively use the available space within the Crawford cell. The flasks were positioned with their bases perpendicular to the direction of propagation of the electric field. Since no stirring was provided, the cells which were immersed in a biological nutrient medium settled to the bottom of the container forming essentially a monolayer. The SAR which specifies the rate of energy deposition in the cell suspension clearly depends on the volume of the nutrient covering the cell monolayer in each flask. Experiments which require the use of radioactive tracers, for instance tritiated uridine, make it desirable to minimize the volume of the nutrient. Long term experiments with large concentrations of cells may require a larger volume of nutrients. Therefore, depending on the requirements of a particular experiment it may be necessary to change the volume of the nutrient used. To satisfy these requirements SAR measurements were carried out with the tissue culture flasks filled with 1.5 ml, 2 ml, 5 ml, 10 ml, and 15 ml of nutrient. The results of these measurements are shown in Figure 1 and Table I.

TABLE I

Volume/flask (ml)	α
1.5	180.6 ± 7.6
2.0	192.1 ± 7.4
5.0	298.8 ± 9.8
10.0	
15.0	

P_{inc} = α*SAR. Proportionality constants α relating SAR (mW/g) to the incident power (mW) for the Crawford cell loaded with 4 25 cm² flasks.

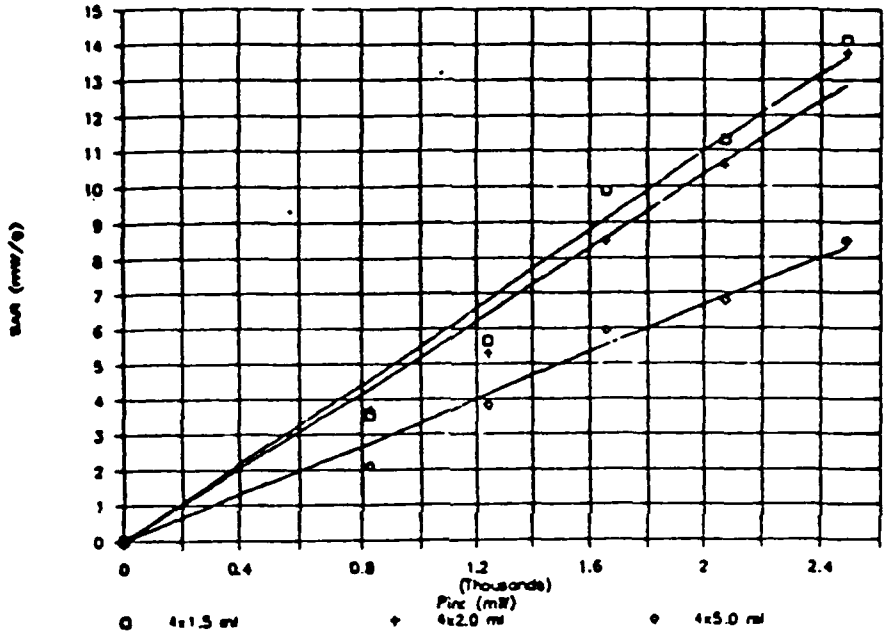

Fig. 1 SAR vs. P_{inc} for Crawford cell with four 25 cm^2 tissue culture flasks.

2. ELF irradiation of cells

2.1 Solenoid based ELF exposure system

A system for exposure of attached cells and cells in suspension to ELF ac magnetic fields was set up using a μ-metal shielded, 18 inch long, 4 inch ID solenoid. The system block diagram is shown in Figure 2.

Exposures using this system can be carried out in the frequency range between DC and 400 Hz with magnetic fields of up to 15 Gauss. The reference resistor was included in the circuit to provide a convenient means of determining the required level of the output signal from the amplifier to produce a desired magnetic flux density in the solenoid. The voltage drop across the reference resistor is proportional to the magnetic flux density.

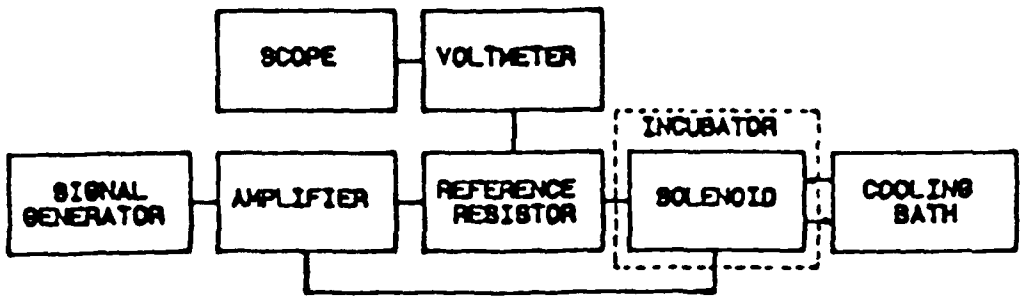

Fig. 2 Block diagram of ELF exposure system.

Measurements to determine the proportionality constant were carried out at various frequencies using a Bell 620 Gauss meter. The results are shown in Figure 3 and Table II.

TABLE II

Frequency (Hz)	β
40	0.1970 ± 0.0024
50	0.2004 ± 0.0016
60	0.2073 ± 0.0015
72	0.2193 ± 0.0014
80	0.2278 ± 0.0013
90	0.2380 ± 0.0009
100	0.2486 ± 0.0024

$V_s = \beta * B_o$. Proportionality constants β relating B_o (Gauss) to the voltage drop across the reference resistor (volts).

A plexiglass sample holder with shelves positioned at one inch intervals was built to accept 50 mm diameter round tissue culture dishes. This sample holder allows placing of the biological samples within the region of uniform magnetic field of the solenoid. In this configuration, the culture dishes rest perpendicular to the direction of the magnetic field.

In order carry out the experiments at a controlled temperature, the solenoid was placed within a water jacketed incubator. Temperature measurements inside and around the solenoid were carried out with magnetic fields of up to 10 Gauss with the incubator set at 37°C. To make these measurements type T thermocouples were immersed in the liquid medium contained in each culture dish of the fully loaded sample holder as well as in dishes outside the solenoid. Each culture dish was filled with 5 ml of nutrient medium.

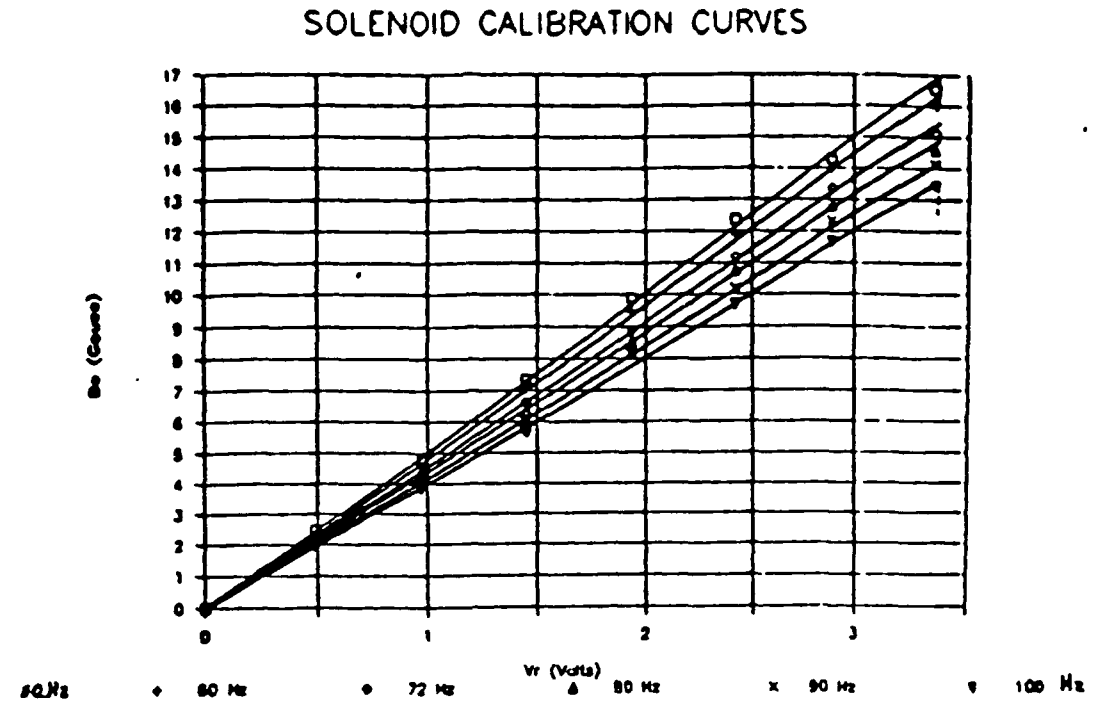

Fig. 3 B_o vs. V_R, the voltage drop across the reference resistor, at various operating frequencies.

In all cases considered, the temperature in the samples inside the solenoid was found to be greater by up to 2°C than the temperature in the samples elsewhere in the incubator. This temperature increase was determined to be due to IR heating associated with the solenoid. To alleviate this problem, a cooling coil was built of 1/4 inch OD flexible copper tubing and placed inside the solenoid. The magnetic field profile within the solenoid was not affected by the presence of the coil as long as the coil was fit with spacers to prevent succesive turns from touching each other. Water from a constant temperature circulating bath was made to flow through the coil. Further temperature measurements indicated that with this configuration and the appropriate choice of set temperature for the water bath a uniform temperature could be obtained.

Magnetic field measurements to determine the uniformity of the field within the solenoid were made at various points on cross-sections separated by one inch intervals along the axis of the solenoid. The measurements were carried out with a Bell 620 Gauss meter and an axial probe. Figure 4 shows a diagram of the axial cross-section of the solenoid with the sample holder and sample containers. Figure 5 shows points on a given transverse cross-section and along the length were the magnetic field was measured. The magnetic field profile was found to be axially uniform within ±5 inches from the center of the solenoid, and transversally uniform within a radius of 1.8 inches from the center axis.

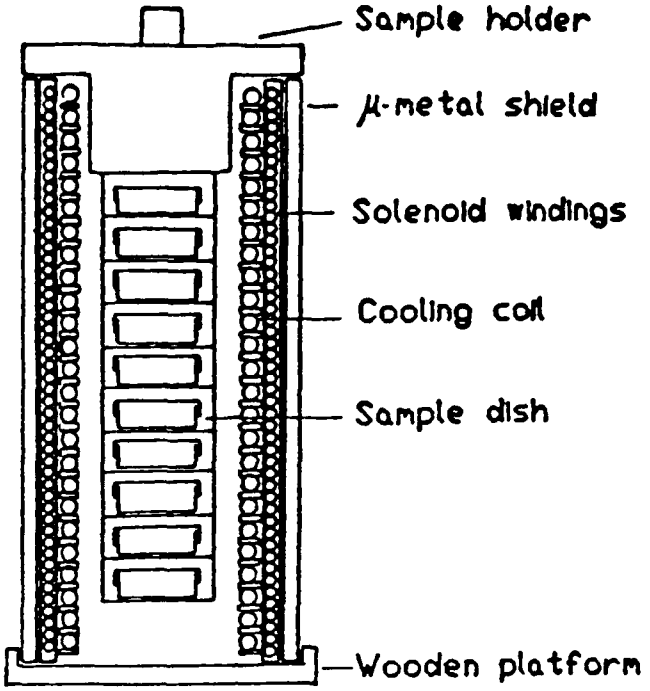

Fig. 4 Axial cross-section of solenoid showing plexiglass sample holder and location of sample containers.

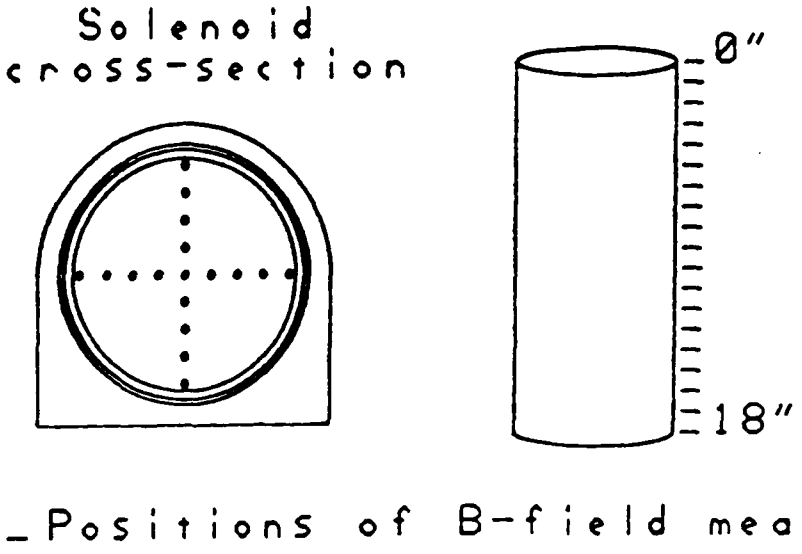

Fig. 5 Diagram of solenoid showing points on a given cross-section and levels along the length where the magnetic field was measured for calibration.

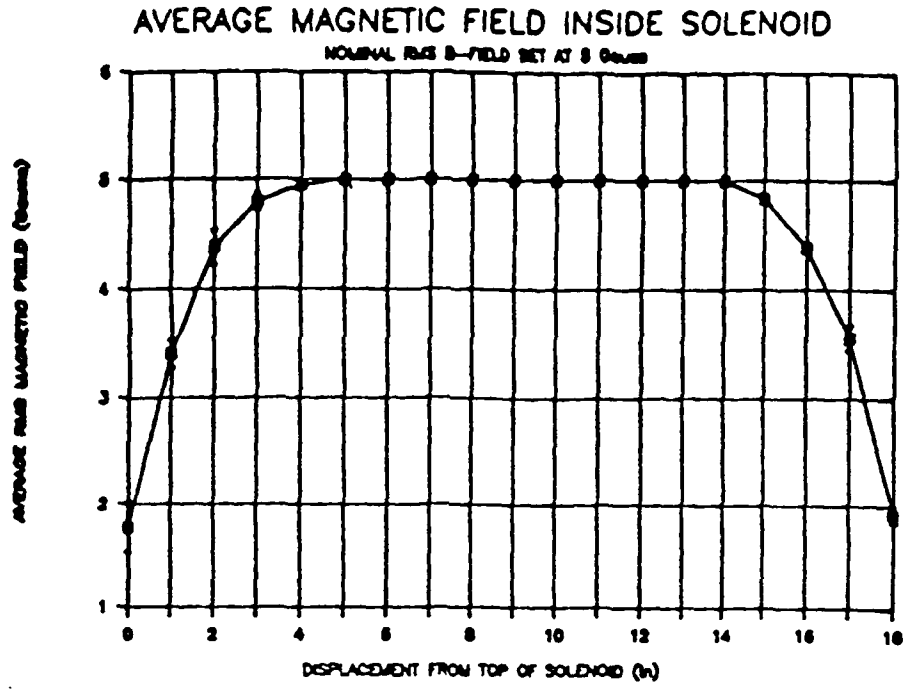

Fig. 6 Magnetic field distribution inside the solenoid obtained by averaging measurements on planes separated by one inch intervals along the length of the solenoid.

Figure 6 shows the average field on each cross-section plotted with the standard deviation as a function of position along the axis of the solenoid. Where no standard deviation was measured, non is shown. When the sample holder is placed in the solenoid the sample containers are located within ±5 inches from the center of the long axis of the solenoid. Therefore, these results indicate that all samples are indeed exposed to a very uniform magnetic field.

It has been reported in the literature[1] that extremely low magnetic fields of the order of 5 μT (1μT=10 mG) can cause measurable biological effects. Fields of this magnitude can arise from sources which might be present in any laboratory environment, such as motors, heaters, and in general any current carrying device. This prompted us to evaluate the background magnetic fields present around our ELF exposure system including the area where control samples are placed. The Hall effect magnetic field probes available to us were not sensitive enough to accurately measure very small fields. Instead, measurements were performed using a 100 turn search coil with a 1.2 cm^2 cross-sectional area. The calibration constant of this coil at 60 Hz was found to be 5 μV/μT. Clearly, this search coil is directional and therefore measurements in orthogonal directions were needed to completely characterize a field distribution. The solenoid is contained within the left chamber of a two chamber incubator.

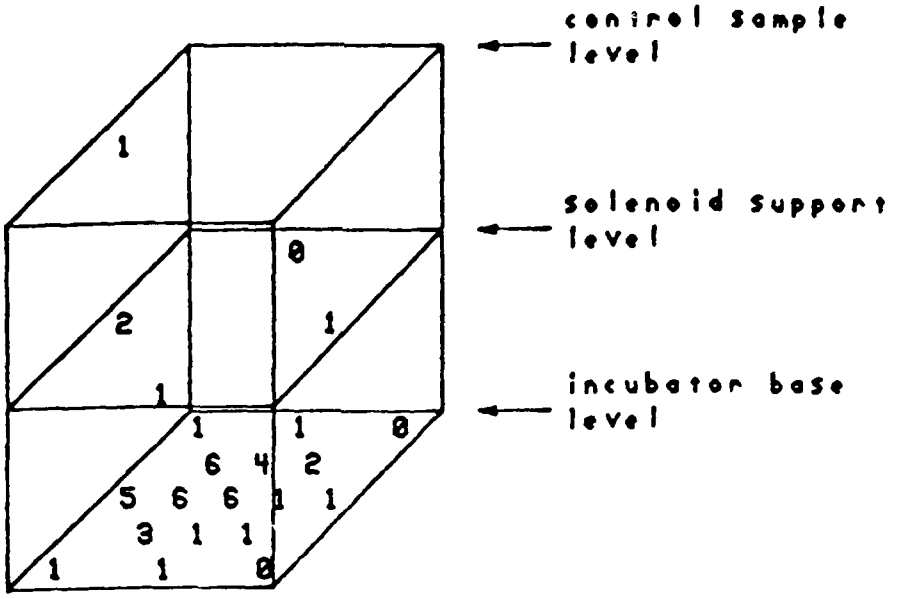

Fig. 7 60 Hz magnetic fields measured inside the left hand side chamber of the incubator used with the solenoid system. Measurements were taken while the incubator was regulating, with the pick-up coil placed in the vertical direction. With the regulation off the field were negligible.

During a normal exposure the sample are placed within the solenoid, while the controls are placed outside the solenoid but within the same chamber. The possible sources of extraneous magnetic fields closest to the area within the incubator chamber containing the solenoid are the heaters of the incubator and the compressor motor of the cooling coil bath located above the incubator. With the magnetic field of the solenoid off, the compressor off, and the heating coils off, the measured field in all directions was not different from the background level. Similarly, no effect was observed upon turning on the compressor. However, when the heater coils of the incubator were turned on a vertical field of approximately 6 μT was measured inside the incubator at the base of the chamber containing the solenoid. This field tended to be higher toward the center and left of the incubator becoming negligible on the right side. A diagram with these measurements is shown in Fig 7. A measurement at the position where the control samples are normally placed, showed that a vertically oriented field of approximately 2 μT was present there when the heater coils of the incubator were on. Further measurements in and around the control sample area with all extraneous fields off and the solenoid field on at approximately 10^{-3} T (10 Gauss) showed no difference with the background level.

2.2 Helmholtz coil based ELF exposure system

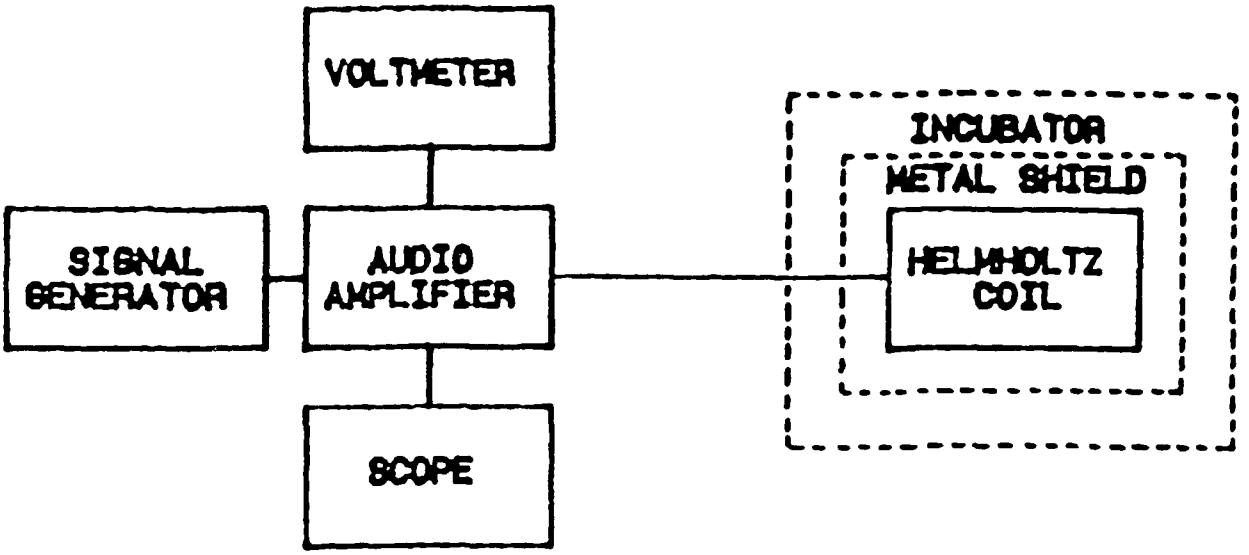

Fig. 8 Block diagram of ELF exposure system using a Helmholtz coil to produce the magnetic field.

Biological effects from ELF exposure using Helmholtz coils have been reported in the literature. In some cases[2] cell suspensions are exposed in containers positioned with their bases parallel to the direction of the magnetic field. This configuration is unlike that used in our solenoid system. In order to reproduce the experimental conditions under which the above mentioned effects were observe, a new ELF system was set up using a Helmholtz coil as the magnetic field source. A block diagram of the system is shown in Fig 8. The Helmholtz coil, completely shielded in an 11"x11"x10" μ-metal box, was placed in the right chamber of a two chamber incubator. Measurements with the search coil showed no field leakage inside the μ-metal box from external sources, principally the incubator heater coils, and no field leakage outside the μ-metal box with fields up to 100 μT from the Helmholtz coil. The distortion of the magnetic field within the Helmholtz coil due to the μ-metal box was also measured using a 100 μT field. The results are shown in Fig 9. In order to minimize extraneous field effects on the control sample, a smaller μ-metal box approximately 3"x5"x4" was built. Measurements conducted by placing the box within the Helmholtz coil indicated that it can addequately block fields up to 100 μT. During a normal exposure the control samples are to be located inside this μ-metal shield within the left chamber of the incubator.

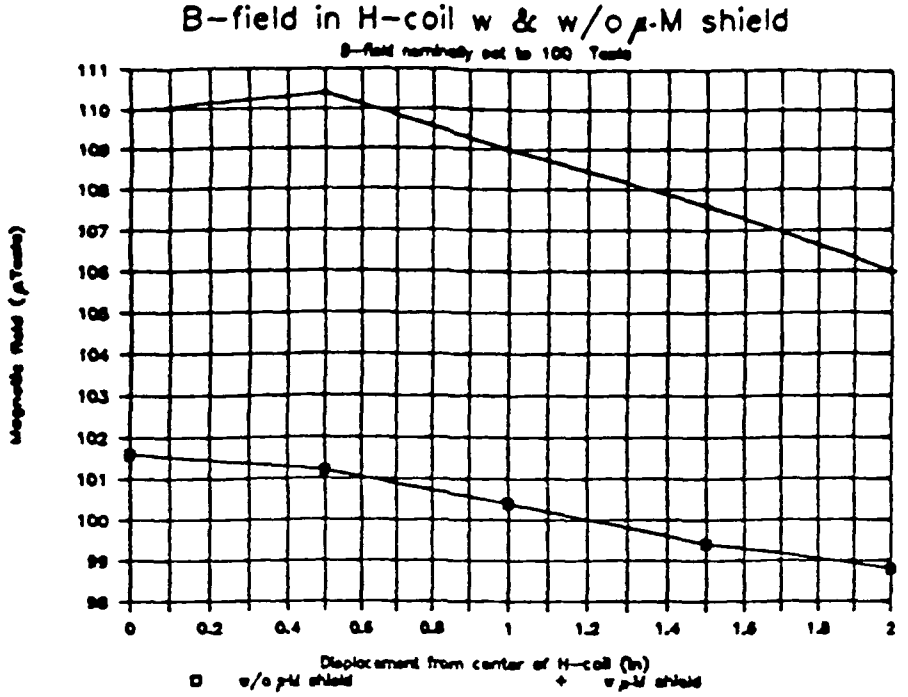

Fig. 9 Variation in the B-field with displacement from the center of the Helmholtz coil for a fixed coil driving voltage, with and without the metal shield.

3. Electric field distribution studies

Considerable effort is currently being devoted by many investigators to the study of biological effects of ELF electromagnetic fields. While the magnetic field can be measured directly, there is much confusion about quantification and reporting of the induced electric field. During this period we have been investigating methods to measure the magnitude of the electric field induced within samples of NaCl solutions. These solutions are of equivalent conductivity to Eagle's minimum essential medium often used as a cell nutrient medium in studies of biological effects of ELF fields.

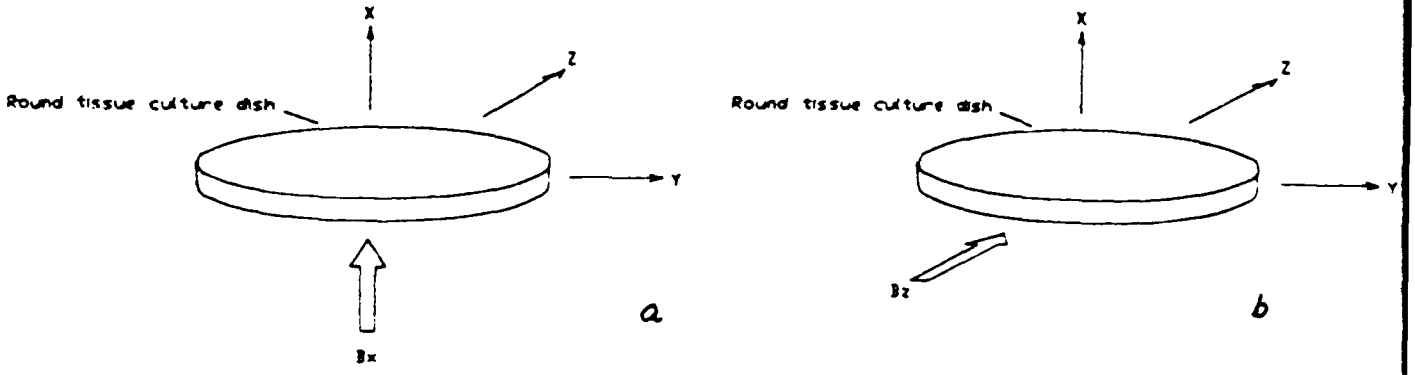

Fig. 10 Commonly used ELF exposure configurations: a) perpendicular, b) parallel.

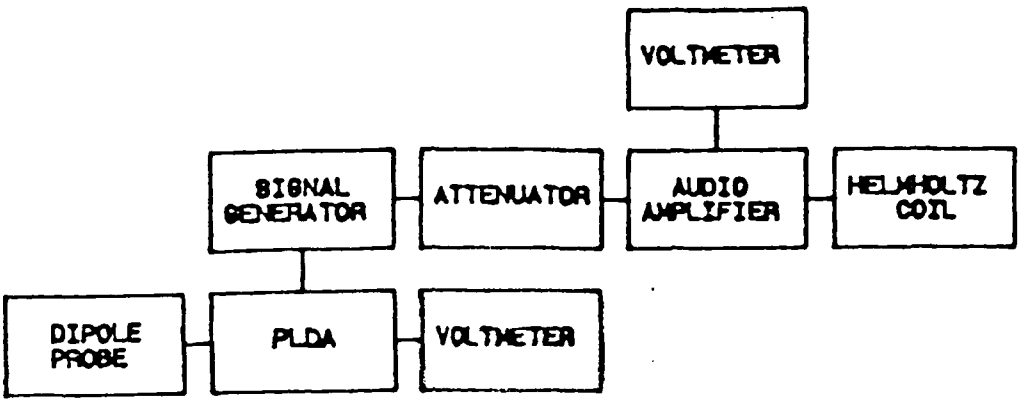

Fig. 11 Block diagram of Helmholtz coil and dipole probe with associated instrumentation.

Two exposure configurations are commonly used to expose biological cells to electromagnetic fields. One in which the sample container is placed with its base perpendicular to the direction of the magnetic field (perpendicular configuration, Figure 10a), and the other one in which the sample container is placed with its base parallel to the direction of the magnetic field (parallel configuration, Figure 10b). Electric field measurements in both configurations were made using a 950 μTesla, 400 Hz magnetic field produced by a Helmholtz coil. The magnetic field was measured using a Bell 620 gaussmeter with an axial Hall probe. A salt solution (0.15N NaCl) with conductivity equivalent to the cell nutrient medium was used for all measurements. A block diagram of the exposure system is shown in Figure 11.

3.1 Design of electric field probe

The direct measurement of small electric fields poses problems associated with unwanted detection of electromagnetic interference and with sensitivity. In this study, electric field measurements were performed using a thin wire short electric dipole. Use of a probe of this type for the determination of E-field variations in containers with cylindrical and rectangular shapes has been previously reported in the literature[3] . Our probe was made using a shielded twisted pair of individually shielded gauge 24 wires Belden # 8640, with a 1000Ω shunting resistor placed at the dipole elements. The resistor allows leakage of the charge which would otherwise build up on the leads. The dipole elements were made of 24 gauge platinum wire coated with platinum black. Coating of the platinum wire with platinum black considerably improved the sensitivity of the probe. A diagram of the probe is shown in Figure 12

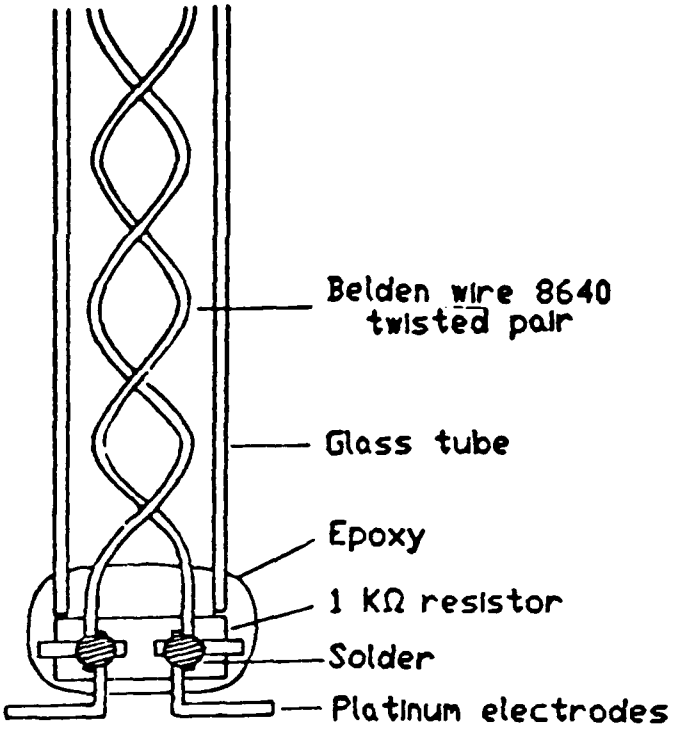

Fig. 12 Detail of short dipole electric field probe.

When placed in an electric field the dipole probe provides a voltage output which is proportional to the magnitude of the field strength in a direction parallel to the dipole elements. In order to measure the magnetically induced electric field the probe cable must be placed parallel to the direction of the magnetic field. This minimized inductive pick up by the cable. In this study, the induced electric fields were small and thus required the use of a narrow band amplifier to improve the signal to noise ratio of the probe. In order to obtain the absolute values of the electric fields the probe was calibrated by making measurements in a configuration for which the induced E-field can be easily calculated. This configuration is that of a circular container, such as a tissue culture dish, filled with an aqueous conducting solution, positioned at the center of the Helmholtz coil and oriented such that the magnetic field is perpendicular to the base of the dish. Using Faraday's law, the induced electric field for a sinusoidally varying magnetic field is given by $E=\pi fBr$, and the dipole voltage by $V_D=K2\pi fBr$, where f is the operating frequency, B is the magnetic field strength, r is the radial position from the center of the container, and K is the calibration constant.

At a given frequency f and solution conductivity σ the value of the probe constant K determined from measurements at different radii showed little variation indicating that the response of the probe was linear. The response of a bare dipole probe is expected to change according to the impedance characteristics of the medium in which it

is immersed. The equivalent circuit of this probe is the parallel combination of a capacitance C_e and a conductance G_e which are a function of the medium. Based on this equivalent circuit, the probe impedance is mostly resistive at low frequencies and therefore would be affected by the conductivity of the medium. Measurements were carried out to determine the variation in the probe constant as a function of the normality of the solution at 400 Hz (Figure 13). The results show that the probe constant changes slowly with conductivity. A four fold increase in conductivity corresponds to a 20% increase in the probe constant. For f=400 Hz and σ=1.5 S/m, the calibration constant was found to be K=0.25 m.

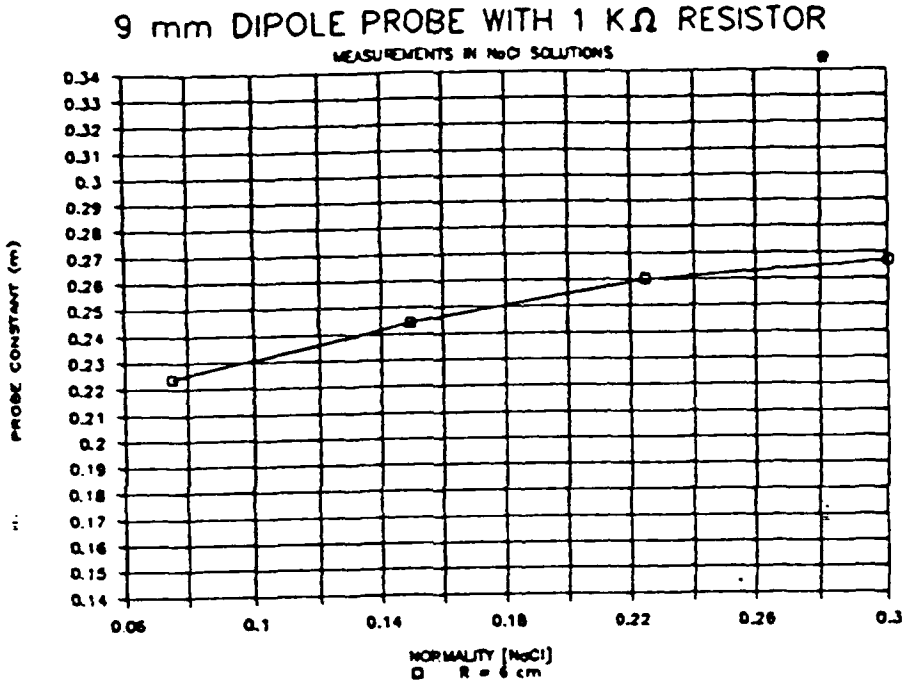

Fig. 13 Variation in the calculated probe constant with increasing normality of the sample medium. The probe was positioned at a radius of 6 cm from the center of the sample container.

3.2 Construction of probe positioner

In order to map out the electric field within the region of uniform magnetic field of the Helmholtz coil, be it in air or inside a liquid sample, two probe positioners were designed and built. One is a r-theta positioner which allows translation of the probe from the center of symmetry and then rotation about it. The other is an x-y positioner which allows translation of the probe at orthogonal directions on the same plane. In both cases the probe can be translated along and rotated about its own axis. The positioners are mounted on a table of adjustable height which can be moved over the Helmholtz coil and centered with respect to it by careful adjustment.

3.3 Electric field measurements in circular dishes oriented in the perpendicular configuration

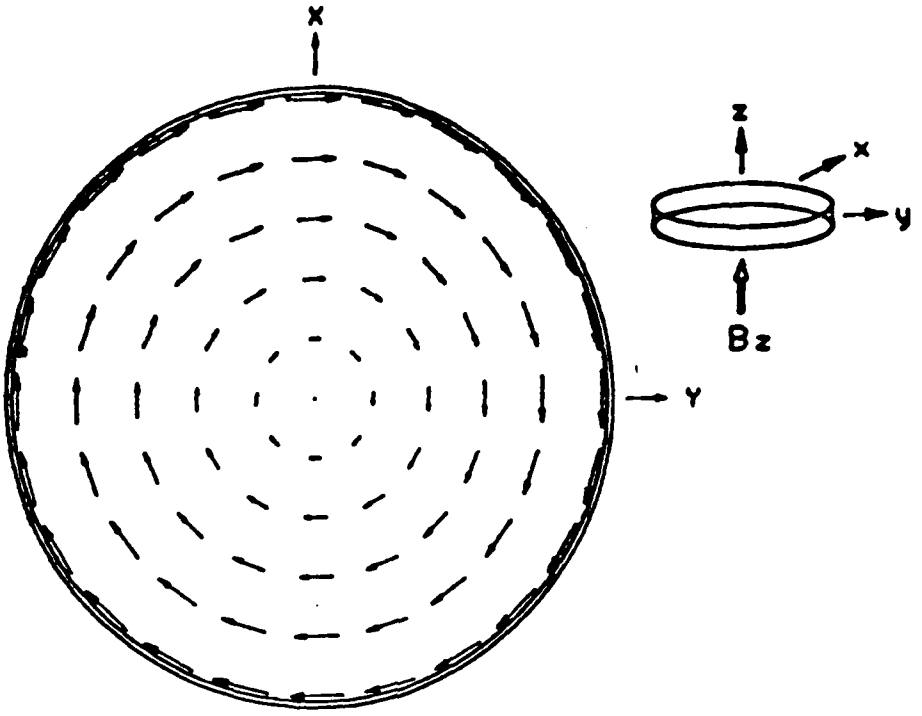

Fig. 14 E-field distribution inside a round container with the B-field perpendicular to the base of the dish. The arrows show the direction and relative magnitude of the E-field.

For this configuration (Figure 10a) Faraday's law predicts that the magnitude of the electric field increases linearly with radius starting from zero at the center of the container, Figure 14. Measurements with the container placed at the center of symmetry of the Helmholtz coil showed that the tangential component of the field increased linearly with radius while the radial component remained constant thoughout. The non-zero value of the radial component represents a background level independent of the applied magnetic field. These measurements showed the validity of the probe to measure electric fields.

It is clear that the induced electric field measured in air or in conduct g samples placed at the center of Hemlholtz coil has its center of symmetry coinciding with that of the coil. In order to show that sample positioning is not critical in this configuration, measurements were conducted using 50 mm circular tissue culture dishes filled with 0.15N NaCl placed within the Helmholtz coil at points displaced from its center axis. These measurements showed that the linearity of the electric field with the radius was maintained regardless of where the dish was placed within the region of uniform magnetic field of the Helmholtz coil.

3.4 Electric field measurements in circular dish with annular rings oriented in the perpendicular configuration

The induced electric field within samples placed in the perpendicular configuration varies linearly with radius. Thus, cells exposed in this configuration are subjected to a wide range of electric fields. If the ELF effects are caused by the induced electric fields, this is clearly a very undesirable situation. A possible solution is to confine the cells in narrow annular rings whithin which the range of E fields can be kept within reasonable bounds. Rings of large diameter are more advantageous since the percent deviation from the mean field decreases with increasing radius. A large diameter and reasonable width are also desirable in order to have an adequate surface area over which the cells can be properly distributed and allow sufficient room to dispense and withdraw the sample.

Measurements in 50 mm tissue culture dishes separated into various compartments by acrylic annular rings showed that the magnitude of the electric field in each compartment corresponded to the expected field at the same radius in the undivided container. Due to the diameter of the stem of the dipole probe measurements at a single radius were made in each compartment. As in the previous case, the linearity of the electric field with the radius was maintained when the sample was displaced from the center of the Helmholtz coil.

3.5 Electric field measurements in circular dish oriented in the parallel configuration

The electric field distribution for the parallel configuration was calculated by McLeod et al. and shown to vary with the height of the liquid. The results suggest that this field should be relatively uniform at the base of the container where the cells, originally suspended in the nutrient medium, eventually settle [Figure 15]. Our electric field probe was shown to operate properly only when placed with its output cable parallel with the direction of the magnetic field. In order to test the validity of the theoretical result for this configuration with this constraint, measurements were conducted using containers made from 2.5 inch diameter acrylic tubing cut to various lengths corresponding to different liquid heights, sealed at both ends, and cut in half along the length of the tube to make half-pill box shaped vessels. The containers which before cutting were roughly equivalent to 50 mm tissue culture dishes, were placed within the Helmholtz coil as shown in Figure 16. Measurements were carried out on the container wall corresponding to the base of the dish. For the container with shortest height (1.5 cm), the induced E-field along the bottom is relatively uniform within a radius approximately 5% smaller than the radius of the container. As the height of the container increases, the E-field becomes progressively less uniform. These results corroborate the theoretical predictions made for the case of rectangular containers.

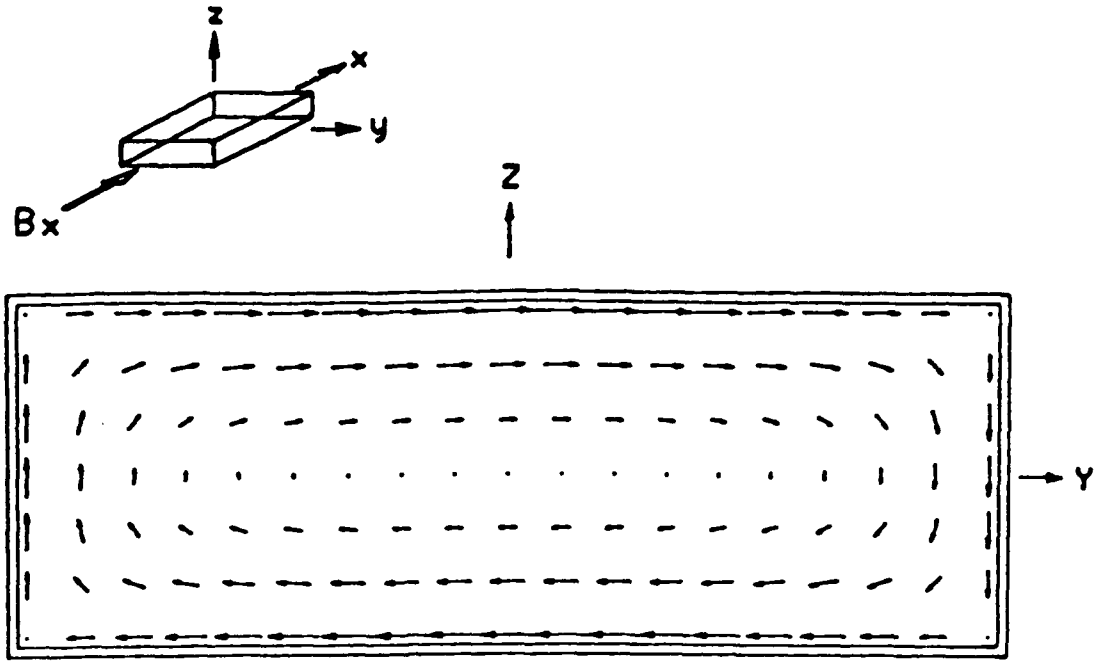

Fig. 15 E-field distribution inside a rectangular container with the B-field parallel to the base of the container. The E-field was calculated using McLeod's results[3]. The arrows show the direction and relative magnitude of the E-field.

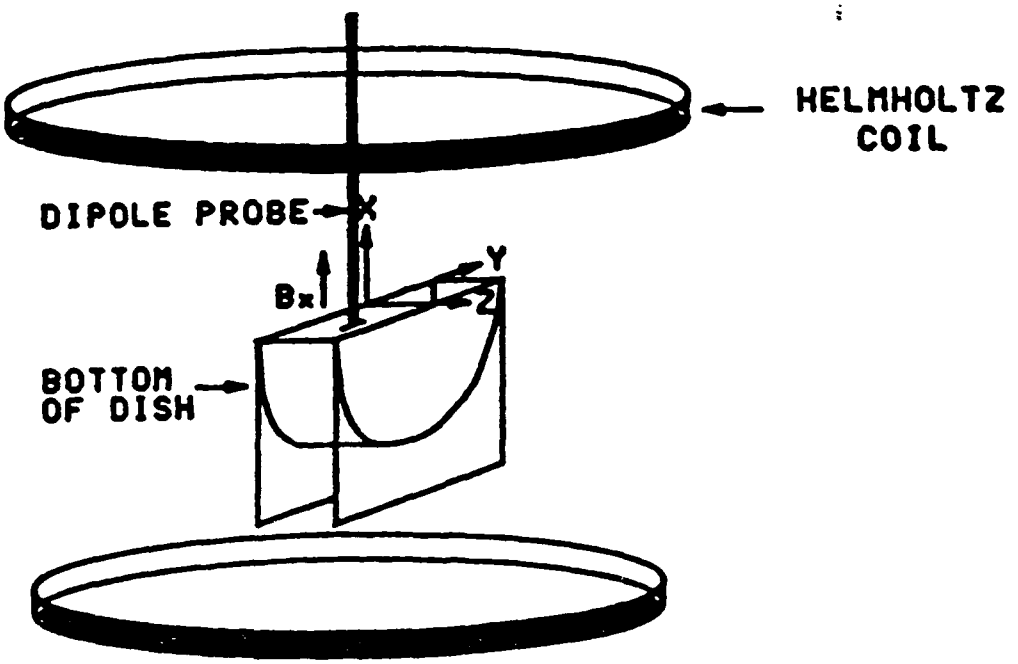

Fig. 16 Cut-out circular container placed within the Helmholtz coil such that the bottom of the container is parallel to the direction of the B-field.

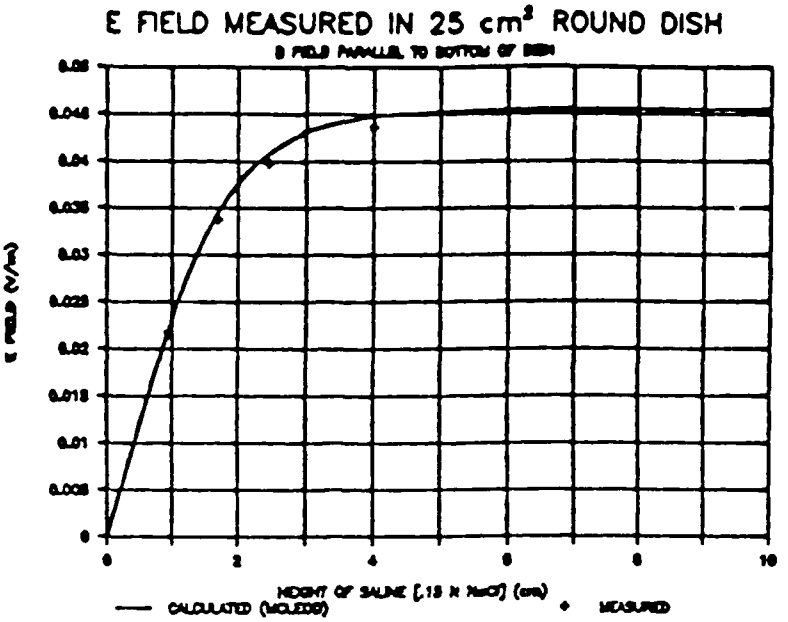

Fig. 17 E-field measured at the botom of cut-out circular containers of increasing height filled with .15 N NaCl with the B-field parallel to the bottom of the container. The solid line represents values calculated using McLeod's results[3].

Fig 17 shows a comparison between predicted and measured E-field values close to the center of symmetry of the container as a function of the height of the liquid.

3.6 Electric field measurements within region with large concentration of cells

A cell suspension, which was considered as a homogeneous medium for the calculation of the induced electric field, is in fact composed of two phases one consisting of a high concentration of cells, which upon settling are in close proximity to one another, and the other consisting of the cell free nutrient medium. A solution consisting of biological cells in suspension is expected to have a large dielectric increment. A highly concentrated solution of packed cells can be said to approach the construct of a tissue. Muscle tissue for example has a dielectric increment of the order of 10^6, on the other hand, its conductivity increment is of the order of 10^{-6} S/m which is negligible compared with its static conductivity value of approximately 0.125 S/m. Therefore, cells which have settled in a nutrient medium, form a two phase system with widely different permittivities and conductivities differing by a small but finite amount. It has also been speculated that due to the volume excluded by the cells, the conductivity of the cell phase should be considerably lower than that of the cell free medium.

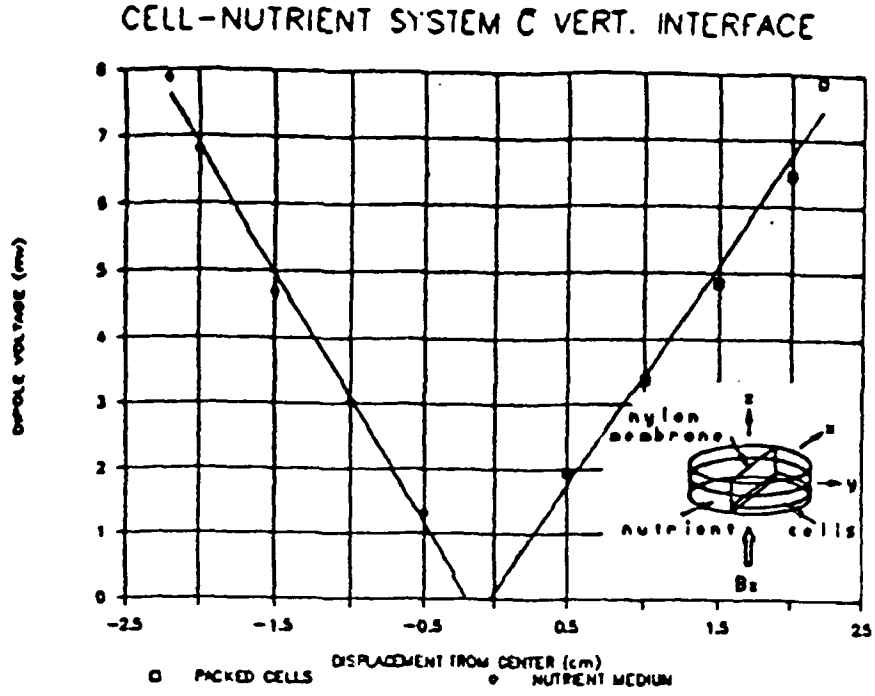

Fig. 18 Variation in the E-field with displacement from the center of the divided container. The right side shows the variation in the volume with the packed cells while the left side shows the variation in the cell free medium.

The two phase nature of a settled cell suspension is important only in the parallel configuration where the electric field lines traverse the interface between the two phases. In this case, charge build up at the interface between the two phases, which occurs if the conductivities are different, can significantly alter the electric field distribution. In order to perform measurements in both phases in the parallel configuration, it was necessary to take into account some practical considerations. The electric field probe currently on hand can be used effectively only when the axis of the probe is parallel to the direction of the magnetic field. In spite of its insulated twisted wire construction with individually insulated leads, when placed perpendicular to the direction of the magnetic field the probe picks up a large extraneous voltage as it cuts through the lines of magnetic field. Therefore, a two phase system allowing placement of the probe parallel to the direction of the magnetic field was needed to perform this measurement. The approach followed was to build a round sample dish separated into two compartments by a 10μ mesh nylon membrane permeable to the ions in the saline solution but not to the biological cells. Measurements were carried out with biological saline in one compartment and a large concentration of HL-60 cells in the other. The cells were allowed to settle for about 30 minutes before performing the measurement. Fig 18 shows the variation of the dipole voltage V, with the displacement R from the center of

the container on both sides of the container. In this case, the slope, $|\Delta V/\Delta R|$, in the cell free medium is somewhat larger than in the medium with cells. Since the fields were measured with a bare dipole probe whose response is sensitive to the characteristics of the medium, the observed difference could be attributed calibration differences in the two media and not necessarily to any variation in the electric field. Further measurements will be conducted using protein gels as analogs for the phase containing packed cells.

4. Dielectric measurements of polyelectrolytes

The response of biological cells to electromagnetic fields can be analyzed on two levels, the response of the cell and its environment, and the response of components internal to the cell. Amongst these components is deoxyribonucleic acid (DNA) which contains the genetic code vital for cell survival and proliferation. DNA is present in the cell as a charged macromolecule in solution forming a polyelectrolyte. In common with other polyelectrolytes it contains a condensed ion layer the nature of which is dictated by the distribution of charges along the entire molecule, that is the charge density. The effect of the condensed ion layer on energy absorption as a function of frequency can be studied can be studied through dielectric measurements.

Two dielectric cells were designed for this purpose, one to cover the range between 100 Hz and 40 MHz and the other for frequencies above 45 MHz. The low frequency cell was used with a Hewlett Packard 4194A Impedance/Gain Phase Analyzer, while the high frequency cell was used with a Hewlett Packard 8510 Network Analyzer. The low frequency cell is a capacitive cell made after a design used by Dr. K. Foster. This cell has platinum electrodes coated with platinum black to minimize electrode polarization. Temperature control is provided by a circulating bath surrounding the sample chamber. The high frequency cell is of the coaxial type and was designed based on a GR-900 connector. The cell design was described in the second annual report. The GR-900 connector is rated to operate up to 8.5 GHz, however, measurements indicated that this cell provides adequate performance only up to 1.5-2 GHz.

Polyelectrolytes have common features which can be investigated by studying particular compounds. Since synthetic polyelectrolytes are easier to purify and handle, all measurements during this reporting period were conducted using synthetic compounds. To gain familiarity with the available dielectric measuring systems, measurements with potassium (K) polyvinyl sulfate were carried out between 100 Hz and 2 GHz. At frequencies below about 50 KHz the calculated values of the permittivity were in error due to electrode polarization which persisted in spite of using electrodes coated with platinum black. Conductivity measurements appeared to be mostly unaffected by this problem. Solutions containing 0.1%, 0.2%, and 0.4% of the polymer

were measured. As expected, the low frequency conductivity increased linearly in proportion to the concentration of the polymer. Some difficulties were also encountered with the permittivity measurements at frequencies above 10 MHz associated with self-inductance of the low frequency cell. This problem was corrected for by using a feature of the HP 4194A which permits calculation of elements of the equivalent circuit of the dielectric cell. Problems with the high frequency cell were related to loss of calibration which caused straneous resonances at frequencies greater than about 1.5 GHz. In some cases, the data obtained with the low frequency cell did not match well with that obtained with the high frequency cell at the cross over frequencies. These errors were not easy to eliminate, however, careful measurements diminished the problem. Since the measurement of interest was the dielectric increment, or alternatively the conductivity decrement, relative measurements were sought with reference to a NaCl salt of equivalent low frequency conductivity. To this end, dielectric measurements were conducted on various NaCl solutions. The dielectric increment vs. frequency of K polyvinyl sulfate relative to NaCl salts of equivalent low frequency conductivity shows two well defined relaxations with center frequencies at approximately 1 MHz and 50 MHz. A third relaxation at higher frequencies is also apparent. Clearly, a definite determination of these relaxations requires fitting of the data to an appropriate model.

The emphasis of this work has been to attempt to explain the dielectric relaxations observed in polyelectrolyte solutions in terms of the well known phenomenon of counterion condensation. Counterion condensation is a characteristic property of polyelectrolytes. Its occurrence was originally predicted by Oosawa[4], but it was Manning[5] who provided a more complete theory on the basis of which a wide range of thermodynamic and physical properties of polyelectrolytes can be derived.

In an environment containing a single species of counterions, condensation depends solely on the valence of the counterions and the charge density parameter ξ defined as

$$\xi = e_o^2/\epsilon kTb \qquad (1)$$

where e_o is the protonic charge, ϵ is the permittivity of the solvent, k is Boltzmann constant, T is the Kelvin temperature, and b is the average spacing between charged sites on the polyion. Condensation occurs when the condition $\xi \geq 1/z$ is met.

When electroneutrality of the polyelectrolyte is provided by monovalent counterions, the theory predicts counterion condensation will occur when the axial charge density parameter ξ reaches the critical value $\xi = 1$, below this value no condensation is expected. Since ξ is inversely proportional to the permittivity ϵ of the

solvent, variations in ϵ can provide a means of changing the axial charge density thus allowing the study of dielectric properties of polyelectrolyte systems in terms of counterion condensation. Similarly, changes in the charge spacing b or the temperature T also lead to changes in ξ. Since T is the absolute temperature, ξ is not very sensitive to changes in T within ranges not causing depolimerization. The charge spacing b can be changes for instance by changing the pH of the solution which changes the degree of neutralization.

4.1 Determination of counterion condensation by measurements of the static conductivity

In order to investigate to investigate the nature of the dielectric relaxations in terms of counterions condensation it is of particular interest to perform measurements at under conditions points close to the critical point for condensation. Thus, it is first necessary to device a means to show the occurrence of this phenomenon. The objective of this work was to attempt to demonstrate the occurrence of counterion condensation by measurements of the static conductivity

Experimental measurements of the activity coefficients of solutions of polyelectrolytes with added salts have lead to the conclusion that the activity of counterions can be expressed as the sum of independent contributions from the counterions from the polyelectrolyte and the added salt[6]. Similarly, the conductivity of the solution is the sum of the conductivities due to the pure electrolyte and the pure salt. The static conductivity of the pure electrolyte is due to free ions, that is ions not trapped or condensed in the potential well from the combined coulombic fields of the charges on the polyelectrolyte. Since theory predicts that condensation is a threshold phenomenon, the static conductivity of a polyelectrolyte solution measured as a function of the degree of ionization α should show a discontinuity at the critical value of α corresponding to $\xi = 1$. Two approaches were followed to attempt to demonstrate the occurrence of counterion condensation through measurements of the static conductivity, these are described below.

4.1.1 Control of the magnitude of the charge density parameter through changes in the permittivity of the solvent

A solvent which can provide continuous variability in ϵ in the range 33 to 80 is the methanol-water system. Dielectric measurements of methanol-water mixtures with NaCl were conducted in order to investigate the behavior of the conductivity of these systems due to the addition of simple salts. Knowledge of this behavior is important to the understanding of the dielectric response of polyelectrolytes in methanol-water mixtures since changes in ϵ cause not only changes in the axial charge density of the polyelectrolyte but also in the conductivity of free ions.

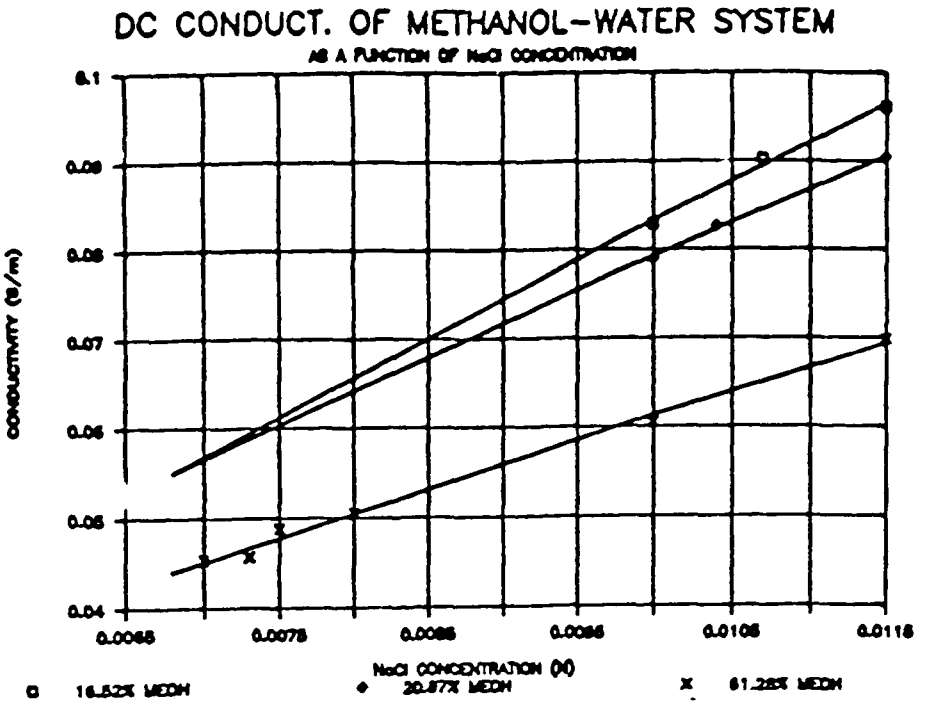

Fig. 19 DC conductivity vs. NaCl concentration for solutions containing 16.52, 20.87, and 61.28 weight percent methanol in water.

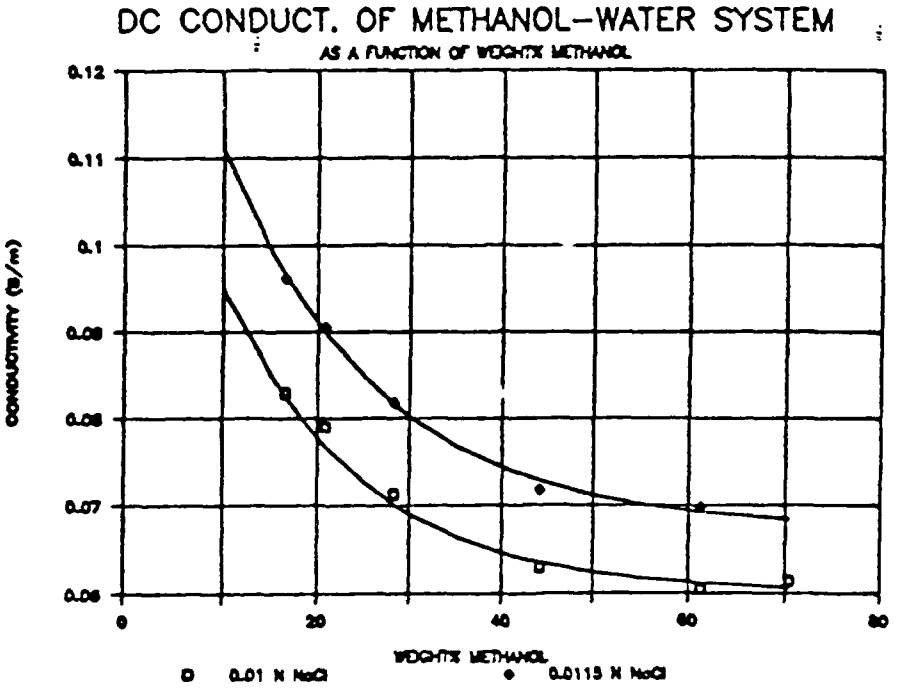

Fig. 20 DC conductivity vs. weight percent methanol in aqueous solutions containing 0.01 N NaCl and 0.0115 N NaCl.

solutions containing 0.01 N NaCl and 0.0115 N NaCl.

Low frequency (<600 Hz) conductivity data for methanol-water mixtures with NaCl yielded relationships which were generally linear as a function of the salt concentration for solutions with a fixed proportion of methanol. For a given salt concentration, the data for conductivity as function of weight percent methanol in water was fit to an equation of the form $\sigma = a + b\, e^{-cw}$ where σ is the conductivity, w is the weight percent methanol, and a, b and c are constants. These results are shown in Figures 19 and 20.

To show the occurrence of counterion condensation conductivity measurements were carried out with 6-6 Ionene bromide, a positively charged polyelectrolyte, dissolved in mixtures of methanol and water in which the weight percent of methanol ranged from about 16 to about 70. These measurements were carried out using the low frequency cell and the HP 4194A Impedance/Gain Phase Analyzer. The break in conductivity expected at $\xi=1$ was not observed. This was attributed to possible contamination of the stock sample of the polymer. Future measurements will be made with newly purified samples.

4.1.2 Control of the magnitude of the charge density parameter through changes in pH

The charge density parameter can also be varied by changing the pH of the solution which changes the degree of neutralization. To demonstrate the occurrence of counterion condensation through pH variations, measurements were conducted using sodium polyacrylate solutions. In order to obtain a stable pH the polyacrylic acid was dissolved in appropriately selected buffers.

The polyacrylic acid solutions used in these measurements were prepared as follows. A stock solution of sodium polyacrylate (NaPA) was prepared by dissolving equal molar amounts of polyacrylic acid and sodium hydroxide in deionized water. The resulting solution was passed through an Amberlite IR-120 ion exchange column and subsequently dialyzed for three days with three water exchanges. The concentration of NaPA after dialysis was estimated at .4%. Ten pH buffer solutions were prepared with nominal pH in the range 3.8 to 8.0. The actual pH values measured with a Fisher pH meter fell within 2% of the nominal values. Buffers with pH 3.8, 4.7, 5.2, and 5.6 were prepared using a sodium pthalate buffer. Buffers with higher pH's were prepared using a sodium phosphate buffer. In both cases the buffer strengths were chosen to provide adequate buffering capacity. The samples tested were prepared by mixing the NaPA stock solution with the buffer solutions in a 1:1 proportion by volume and then diluting the mixture 1:1 with deionized water. Sample buffers of equivalent ionic strength were also prepared by substituting deionized water for NaPA in the first dilution step.

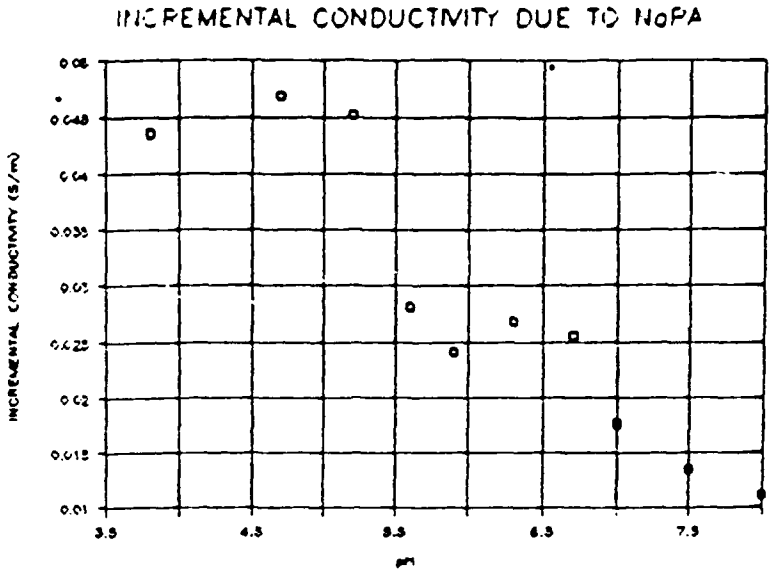

Fig. 21 Incremental conductivity due to the presence of Na polyacrylate (NaPA) as a function of pH in pH buffered NaPA solutions.

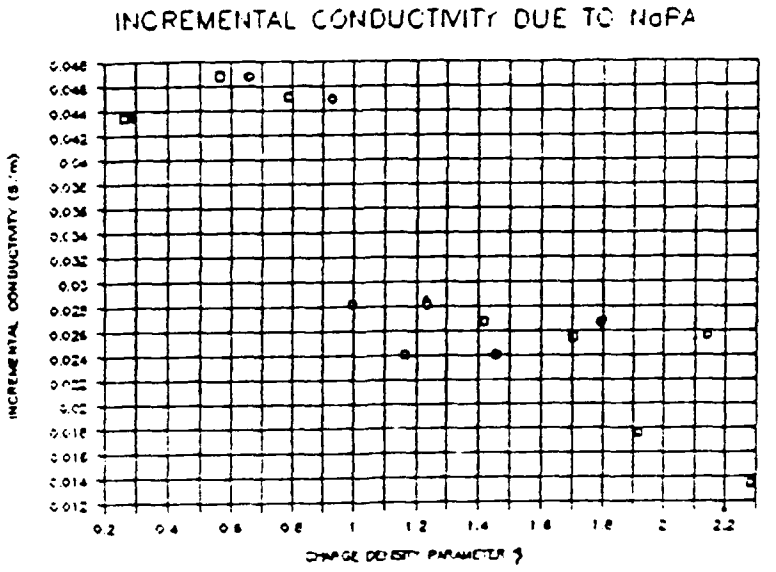

Fig. 22 Incremental conductivity due to the presence NaPA as a function of the axial charge density parameter ξ in pH buffered NaPA solutions.

The conductivity measurements were carried out using the low frequency dielectric cell and the HP 4194A Impedance/Gain Phase Analyzer (IGPA).

Since the additivity rule is considered a good approximation to the total conductivity of polyelectrolyte solution with added salts, the contribution to the conductivity due to the presence of the polyacrylic acid in the buffer solutions was calculated as the incremental conductivity over that measured for the buffer solutions without the polyacrylic acid. The conductivity of the buffer solutions increased from 0.19 S/m for the buffer with the lowest pH (3.8) to 0.39 S/m for the buffer with the highest pH. As shown in Fig. 21, the incremental conductivity is approximately constant for pH values below pH 5.5 showing a sharp discontinuity above this value. Knowing that the pH changes the value of the charge density Ç, it is reasonable to assume that this break in the incremental conductivity corresponds to the onset of counterion condensation.

For weak polyacids, such as polyacrylic acid, the pH can be calculated using the following equation (Alexandrowicz and Katchalsky[7])

$$pH = pK_o + \log[\alpha/(1-\alpha)] + \Delta pK \qquad (2)$$

where pK_o is the dissociation constant of the ionizable group of the monomer, α is the degree of ionization, and ΔpK is incremental value of the dissociation constant due to the polyion. The measured conductivities of the buffer solutions were used to calculate the equivalent salt (NaCl) concentration, C_{eq}, of each buffer, by applying the empirical relations of K et al [] The values of C_{eq} were found to be in the range 0.019 M/l to 0.039 M/l. The monomeric concentration of the polymer was estimated to be 0.1% in each sample corresponding to 0.0106 M/l. Under these conditions the polyion is present in excess salt, therefore, curves shown in ref [7] which relate ΔpK to the degree of ionization were used to calculate equations (fourth order polynomials) of ΔpK vs α for each buffer solution. Knowing the pH of each buffer, eq(2) was solved iteratively for α. The corresponding values of ξ were calculated using $\xi=2.85\alpha$ (Manning[8]). Fig 22 shows the incremental conductivity as a function of the charge density. Counterion condensation is seen to occur above $\xi=1$.

Dielectric data as a function of frequency for each sodium polyacrylate buffered sample will be analyzed in a future report in light of the conductivity data showing the occurrence of counterion condensation.

References

[1] J. Juutilainem, M. Harri, K. Saali, T. Lahtinen, "Effects of 100-Hz magnetic fields with various waveforms on the development of chick embryos", Radiation and Environmental Biophysics, 25, 65-74, 1986.

[2] R. Goodman, C. A. Basset, A. S. Henderson, "Pulsing electromagnetic fields induce cellular transcription", Science Magazine, 220, 1283-1285, 1983.

[3] B. R. McLeod, A. A. Pillar, M. W. Sampsell, "Electromagnetic fields induced by Helmholtz coils inside saline filled boundaries", Bioelectromagnetics, 4, 327-370, 1983.

[4] F. Oosawa, Journal of Polymer Science, 3, 421, 1957.

[5] G. S. Manning, "The molecular theory of polyelectrolyte solutions with applications to the electrostatic properties of polynucleotides", Quarterly Review of Biophysics II, 2, 179-246, 1978.

[6] F. Oosawa, Polyelectrolytes, Marcel Dekker, New York, 88, 1971.

[7] Z. Alexandrowics, A. Katchalsky, "Colligative properties of polyelectrolyte solutions in excess salt". Journal of Polymer Science: Part A, 1, 3231-3260, 1963.

[8] G. S. Manning, "Limiting laws and counterion condensation in polyelectrolyte sclutions: I. Colligative properties", The Journal of Chemical Physics, 51, 924-933, 1969.

CHAPTER IV

EXPERIMENTAL BIOLOGICAL STUDIES

Biological research in Project Year 3 was centered on: (1) an investigation, using 2-D gel electrophoresis analysis, of possible ELF (extremely low frequency)- and microwave-induced alterations in synthesis of specific proteins; (2) examination of possible ELF enhancement of specific mRNA synthesis; (3) experiments centering around the enhancement of total RNA synthesis after short term ELF exposure; and (4) investigation of the role of ELF and microwave exposure to alterations in specific activity of the enzyme ornithine decarboxylase. Two of these areas, (3 and 4) have revealed interesting effects which promise extensive opportunities for further investigation. The other two areas of research have revealed no field-specific effects, and will be terminated unless new avenues of investigation can be opened.

1. Effect of microwaves and ELF on protein translation

Methods:

HL-60 cells, at $3x10^6$ per dish, were plated into culture dishes in Eagle's Minimum Essential Medium with 10% fetal bovine serum (complete MEM). Dishes for ELF exposure in a solenoid device were of a concentric ring design, fabricated by gluing acrylic cylinders into a standard 60 mm culture dish. Such "fabricated" dishes provided two concentric chambers, one defined by walls positioned at radii of 6.4 and 11.1 mm, and the other by walls at 22.8 and 27 mm. These chambers were designed for experiments in which two cell populations, each exposed to a different, but defined, electric field could be exposed simultaneously to an identical magnetic field. For the purposes of the 2-D electrophoresis experiments only the outermost chamber, where electric field strength was highest, was used. Standard 25 cm^2 culture flasks were used for microwave exposures in a Crawford cell.

The medium in which cells were plated varied with the particular experimental procedure. In some instances cells were plated in complete MEM and irradiated for 30 min to 3 hr, with the medium being then replaced by methionine-deficient MEM plus 30 μCi/ml ^{35}S-labeled methionine for 30 to 90 min. of continued exposure in the Crawford cell or solenoid. For shorter term exposures, 45 to 90 min, cells were plated directly in the labeling medium immediately prior to onset of irradiation. Under conditions where cells were to be continuously labeled for several hours the labeled methionine was added to complete MEM so that incorporation

of the label would occur gradually during the duration of the experiment. In some ELF experiments cells were exposed to 0.1 or 1 G magnetic fields for 16 hr before labeling, and an additional 1 hr in the field with isotope labeling.

ELF exposures were at 0.1, 1, 5 or 10 Gauss magnetic fields with modulation at 60 Hz. Crawford cell exposures were done using 0.9 GHz microwaves, with 80% amplitude modulation at 60 Hz and an SAR of 2 mW/g.

Two-dimensional gel electrophoresis was conducted according to the methods of Hochstrasser et al (1988). Briefly, first dimension samples were isoelectric focused using a pH gradient of 3-10. For analysis of alkaline proteins some samples were separated under non-equilibrium conditions of isoelectric focusing to prevent the breakdown of the alkaline portion of the pH gradient which occurs under the normal focusing procedure. The first dimension tube gels were then equilibrated with SDS-containing sample buffer, laid onto 10% polyacrylamide slabs and separated according to molecular weight. Gels were equilibrated in a water soluble fluor, dried under heat and vacuum, placed into contact with X-OMAT RP X-ray film for 3-5 days, and fluorographs obtained. The 2-D fluorographs were analyzed with a Visage 60 computer densitometry system which allowed spot matching and comparisons between matched experimental and control specimens.

Results:

Sample to sample accuracy of the gel analysis system was checked by running four aliquotes of a single sample, preparing 2-D gels from each and analyzing with the Visage 60. One sample was chosen as the standard, and ten spots compared for integrated intensity between it and the other three samples. Average factor differences for integrated intensities of the ten spots for the three comparisons were: 1.3066 ± 0.2240, 1.1194 ± 0.1786 and 0.9876 ± 0.1240. These results indicated that differences in spot integrated intensities of less than 20% were not significant by these methods, but that differences of 50% or more should be considered critically as representing possible field-induced translational differences. To allow for slight differences in overall loading of samples from different specimens a normalizing function, built into the computer program, was sometimes used. This allowed overall alteration of one set of averaged spot integrated intensities to match that of another gel, compensating for loading error, and allowing a search to be conducted for those protein spots considerably enhanced relative to those on the other gel.

Twenty-five experiments were conducted and evaluated for translational effects of ELF or microwave exposure. Eight two dimensional gels were run for each experiment, with duplicates for each of four samples. Duplicate gels were compared by eye and the

gel offering the best resolution of a pair was selected for computer analysis. Most experiments were evaluated using a 3-10 pH gradient in the first dimension. Such gels yielded between 700 and 900 labeled spots, but the protein spots in the alkaline Pi region were typically streaked and poorly resolved. This situation is common with standard 2-D techniques, due to breakdown of the pH gradient during the extended time period required for proteins to focus (Cellis and Bravo, 1984). To achieve better resolution of the alkaline region both standard 2-D and also non-equilibrium gels were run for the same samples.

None of the fluorograms from the different experiments displayed any consistent, significant differences in radiolabeling of specific polypeptides when comparisons were made between experimental and control samples. Where dramatic differences in integrated intensities for spots were reported from computer analysis, carefyk sude-by-side examination of the two gels showed that the result was due to failure of the computer to resolve two spots on one of the gels, thus adding the intensities of two spots into one on its report, or from similar differences that arise in resolution between two different gels. Thus, within the limits of the system, no differential synthesis for particular polypeptides could be accounted for on the basis of exposure to ELF or microwave fields.

To determine that changes in differential protein synthesis could, in fact, be detected by the 2-D system employed, an experiment utilizing heat shock was conducted. HL60 cultures were subjected to heat shock conditions of 42° C for 90 min. with subsequent ^{35}S-methionine labeling of proteins for a 2 hr interval following the heat shock. Analysis of the resulting fluorograms illustrated 2 to 4 times enhanced synthesis of 5 heat shock proteins, all in the acid to neutral Pi range, by experimental relative to control samples, with other proteins showing equivalent integrated intensities and so showing unvaried synthesis rates. These differences in translation were readily detectable with the Visage 60 system, and serve to substantiate the lack of enhancement of translation we observed for ELF or microwave exposed cultures.

To assess whether overall protein synthesis, as contrasted to that for specific proteins, might be elevated in exposed cells a series of specific activity measurements was conducted, examining incorporation of labeled methionine into total cell protein under conditions of ELF (10 Gauss, 60 Hz, 1, 2, 3 and 5 hr) or microwave (1 or 3 SAR, 2.5 and 5 hrs) exposure. In each case examined the incorporation of labeled methionine into total cell protein for experimental specimens was within a range of 0 to 15% of that measured for controls. There were, thus, no indications that alteration of translation, either for individual polypeptides, or for total cell protein, was produced by exposure of cells to ELF or to modulated microwaves.

2. Effect of ELF on synthesis of specific mRNA

Work that has been reported by others at national meetings, and has been, to date, published in abstract form (see Wei, et al, 1989; manuscript by same authors , Biochimica Biophysica Acta, in press) has indicated that exposure to ELF fields can enhance the synthesis of particular mRNAs by factors of three to four fold after exposure times of less than 30 min. We have sought to clarify and extend these observations by examining the relative levels of the mRNAs for the c-myc, histone H2B and actin genes after exposure to a range of ELF field conditions. The goal of this work was to examine alterations in synthesis by ELF signals, and then to extend these observations to conditions of continuous wave and modulated microwave exposures.

Methods:

HL60 cultures were plated in concentric rings of the fabricated annular dishes at cell densities of 10^7 cells per chamber. Dishes were exposed in a solenoid device to 60 Hz ELF fields ranging from 0.1 to 10 Gauss, for time periods ranging from 10 min to 8 hr. Control cultures were maintained in the same incubator chamber, but positioned outside the solenoid where measurements had indicated that no measurable fields from the solenoid were present. Alternatively, a second exposure system using Helmholtz coils was employed. In this system 1.2×10^7 cells were placed into 60 mm diameter petri dishes for exposure. Since positioning of the coils was vertical, relative to the bottom of the culture dish, annular chambers were not necessary in this system which provides relatively constant electric fields across the cells' growth surface. Exposure conditions for the Helmholtz system ranged from 0.01 to 10 Gauss, 60 Hz, for 10 to 40 min.

Following exposure cultures were harvested, washed in PBS and either stored as frozen pellets or processed immediately for RNA extraction. Initial RNA extractions were done using a "chaos" buffer technique in which cells were lysed in a buffer containing 4.2 M guanidinium salts, 25 mM Tris, pH 7.5, 0.5% sarkosyl and 100 mM β-mercaptoethanol. RNAs were then extracted with phenol:chloroform and precipitated with isopropanol. Early in the grant year, however, a new RNA extraction procedure was employed based on the method of Chomczynski and Sacchi (1987). This method proved not only more rapid, but yielded approximately 4 times more RNA per cell pellet, and so has been used routinely for all subsequent work.

Extracted RNAs were blotted onto nylon membrane using a "dot blotting" device. Each sample was blotted six times, with each blotting employing successive 2-fold dilutions to provide dots corresponding to 4 to 0.13 μg total RNA. Blots were probed under hybridizing conditions with ^{32}P-labeled cDNAs for the mRNAs of the c-myc, histone H2B and actin genes. Following hybridization, blots

were washed and processed by exposing them to XOMAT-AR5 film at -75° C with an intensifying screen. Developed autoradiograms were scanned with a Visage 60 densitometric system for analysis of the integrated intensity of each spot. The series of dilution spots chosen for analysis was selected by determining which series were within the liner range of response of the film relative to spot densities. Individual probes were removed from blots by incubation at 65° C in buffer containing 5 mM Tris-HCl, pH 8.0, 0.2 mM EDTA, 0.05% pyrophosphate and 0.1X Denhardt's reagent; blots were then reprobed with other cDNAs.

Repeatability of the dot blot system was tested by preparing several identical cell pellets and processing each pellet individually, or by preparing replicate samples from a single RNA extraction. In either case the range of error for amount of cDNA probe bound to the identical specimens in a series was found to be ± 20%. Thus, differences in results in the range of 1.5 - 2 times for a specific message would be readily detected.

For experiments done in the Helmholtz coil system, and some with the solenoid system, RNAs were dot blotted, as above, but samples were additionally separated electrophoretically in an agarose gel system prior to blotting. Such "Northern" blots allowed not only an assessment of the relative binding of cDNA probes to a sample, but provided assurance that binding is to an mRNA of the appropriate molecular weight. Except for the electrophoresis step and blotting onto the nylon membrane, all processing steps were the same as for dot blots.

Results:

ELF exposures performed in the solenoid system provided for comparisons of samples simultaneously exposed to the same magnetic field, but to two different electric fields, by use of two cultures in separate concentric chambers of the fabricated culture dishes. Exposure times ranging from 10 min to 8 hr, and 60 Hz fields ranging from 0.01 to 10G were employed. Although particular samples in a given experiment showed occasional variation in the amount of cDNA probe bound relative to control samples, none of the many experiments conducted gave any results that were interpretable as showing any consistent transcriptional effect related to intensity of either the magnetic or electric fields. Typical results are presented in Figure 1A, in which it is seen that minimal variation occurred in the amount of probe bound when experimental and control samples from a given time point were examined.

Exposures using the Helmholtz coil system likewise showed no time-dependent pattern of alterations in specific mRNA levels (Figure 1B). Field intensities in these experiments ranged from 0.01 to 1.0 Gauss, bracketing the range of magnetic field strengths (0.1 Gauss) calculated to be used in a series of experiments for

which 3-4-fold enhancements of specific mRNAs were reported (Wei, et al, 1989; and manuscript in press, Biochemica and Biophysica Acta).

Northern blot analyses of the RNAs from both solenoid and Helmholtz coil exposures also showed no differences in binding of specific probes (Figure 1C,D). These experiments did, however, serve to confirm the specificity of the probes for mRNAs of the correct molecular weight. In some cases it was found that a probe displayed binding to rRNA species in addition to its specific mRNA. This was found to be the case for the c-myc probe, which displayed some binding with the 18S and 28S rRNA species. Such non-specific binding would not be discriminated in the dot blot system, and so would provide background signal since no electrophoretic separation is done prior to hybridization.

These results contrast with those we obtained early in the work in which an approximate 2-fold enhancement of c-myc message was reported after 45-60 min exposure to a 10 Gauss, 60 Hz field. We have found that these results were inconsistent, however, and probably reflect errors connected with the initial learning and standardizing of technique. As the experiments became routine, such differences in labeling were eliminated. By this time there have been many well controlled experiments, conducted with a variety of exposure conditions. None of these experiments has shown any consistent effect of ELF fields on transcription of specific messages.

3. Effect of ELF on synthesis of total cellular RNA

Published work, based on studies of dipteran salivary glands, has provided evidence for enhanced synthesis of mRNAs as a result of ELF exposure (Goodman et al, 1983; Goodman et al, 1986; Goodman et al, 1987). This was shown by differential RNA puffing of specific salivary chromosome bands, and by sucrose density gradient analysis of cellular RNA, for tissue exposed to ELF signals of the type used to enhance bone healing. The results from the sucrose density technique were particularly intruiging, since the incorporation of tritiated uridine was enhanced in the portion of the gradient corresponding to mRNA, but not in the regions which correspond to the major rRNAs. Similar RNA analyses, done with mammalian HL60 cultures, have been reported at national meetings by the same authors. Such results would indicate that ELF fields selectively influence translation of mRNAs but not rRNAs.

In conjunction with our analysis of the synthesis of specific mRNAs, as discussed above, we decided also to investigate the synthesis of total cellular RNA and the influence of electromagnetic fields upon it. The goals of our experiments were to replicate known ELF effects, investigate the basis of these effects, and then extend the experiments by examining alterations in transcription produced by microwave exposures. The techniques

employed also promised an alternative method to investigate which, if any, specific categories of RNAs were influenced by electromagnetic fields.

Methods:

HL-60 cells were exposed to 60 Hz ELF fields using a solenoid device in which the magnetic fields, oriented perpendicular to the cells' growth surface, were of constant value throughout the dish, but the electric fields varied from 0, at the center of each dish, to values increasing linearly with the radius. Initial exposures were done with $8x10^6$ cells, in complete Minimum Essential Medium, plated into 60mm diameter petri dishes. Experimental cultures were exposed to 10 Gauss magnetic fields for periods up to 4.5 hr, and in some instances to 24 hr. Control cultures were placed in the same incubator chamber outside the solenoid. Dishes were placed sequentially into the incubator so that samples for all time points would complete their exposure/control times simultaneously. Cells were pulsed with ^3H uridine (20 μCi/mL) for the final 15 min. At the end of the labeling period cells were harvested, washed twice with cold phosphate buffered saline (PBS), lysed with a 0.5% SDS buffer, and the RNA precipitated with 10% cold trichloroacetic acid. Lysates were collected on filters and counted in a liquid scintillation counter.

Subsequent experiments were performed in similar fashion except that the dishes with concentric, annular compartments were used to provide chambers in which cells would experience relatively defined electric fields. These dishes consisted of either the fabricated dishes with concentric chambers (described above) or organ culture dishes which contained a central well with a radius of 9 mm, surrounded by an outer well with its inner wall positioned at 12 mm, and its outer wall at 32 mm along the dish's radius. With such annular dishes $4x10^6$ cells were placed into each chamber.

For some experiments RNAs, in formamide and formaldehyde, were fractionated by separating them electrophoretically in an agarose gel, and then slicing the gel into multiple pieces along the axis of separation using a device holding several razor blades. These agarose slices were placed into scintillation fluor, melted in a microwave oven, and counted in a liquid scintillation counter. Sizing of the RNAs in each slice was done by comparison with the relative mobilities of RNA standards run in adjacent lanes of the same gel.

Results:
Pulse Labeling of Total RNA

Initial results, exposing cells in 60mm petri dishes to 10 Gauss, 60 Hz fields, indicated an enhancement of transcription to occur in exposed cultures. Between 0.5 and 1 hr following onset of irradiation, incorporation of ^3H uridine into the RNA of exposed

cells was enhanced by 35-55% over control values. This elevated transcription declined by 2 hrs, but increased to near maximal values by 3 hrs before declining again. Such experiments were subsequently conducted over exposure periods ranging to 24 hrs. Results of such longer exposures, shown in Figure 2, indicated the enhanced incorporation of label is transient, reaching control values by approximately 20 hrs exposure. These experiments were all done using the standard 60 mm culture dish, without cocentric compartments.

These results indicated a definite effect of the electromagnetic field on RNA metabolism. Given the radially-varying electric field produced in the solenoid exposure system, it was decided to conduct subsequent experiments using culture dishes in which concentric annular chambers were present. Such dishes would provide for 2 experimental cultures, each exposed to a uniform magnetic field but to different electric fields. Small widths of the annular chambers would mean that cells within the chamber would experience limited variance in the electric field. Most such experiments were done using standard organ culture dishes, but some were done with the fabricated 60 mm culture dishes.

Results from an experiment done in the organ culture dishes are shown in Figure 3A. Cells in the outermost well, experiencing an electric field of 1.5 mV/m, showed higher incorporation of labeled uridine, relative to controls, than did cells in the inner well, which were exposed to the same 10 Gauss magnetic field, but an electric field of 0.33 mV/m. Similar results were obtained with two cell populations placed into concentric annular chambers in the fabricated dishes, except that the spatial separation of the two chambers was not sufficient to give such large differences in electric fields, and differences in incorporation of tritiated uridine were, correspondingly, not as pronounced.

Data from this work indicated that the electric field may be the major factor in determining the rate of transcription since the magnetic field was constant for the two ELF-exposed cell populations. In order to verify this hypothesis exposures were done using cells placed in the outermost well of the culture dishes, but with the magnetic field lowered to 1.0 Gauss, so that the electric field in the outer chamber would approximate the 0.33 mV/m field produced in the inner chamber when a 10 Gauss ELF exposure was used. Results from these experiments are shown in Figure 3B. Enhancement of transcription for inner and outer wells was almost identical when both received identical electric fields, but different magnetic fields. Considered in conjunction with the results from comparisons of inner and outer wells at the same magnetic fields, these data provide strong evidence that alteration in transcription is directly related to the strength of the electric field applied to the cells.

RNA Fractionation

The above experiments were conducted using the incorporation of ^{3}H-uridine into total cellular RNA as the endpoint. Experiments were initiated to determine which of the RNA species accounted for the enhanced synthesis. Fractionation of cellular RNA was accomplished by electrophoresis on an agarose gel, slicing the gel into fragments corresponding to the migrations of RNAs of known sizes, and analyzing the distribution of incorporated ^{3}H-uridine into different RNA fractions.

Examinations of control cultures showed that incorporation was initially highest in a 45S RNA species, but that label was found to shift from the 45S to 28S, 18S and 5S peaks if labeling were prolonged (Figure 4). Although several RNA species are found in the 5S range, making interpretation of the 5S labeling problematic, the time-dependent shift from 45S to 13S and 28S species is typical of the processing of the rRNA 45S precursor species into 18S and 28S rRNAs. Other than these rRNA species and the 5S peak, no major RNAs were resolved, in correspondence to the fact that rRNA constitutes approx. 85% of total RNA synthesis, and that there is a wide range of molecular weights for the many different mRNAs.

The gel fractionation system was utilized to determine whether the rRNA species labeled would display differential transcription in ELF-exposed cultures. This was found to be the case, as is shown in Figure 5. Cultures exposed to 60 Hz, 10 Gauss fields for 60 min, and labeled for the final 15 min of exposure followed by a 15 min chase period, showed higher incorporation of label into the 45S peak than did control cultures. When the chase period was prolonged for 120 min the exposed cells showed higher incorporation of label into 18S and 28S rRNA peaks than did controls, but the label in the 45S peak had diminished.

These results show that the major fraction of the enhanced transcription observed for cells exposed to 10 Gauss, 60 Hz electromagnetic fields can be accounted for by the synthesis of the 45S rRNA precursor, and its processing into 18S and 28S rRNAs.

Continuous Labeling of Total RNA

Since the enhanced incorporation of label into RNA occurred for a pulse administered during the final 15 min of 45-60 min of ELF exposure, it was decided to examine the effects of continuous labeling of cellular RNA during 30-120 min exposure periods. Accordingly, cultures were continuously labeled during the entire period of irradiation. Results of such a continuous labeling experiment are shown in Figure 6. Under conditions of continuous labeling no differences in total incorporated label were observed between exposed and control cultures for periods ranging from 30 to 120 min.

Given this unexpected discrepancy between incorporation of ^{3}H-uridine by pulse vs continuous labeling techniques, the continuous labeling experiments were repeated several times, in each case yielding the same results. In one instance different cultures were simultaneously pulse and continuous labeled during the same experiment, the results showing that pulse labeling continued to demonstrate enhanced transcription in exposed cells, but that continuous labeling produced no difference with controls. These facts, considered in light of the RNA fractionation data discussed below, have suggested that rate of processing of the 45S rRNA precursor may be accelerated in the field, or that the field may alter rates of RNA degradation. Experiments have been initiated to examine these possibilities during Project Year Four. Preliminary results in which ^{3}H uridine was added to culture medium as a pulse for the final 15 min of ELF exposure, and then chased for various times by replacing the labeling medium with one containing a 1000-fold excess of unlabeled uridine, suggest that exposure conditions accelerate processing of the 45S rRNA precursor (Figure 7). These experiments, however, must be repeated.

4. Effect of microwaves on ODC activity

ELF- or microwave-induced effects upon cell metabolism could be manifested by changes in actual levels of particular enzymes, or other proteins, or by alterations in the specific activities of particular enzymes with no change in their actual quantities. We earlier examined the effect of microwave exposure upon the activities of the RNase L and 2',5'-adenylate synthetase system important to regulation of growth and to interferon/anti-viral response (Silverman, et al, 1983). Results from that work indicated that modest levels of enhancement of RNase L, but not 2,5-A synthetase activity could be obtained in L929 cultures. The conditions of exposure employed, utilizing a wave guide system, required that cells be maintained in suspension culture for the duration of exposure (2.45 GHz, continuous wave, SAR of 300 mW/G, 4 hr, heating prevented by a temperature controlled circulation bath). When monolayer cultures of L929 and HL60 cells were exposed using a Crawford cell (0.9 GHz, continuous wave, SAR limited to 3 mW/g to avoid heating), however, no statistically significant alterations for either enzyme activity were found. These results suggested that removal of cells from monolayer augmented RNase L activity slightly, and that microwave exposure further accentuated this increase.

The enzyme ornithine decarboxylase (ODC) was chosen for further investigation of possible field-mediated alterations of enzyme activity. Published work indicates that both ELF fields and 16 Hz amplitude modulated microwaves can enhance activity of ODC in mammalian cultured cells (Byus and Weiner, 1982; Byus et al, 1988). Additionally, ODC activity can be regulated by binding of ligands to cell membrane receptors, with subsequent effects occurring through a second messenger system (Pegg and Williams-Ashman, 1981),

a fact that would be of significance if electromagnetic field effects are primarily manifested at the cell membrane. Phorbol methyl ester (PMA) has been used experimentally as a ligand capable of eliciting elevated ODC response in cultured cells. ODC was also an attractive candidate for study since it is involved with major metabolic pathways for the synthesis of DNA, RNA and proteins.

Work detailed in the previous Annual Report showed that L929 monolayer cultures alter ODC activities in response to progression from stationary through lag to logarithmic growth phases, and that PMA could induce nearly ten-fold increases in ODC activity. Exposures of L929 suspension cultures to microwaves under conditions used for the RNase L work, however, produced no changes in ODC activities from control values. When the Crawford cell became available for microwave irradiation of monolayer cultures, it was decided to extend the ODC work. Results indicate that ODC modulation can be achieved as the result of exposure to amplitude modulated, but not continuous wave, microwave conditions. Cells were also exposed to ELF conditions and assayed for altered ODC activities.

Methods:

ODC Specific Activity Measurements: Cells were removed from culture flasks, washed 3 times in cold PBS and frozen at -70° C for storage. Thawed pellets were suspended in lysis buffer (25mM Tris, pH 7.5, 2.5 mM dithiothreitol, 0.1 mM EDTA, 0.1% Nonidet P-40), and S-10 fractions prepared by centrifugation at 10,000 rpm for 15 min, 4°C. Protein determinations were done by the Bio-Rad coomassie blue method. 100 μg of S-10 sample protein were used in a 250 μL assay mixture including 40 μM L-ornithine, 275,000 dpm L-[^{14}C]-ornithine (approx. 50 mCi/mMole), 4 μM pyridoxal phosphate, 1.25 mM dithiothreitol and 5.0 mM Tris-HCL, pH 7.5. The reaction was carried out by incubation at 37° C, in stoppered test tubes carrying polypropylene wells containing 200 μL of 1M hyamine hydroxide. After 60 min the reaction was stopped by injection of 300 μL 20% TCA through the rubber stopper. Acid-released $^{14}CO_2$ was dissolved in the hyamine hydroxide during a further 30 min incubation at 37° C. The well containing the hyamine hydroxide was removed, the hydroxide neutralized with 5 μL glacial acetic acid, and the well placed into a scintillation vial for counting (Seeley, J.E. and A.E. Pegg, 1983).

Results:

ODC activities were assayed for HL60 cells exposed to 60 Hz ELF, 10 Gauss fields. Over time periods of 0.5 to 6 hr exposure no differences in ODC specific activities were detected between exposed and control samples. Measurements of cell viability, cell numbers and population doubling time for cultures exposed to these conditions up to 72 hr were also found not to vary from control values. These results are in contrast to 2-3-fold enhancements of

ODC activity that have been reported following ELF exposures of other cultured cells (Byus and Weiner, 1982).

L929 monolayer cultures were exposed to microwaves for periods of 2 to 8 hr. Microwave conditions were 0.9 GHz, 60 Hz amplitude modulation (80%) or continuous wave, SAR = 3 mW/g. Each exposed culture was matched with a control maintained in the same incubator chamber but outside the Crawford cell. Results from these experiments showed limited to no differences in experimental and control ODC samples for the 2, 4 or 6 hr. exposures, but 8 hr exposures produced notable results, as shown in Table 2.

Table 2

Exposure Conditions	Ratio ODC Activity, Exposed/Control
8 hr. CW Microwaves	0.93 ± 0.5
8 hr. CW Microwaves	0.82 ± 0.3
8 hr. 60 Hz Mod. Microwaves	2.43 ± 0.5
8 hr. 60 Hz Mod. Microwaves	2.02 ± 0.3

These results indicate that ODC activities can be enhanced by microwave exposure, but that amplitude modulation of the microwave signal is critical for achieving this enhancement. Given the significance of ODC to overall cell metabolism, these results will be confirmed and extended to include additional time points, varied exposure conditions, and the possibility that microwave exposure could enhance the effects of sub-optimal levels of PMA on ODC expression.

DISCUSSION:

Results from the Project Year Three's activities have provided solid evidence for some ELF and microwave field effects, but have shown that no field-related effects can be detected by other assays. Positive results provide leads upon which we are currently expanding work. Negative results will draw certain portions of the project to a close and require anlaysis of our results, relative to those obtained by other researchers, in order to decide whether any aspects of these projects should be continued.

The results showing ELF-enhanced incorporation of labeled uridine into the 45S rRNA precursor and the 18S and 28S rRNAs is of particular interest. Ribosomal RNAs constitute 85% or more of total transcription. It is noteworthy that in published work on dipteran salivary glands (Goodman et al, 1987) enhancements of RNAs in the range expected for mRNAs were reported, but none for the major classes of rRNAs. Since the enhanced rate of synthesis we observed is transient, returning to control values by approximately 20 hr. of exposure, it is not clear what this alteration means in terms of overall cell metabolism, particularly with regard to prolonged ELF exposure. The effect, however, provides solid evidence that it is the electric, and not the magnetic, component of the field which alters cell activity. This fact is exciting, and should aid in further experimental design.

The fact that continuous labeling during exposure does not lead to enhanced accumulation of label in the rRNAs is puzzling and must be analyzed further. Experiments are already in progress to see whether the degradation rate of rRNAs, or the processing rate for the 45S rRNA precursor, are altered by field exposure. Results

from ELF studies will also be extended to microwave exposures, in particular utilizing a comparison of transcription under conditions of continuous wave vs amplitude-modulated microwaves.

In our hands ELF fields, produced using either solenoid or Helmholtz coil systems, have consistently failed to demonstrate any enhancement of specific mRNAs. These data must be reconciled with reports of workers who have reported 3-4 fold enhancement for several different mRNAs after short ELF exposures of HL-60 cells (Wei et al, 1989). Northern blot techniques have been used to verify the specificity of the three cDNA probes used in our experiments, so it is clear that little of the binding we observe in the dot blots can be attributed to non-specific binding of probe to abundant RNA species such as an rRNA. If our results cannot be reconciled with those of investigators who have reported specific mRNA enhancements, we will publish our results since we feel that our attempts to replicate the published data have been thoroughly done and are reliable. This situation would constitute our termination of such experiments.

Similarly, unless new avenues can be found to suggest continuance, the 2-D gel analysis of protein synthesis in ELF and microwave fields will be discontinued. One published work reported alterations in translation of specific polypeptides in response to ELF fields applied to dipteran salivary glands (Goodman and Henderson, 1988). Subsequent work by the same group using HL60 cells, however, has not repeated these results in a clear way and has led to questions regarding the repeatability of the analysis, which was done commercially (Goodman, personal communication). Examination of the published gels for the dipteran work raises questions about the appropriateness of using numerical data from computer analysis without the subsequent careful examination and editing of the detailed gel images. These facts cast doubt upon the reliability of the dipteran work.

Results given in earlier Annual Reports documented minor microwave-stimulated enhancement of one of two enzymes which are part of an interferon-stimulated system in mammalian cells. These data were interesting, and have been submitted for publication, but were felt to be of limited value due to technical limitations of the exposure system and the fact that cells had to be removed from monolayer to elicit the effect. In this report we have detailed our extension of earlier work on another enzyme, ornithine decarboxylase (ODC). Our results, by the end of Project Year 3, showed that 60 Hz, 1 Gauss ELF fields, applied for intervals from 0.5 to as long as 8 hours produce no alterations in ODC specific activity. Microwave exposure, however, using 0.9 GHz, SAR = 3 mW/g, did produce increases in ODC activity after 8 hr exposures, but only when amplitude modulation was applied to the carrier microwave signal. Sixty Hz modulation produced approximately 2-fold increases in ODC activity, whereas continuous wave exposure produced no significant changes from control values. Experiments

confirming the amplitude modulation-specific enhancement have already been completed at the start of Project Year 4, and will be extended by altering physical parameters, such as modulation frequency and amplitude, as well as by investigating the role of the relationship of time and duration of exposure to degree of ODC enhancement.

ODC is a significant enzyme since it is involved in major metabolic pathways for synthesis of DNA, RNA and proteins. ODC activity is related to the state of cell proliferation, which has made it of considerable interest in the study of cancer. The approximately two-fold increase we have observed is far below that which may be obtained by exposure of L929 cells to PMA, where increases of 10-fold or more may be observed; despite this fact, the two-fold difference is of considerable interest since it is only seen when amplitude modulation is applied to the microwave signal. Detailed investigation of these effects will provide a basis for assessing what aspects of microwave exposure produce biological response, allowing more sophisticated experimental design for exploring physical parameters. Additionally, it should be possible to probe the biological origin of enhanced ODC activity, since ODC is regulated by second messenger systems triggered by binding of ligands to specific cell membrane receptors (Pegg and Williams-Ashman, 1981).

FIGURE 1

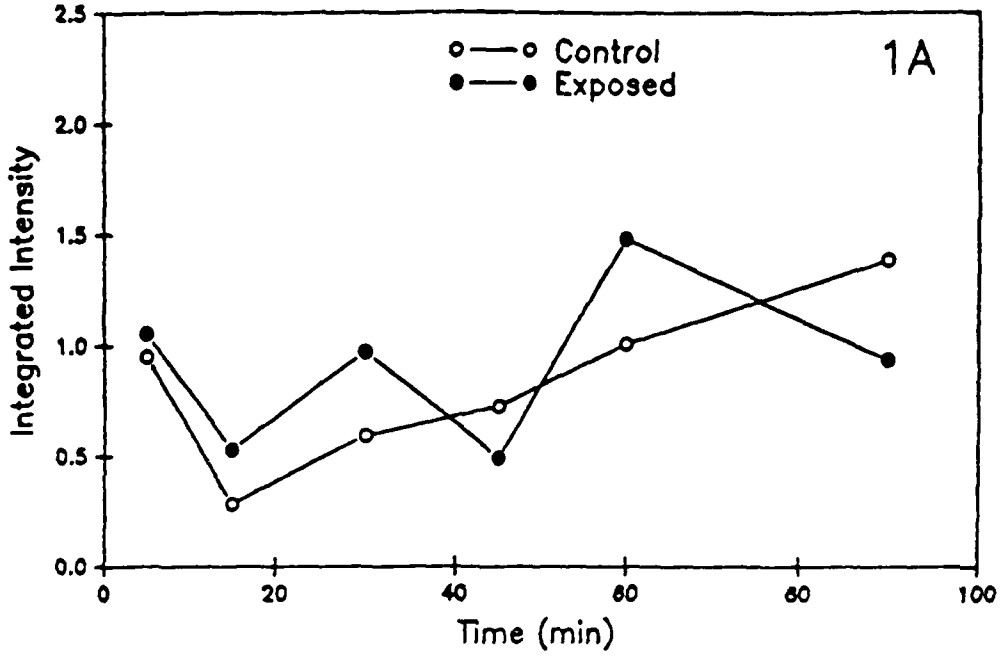
Control
Exposed
1A
Integrated Intensity
2.5
2.0
1.5
1.0
0.5
0.0
0
20
40
60
80
100
Time (min)

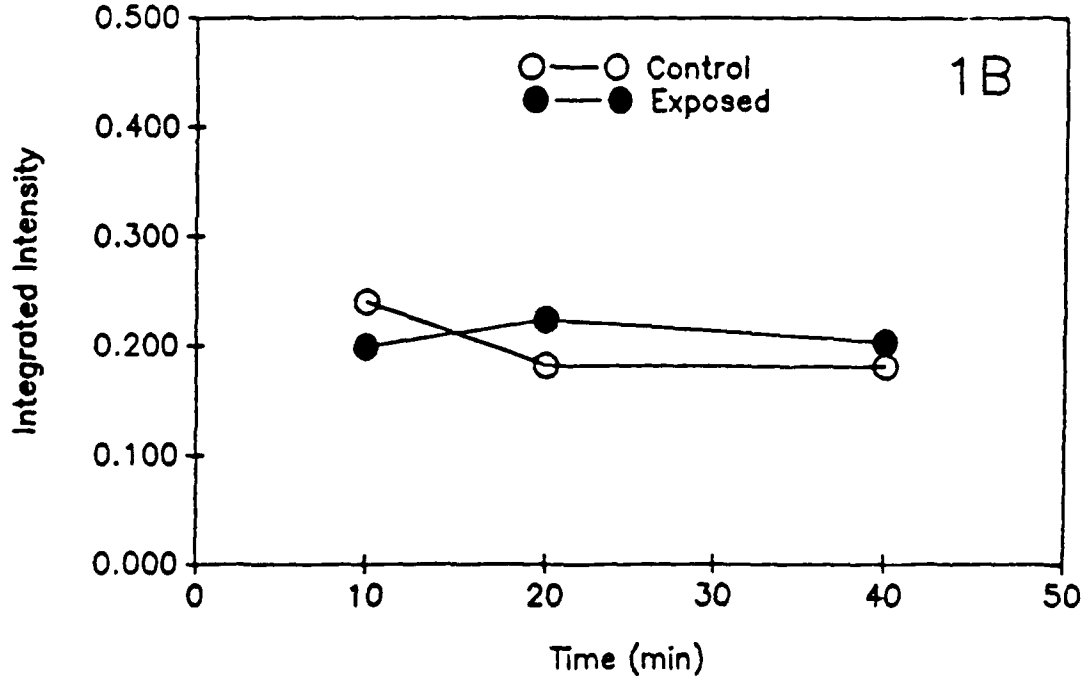
Control
Exposed
1B
Integrated Intensity
0.500
0.400
0.300
0.200
0.100
0.000
0
10
20
30
40
50
Time (min)

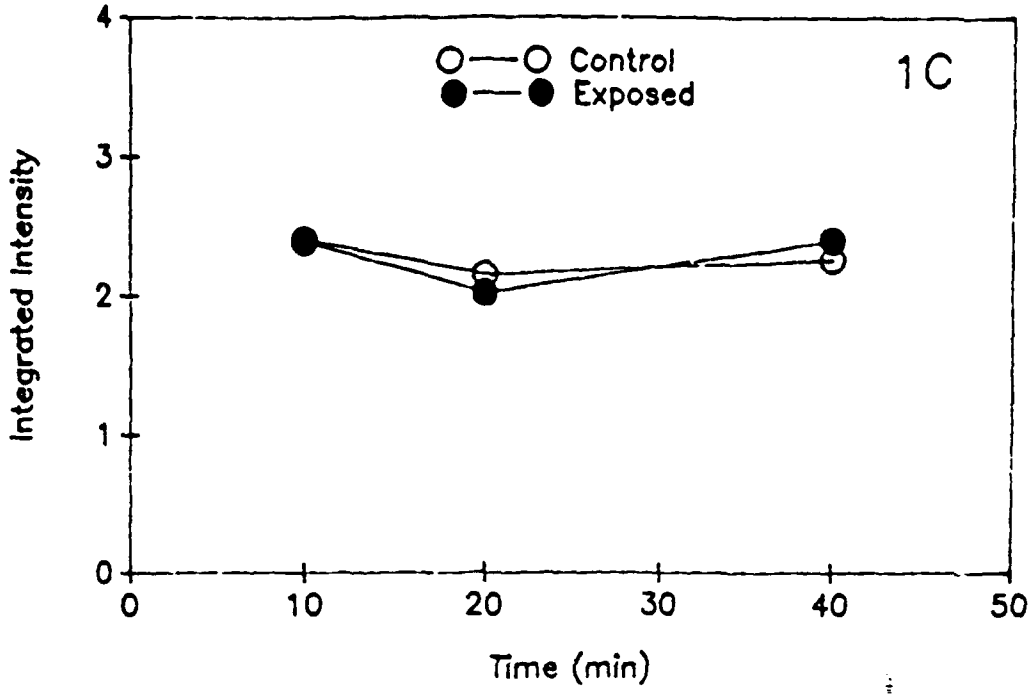
Control
Exposed
1C
Integrated Intensity
0
1
2
3
4
0
10
20
30
40
50
Time (min)

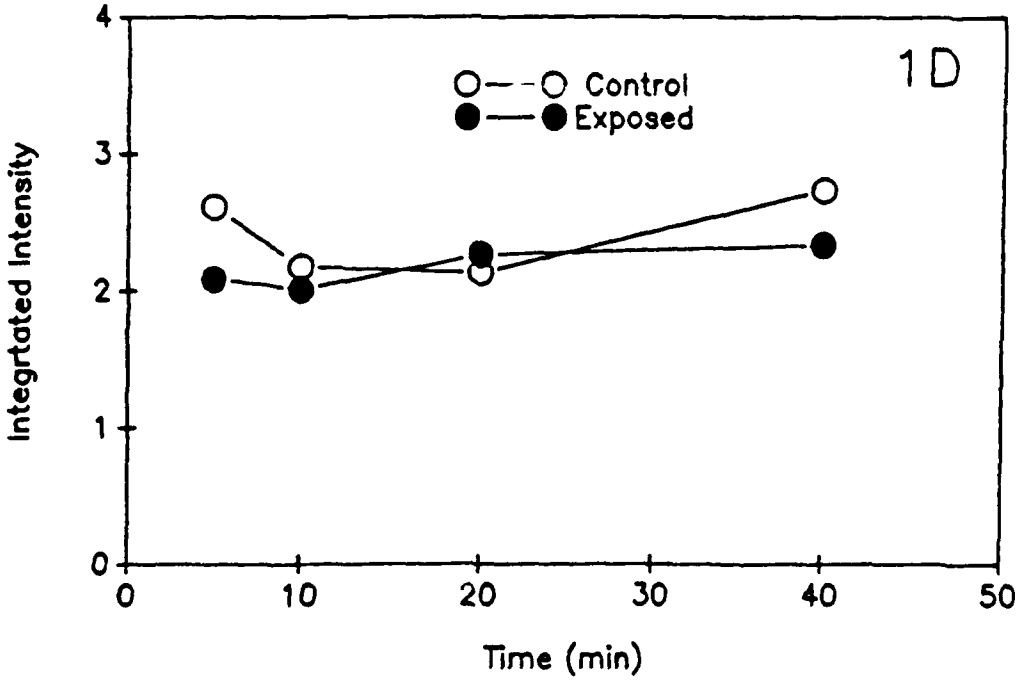
Control
Exposed
1D
Integrtated Intensity
0
1
2
3
4
0
10
20
30
40
50
Time (min)

FIGURE 2

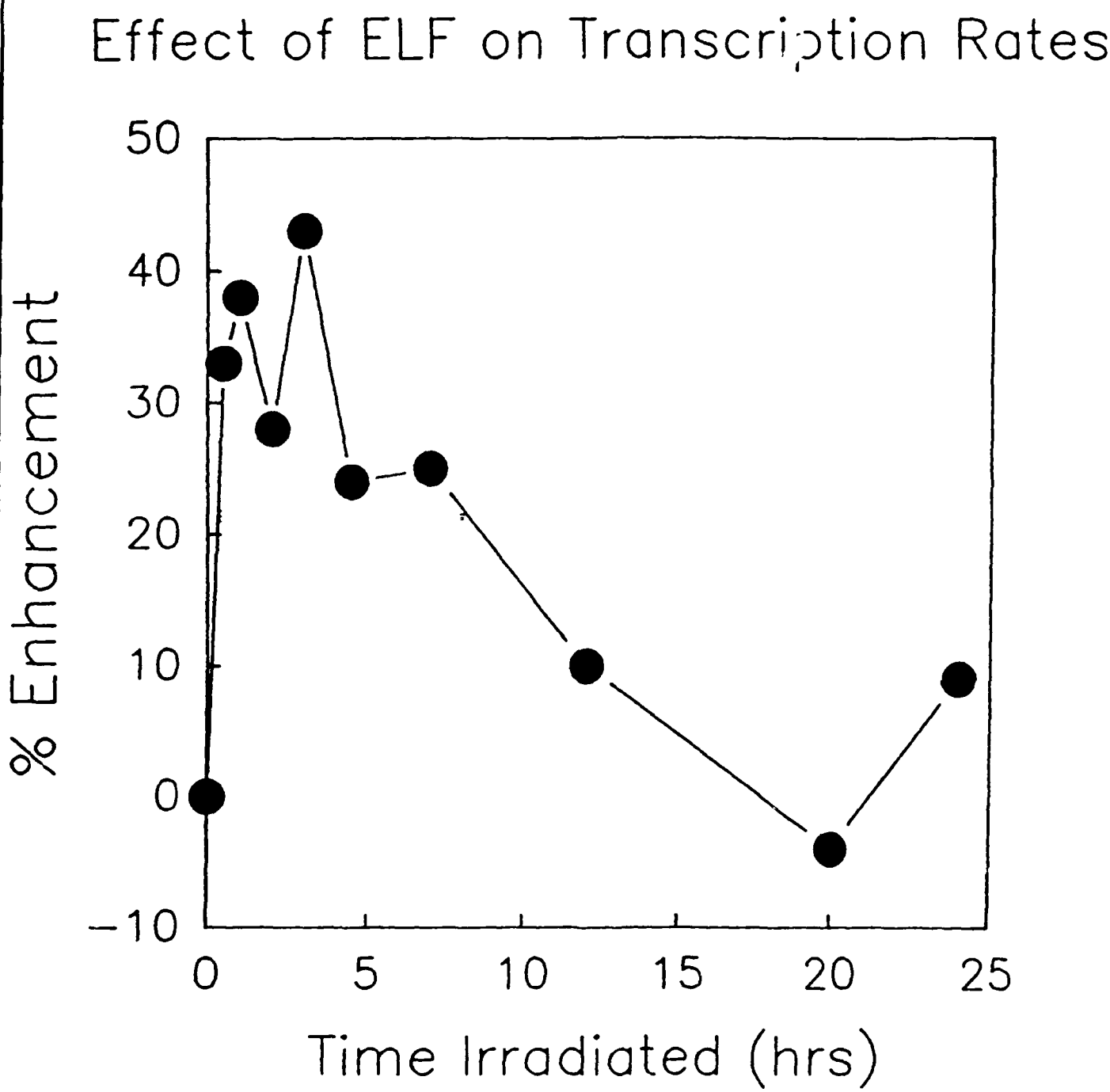
Effect of ELF on Transcription Rates
% Enhancement
50
40
30
20
10
0
-10
0
5
10
15
20
25
Time Irradiated (hrs)

FIGURE 3

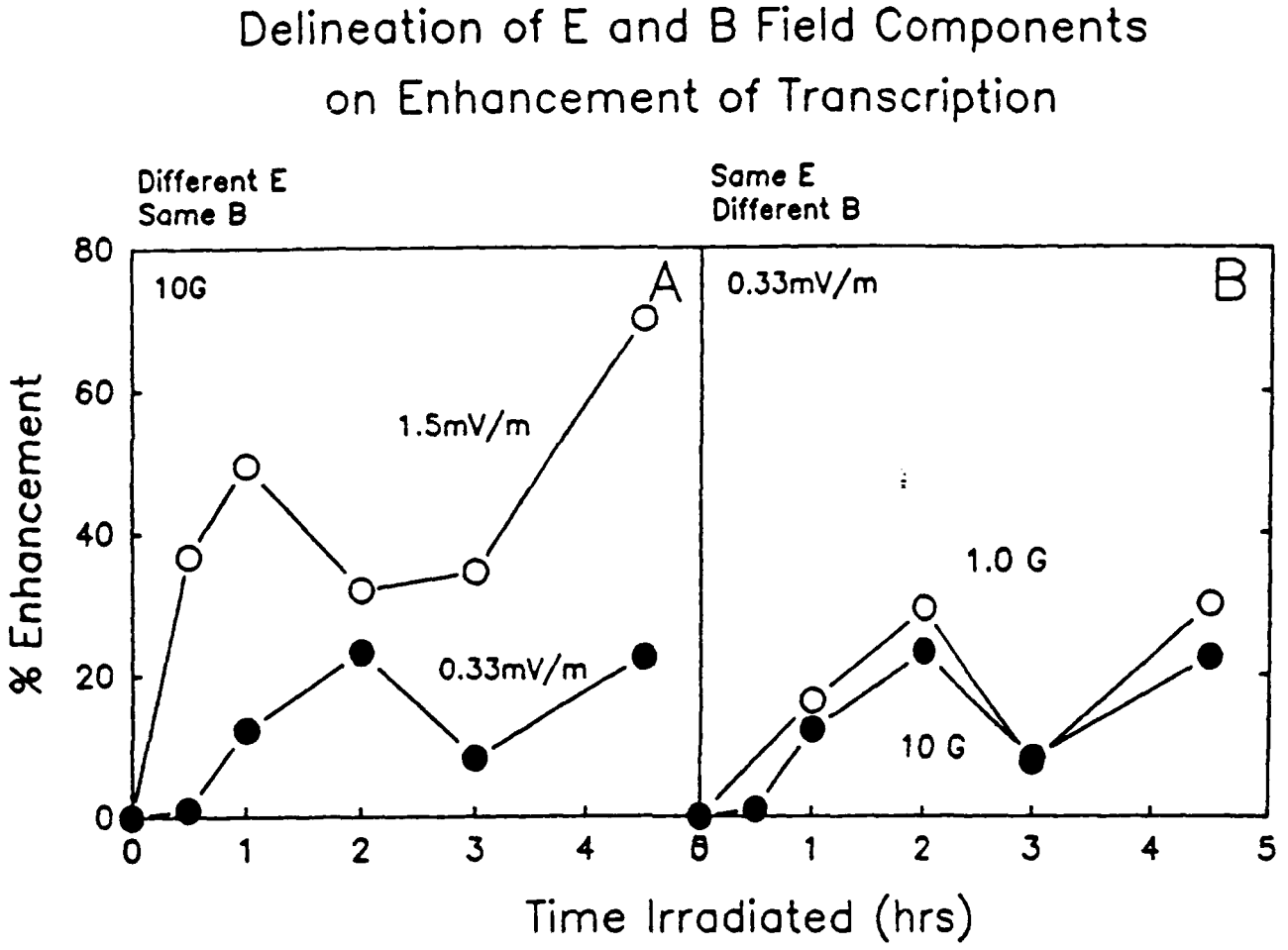
Delineation of E and B Field Components
on Enhancement of Transcription
Different E
Same B
Same E
Different B
10G
A
0.33mV/m
B
1.5mV/m
0.33mV/m
1.0 G
10 G
% Enhancement
Time Irradiated (hrs)
0
20
40
60
80
0
1
2
3
4
5

FIGURE 4

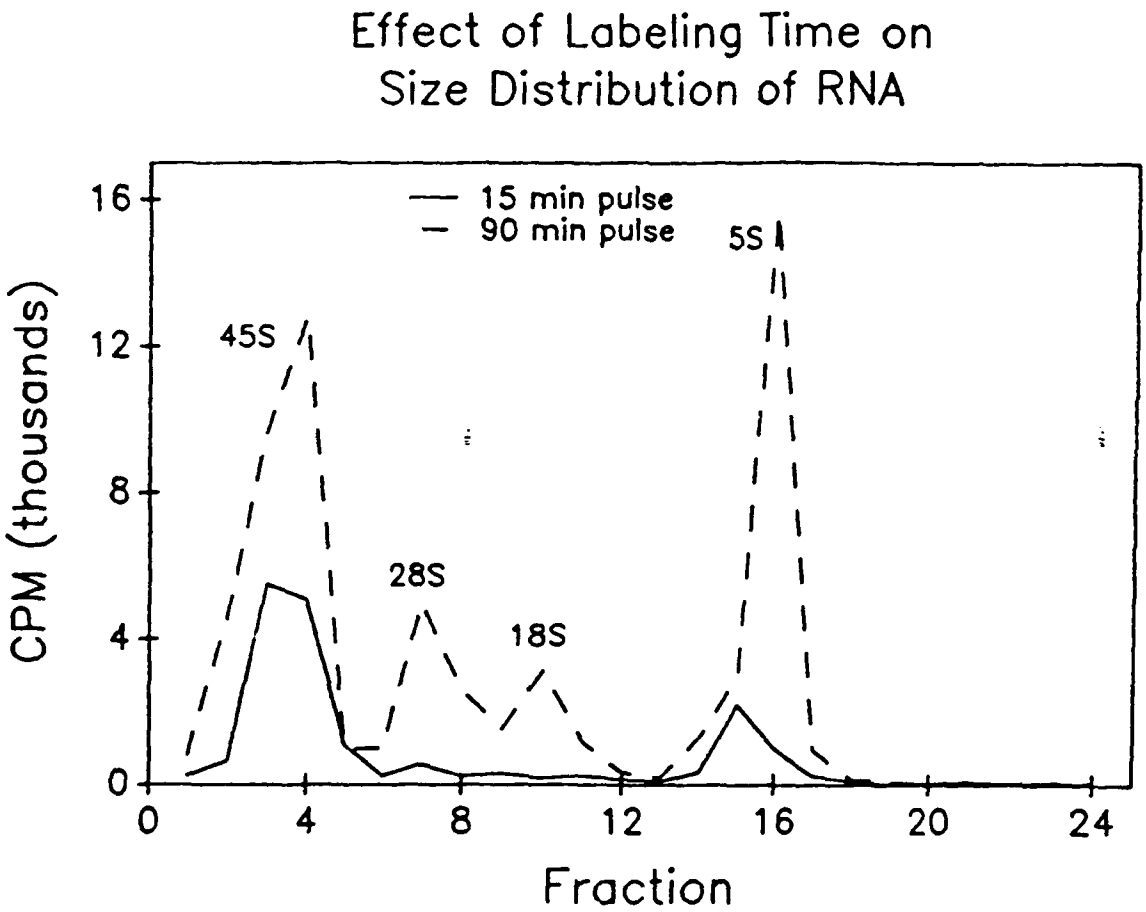
Effect of Labeling Time on
Size Distribution of RNA
15 min pulse
90 min pulse
45S
28S
18S
5S
CPM (thousands)
0
4
8
12
16
20
24
Fraction

FIGURE 5

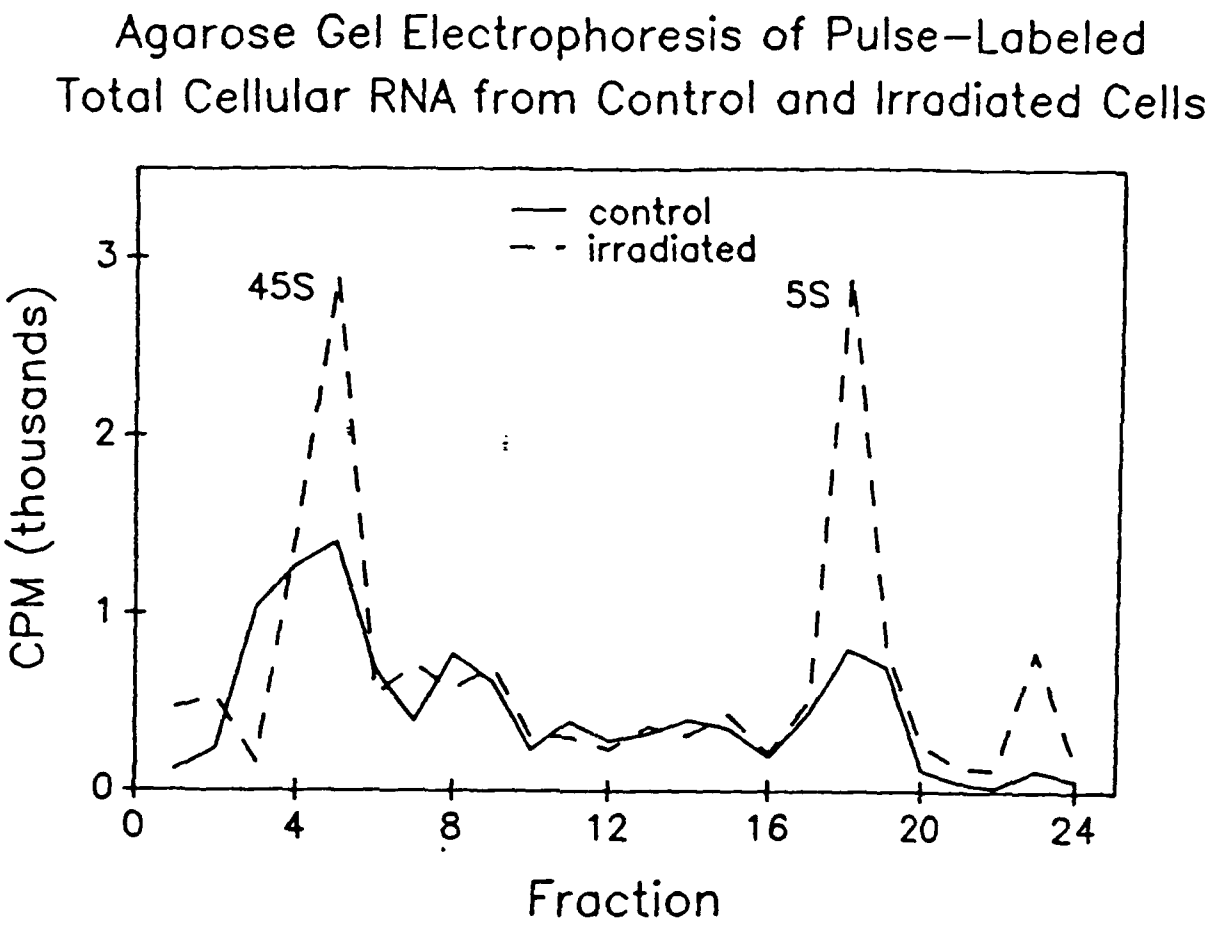
Agarose Gel Electrophoresis of Pulse-Labeled
Total Cellular RNA from Control and Irradiated Cells
control
irradiated
45S
5S
CPM (thousands)
0
1
2
3
0
4
8
12
16
20
24
Fraction

FIGURE 6

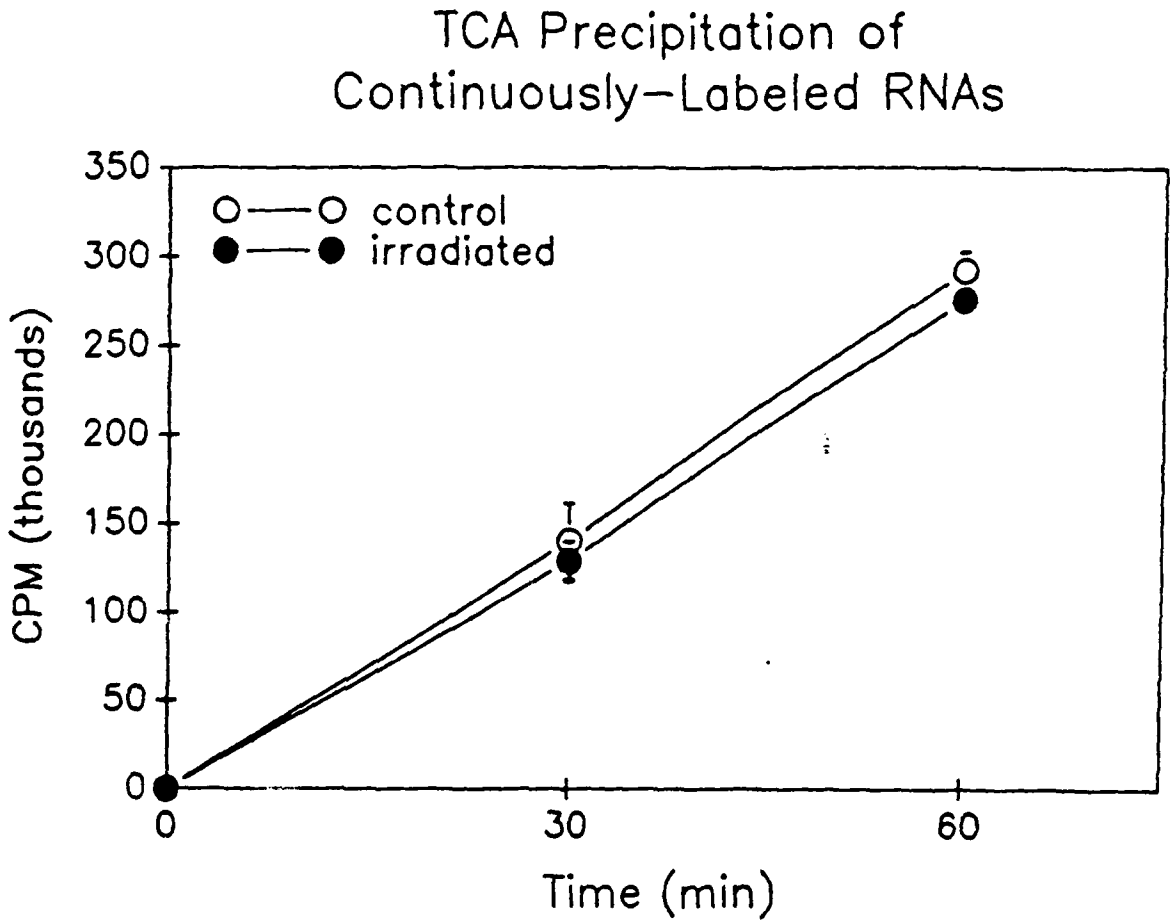
TCA Precipitation of
Continuously-Labeled RNAs
control
irradiated
CPM (thousands)
350
300
250
200
150
100
50
0
0
30
60
Time (min)

FIGURE 7

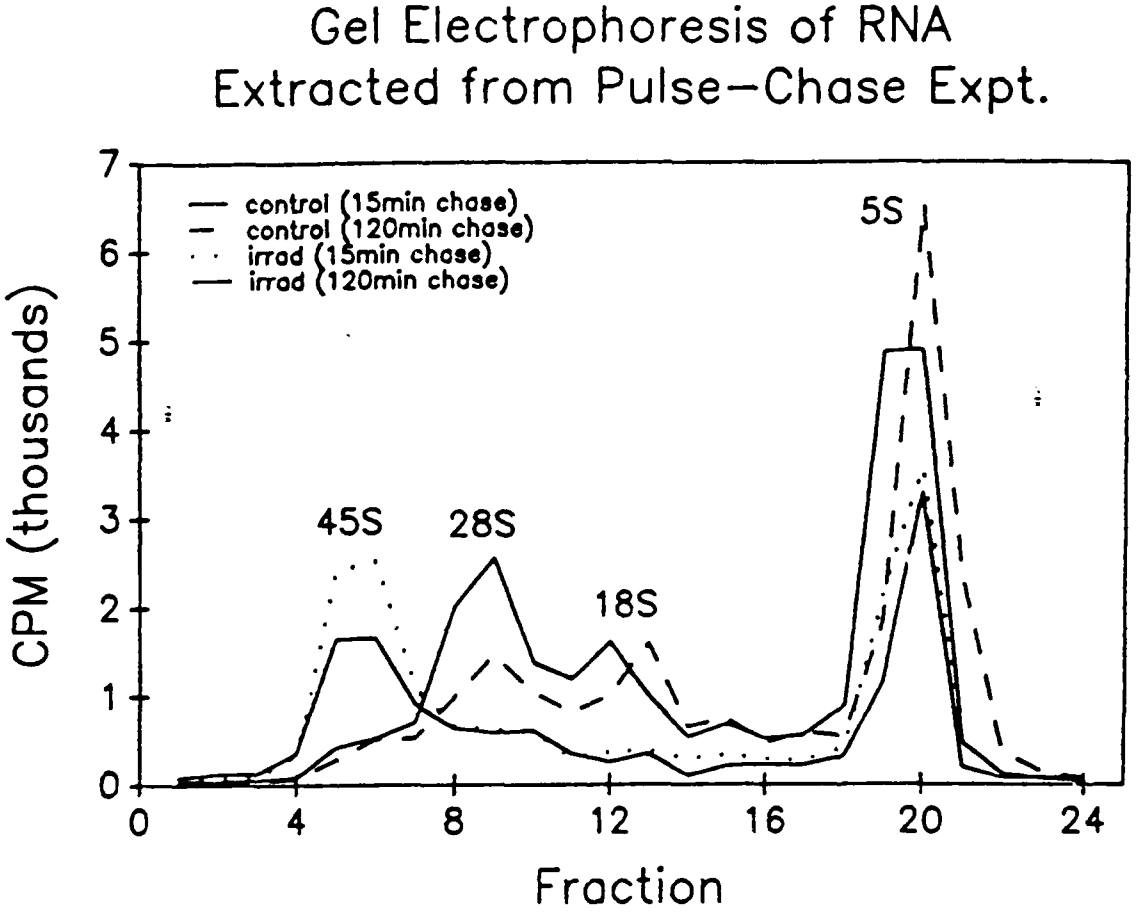
Gel Electrophoresis of RNA
Extracted from Pulse–Chase Expt.
control (15min chase)
control (120min chase)
irrad (15min chase)
irrad (120min chase)
45S
28S
18S
5S
CPM (thousands)
0
1
2
3
4
5
6
7
0
4
8
12
16
20
24
Fraction

FIGURE LEGENDS

Figure 1: Examples of results obtained using cDNA probes to analyze the amounts of specific mRNAs present in samples from total extracted RNA of HL60 cells exposed to ELF fields. All values are measured in units of integrated intensity.

Figure 1A: Comparison of experimental and control values for actin mRNA. Experimental cultures were exposed to a 1 Gauss magnetic field, 60 Hz, in a solenoid device.

Figure 1B: Comparison of experimental and control values for c-myc mRNA. Experimental cultures were exposed to a 0.01 Gauss magnetic field, 60 Hz, in a Helmholtz coil.

Figures 1C and 1D: Integrated intensities of the specific mRNA bands for c-myc (1C) and histone H2B (1D)bands, detected by cDNA probes. Magnetic fields were 0.1 Gauss, 60 Hz, generated by Helmholtz coils (1C) and a solenoid (1D). In all cases where a solenoid device was used cells were maintained in concentric-chambered dishes.

Figure 2: Enhancement of total cellular RNA as a result of exposure of HL-60 cells to a 10 Gauss, 60 Hz field in a solenoid device. Values are expressed as Percent Enhancement, reflecting the incorporation of tritiated uridine into total RNA of exposed relative to control samples. All samples were pulsed with labeled uridine for the last 15 min of their exposure period.

Figure 3: Effect of alteration of electric and magnetic field components on incorporation of tritiated uridine into total cellular RNA of HL-60 cells. Fifteen minute pulses of label were used as for the experiment shown in Figure 2. All exposures were done at 60 Hz.

Figure 3A: Incorporation of labeled uridine relative to control cells was measured for cells in the two chambers of an organ culture dish. Both cultures were exposed to a 10 Gauss but received different average electric fields of 1.5 mV/m (outer chamber) and 0.33 mV/m (inner chamber).

Figure 3B: Incorporation of labeled uridine relative to control cells was measured for 2 different sets of cells. Both sets were exposed to an average electric field of 0.33 mV/m, but different magnetic fields. This was achieved by placing one culture in the center chamber of an organ culture dish and using a 10 Gauss field, and the other in the outer chamber of an organ culture dish and using a Gauss field.

Figure 4: Fractionation, by electrophoresis, of total cellular RNA

from control HL-60 cells given different length pulses of tritiated uridine. Results show that uridine initially (15 min pulse) accumulates in a 45S RNA, and then subsequently shifts to 18S, 28S and 5S RNA species. These results are consistent with processing of rRNAs.

Figure 5: Fractionation of total cellular RNa as for Figure 4, but comparing results for cells exposed to 10 Gauss, 60 Hz magnetic fields relative to control cells. A fifteen minute pulse of tritiated uridine shows enhanced accumulation in the 45S and 5S RNA peaks of exposed cells.

Figure 6: Incorporation of tritiated uridine by continuous labeling. Results show incorporation in counts per minute for control and exposed HL-60 cells. Ten Gauss, 60 Hz fields were used, and label was present for the entire exposure time. Incorporation of label into total cellular RNA was found to be virtually identical for both exposed and control cells.

Figure 7: Results from preliminary analysis, by pulse-chase technique, of the processing of 45S rRNA precursor into 28S and 18S rRNAs. Results indicate that ELF exposure enhances the rate at which the 45S precursor is processed into smaller rRNAs.

REFERENCES

Byus, C.V., K. Kartun, S.E. Pieper and W.R. Ady. 1988. Increased ornithine decarboxylase activity in cultured cells exposed to low energy modulated microwave fields and phorbol ester tumor promoters. Cancer Research, 48:42222-42226.

Byus, C.V. and R.A. Weiner. 1982. The effects of low-energy 60-Hz environmental electromagnetic fields upon the growth=related enzyme ornithine decarboxylase. Carcinogenesis, 3:751-755.

Chomczynski, P. and N. Sacchi. 1987. Single-step method of RNA isolation by acid guanidinium thiocyanate-phenol-chloroform extraction. Analytical Biochemistry, 162:156-159.

Goodman, R., J. Abbott and A.S. Henderson. 1987. Transcriptional patterns in the X chromosome of Sciara coprophilafollowing exposure to magnetic fields. Bioelectromagnetics, 8:1-7.

Goodman, R., C.A.L. Bassett and A.S. Henderson. 1983. Pulsing electromagnetic fields induce cellular transcription. Science, 220: 1283-1285.

Goodman, R. and A.S. Henderson. 1986. Sine waves enhance cellular transcription. Bioelectromagnetics, 7:23-29.

Goodman, R. and A.S. Henderson. 1988. Exposure of salivary gland cells to low-frequency electromagnetic fields alters polypeptide synthesis. Proc. Natl. Acad. Sci., USA, 85: 3928-3932.

Hochstrasser, D.F., M.G. Harrington, A.C. Hochstrasser, M.J. Miller and C.R. Merril. 1988. Methods for increasing the resolution of two-dimensional protein electrophoresis. Analytical Biochemistry, 173: 424-435.

Pegg, A.E. and H.G. Williams-Ashman, 1981, In Morris, D.A. and L.J. Marton (Eds) "Polyamines in biology and Medicine. Marcel Decker, New YOrk, pp. 3-42.

Seeley, J.e. and A.E. Pegg. 1983. Methods in Enzymology, 94: 158-161.

Silverman, R.H., et al. In, E. DeMaeyer and H. Schellickens (Eds) The Biology of the Interferon System, 1983, pp. 189-200.

Wei, L.-X., R. Goodman and A.S. Henderson. 1989. Relationship of transcript quantity to amplitude of sinusoidal electromagnetic signals (60 & 72 Hz). J. Cell Biology, 109: 291a.

DISTRIBUTION LIST

4 copies	Director Walter Reed Army Institute of Research ATTN: SGRD-UWZ-C Washington, DC 20307-5100
1 copy	Commander US Army Medical Research and Development Command ATTN: SGRD-RMI-S Fort Detrick, Frederick, Maryland 21701-5012
2 copies	Defense Technical Information Center (DTIC) ATTN: DTIC-DDAC Cameron Station Alexandria, VA 22304-6145
1 copy	Dean School of Medicine Uniformed Services University of the Health Sciences 4301 Jones Bridge Road Bethesda, MD 20814-4799
1 copy	Commandant Academy of Health Sciences, US Army ATTN: AHS-CDM Fort Sam Houston, TX 78234-6100